DEPARTMENT OF BIOLOGICAL AND ECOLOGICAL SCIENCES (DEB)

PhD Course in GENETICS AND CELLULAR BIOLOGY - XXVII cycle

BIO/13

ROLE OF RAB7A AND RILP IN CELL MIGRATION

PhD student:

Azzurra Margiotta

Coordinator of the PhD course

Prof. Giorgio Prantera

Tutor

Prof. Cecilia Bucci

May 2016

INDEX

ABSTRACT

Rab7a is a small GTPase of the Rab family that regulates late stages of endocytosis. RILP is an important downstream effector of Rab7a, which can be recruited to membrane from cytosol by this GTPase. Rab7a and RILP control together several aspects of vesicular trafficking. This PhD work focuses on the role of Rab7a and RILP in cell migration, which is a cellular process characterized by cell polarization, protrusion of the cell membrane, formation of new adhesions, contraction and retraction of the cell body.

First of all, we demonstrated in wound healing assay that Rab7a modulates cell motility affecting cell velocity and directness. Moreover, Rab7a alters the formation of filopodia by mislocalizing myosin X, an actin motor known to promote the formation of these protrusions. Furthermore, we investigated the role of Rab7a in cell adhesion. We evaluated the ability of control and Rab7a-depleted cells to spread out on fibronectin-coated coverslips and we found that Rab7a depleted-cells showed a lower ability to spread while re-expression of active Rab7a recovered partially the function. Interestingly, activation, localization and intracellular trafficking of β1-integrin, a component of cell-matrix adhesions, were impaired after Rab7a silencing. Furthermore, as Rab7a interacts with Rac1 and vimentin, important factors for cell motility, we investigated the role of Rab7a on the regulation of these proteins. Interestingly, we found that Rab7a silencing impairs Rac1 activation state but not its abundance. In addition, Rab7a regulates vimentin filaments reorientation during migration. In fact, Rab7a depletion reduced the percentage of migrating cells with vimentin filaments facing the wound. We made some Rab7a mutants to investigate deeply the role of Rab7a in cell migration but the preliminary data collected did not show any difference in behavior of these proteins compared to wild type Rab7a. Similarly, Rab7a mutants which are responsible of the onset of Charcot-Marie-Tooth type 2B neuropathy did not act differently from the wild type protein in the performed experiments.

In light of the above, we demonstrated that Rab7a is necessary for proper cell migration, being able to modulate several aspects of this process and by regulating several key proteins.

Then, we characterized the role of RILP in cell migration by evaluating its role on cell motility, microtubule cytoskeleton, cell polarization and adhesion. We demonstrated that RILP controls cell velocity and cell adhesion, but not Golgi apparatus reorientation and microtubules reorganization.

The discovery of the involvement of Rab7a and RILP in cell migration could be of importance both in physiological and pathological situations.

RIASSUNTO

Rab7a è una piccola GTPasi della famiglia delle proteine Rab e regola gli stadi tardivi dell'endocitosi. RILP è un importante effettore di Rab7a che può essere reclutato dal citosol sulla membrana da questa GTPasi. Rab7a e RILP controllano insieme diversi aspetti del traffico vescicolare. In questo lavoro di dottorato si è studiato il ruolo di Rab7a e RILP nella migrazione cellulare, che è un processo importante in tutti gli organismi ed è caratterizzato dalla polarizzazione cellulare, protrusione della membrana plasmatica, formazione di nuove adesioni, contrazione e retrazione del corpo cellulare.

Innanzitutto, si è dimostrato in esperimenti di *wound healing* che Rab7a modula la motilità cellulare influenzando la velocità e la direzionalità delle cellule. Inoltre, Rab7a altera la formazione dei filopodi regolando la localizzazione di miosina X, che è una proteina motore responsabile della formazione di queste protrusioni. Successivamente, si è studiato il ruolo di Rab7a nell'adesione cellulare con la fibronectina, una componente della matrice extracellulare. In particolare, si è valutata l'abilità di cellule controllo e silenziate per Rab7a di aderire su vetrini ricoperti da fibronectina. Si è dimostrato che dopo il silenziamento di Rab7a le cellule presentavano una minor abilità nell'aderire al substrato. Tuttavia, la riespressione della proteina Rab7a attiva ha determinato un recupero parziale della funzionalità. Si è riscontrato, inoltre, un'alterazione nell'attivazione, localizzazione e traffico intracellulare dell'integrina β1, una componente delle adesioni cellula-matrice extracellulare, dopo la deplezione di Rab7a. Questa GTPasi interagisce con Rac1 e vimentina, che sono due proteine importanti per la migrazione cellulare. Pertanto, si è studiato il ruolo di Rab7a nella regolazione di queste proteine. Innanzitutto, si è visto che il silenziamento di Rab7a altera lo stato di attivazione di Rac1 ma non la sua abbondanza proteica. Inoltre, Rab7a regola la riorientazione dei filamenti di vimentina durante la migrazione. Infatti, la deplezione di Rab7a ha ridotto la percentuale delle cellule in migrazione che presentavano i filamenti di vimentina orientati nella direzione di migrazione. Successivamente, si sono creati dei mutanti della proteina Rab7a in modo da valutare meglio il ruolo di Rab7a nella migrazione ma i dati preliminari ottenuti non hanno evidenziato alcuna differenza di comportamento tra le proteine mutate e quella *wild type*. Similiarmente, anche i mutanti di Rab7a che sono responsabili dell'insorgenza della neuropatia di Charcot-Marie-Tooth di tipo 2B non hanno mostrato differenze con la proteina *wild type* negli esperimenti eseguiti.

Alla luce di tutto ciò, si è dimostrato che Rab7a è necessaria per la migrazione cellulare ed è capace di modulare diversi aspetti e proteine chiave di questo processo.

Successivamente si è analizzato la funzione di RILP nella migrazione cellulare valutando il suo ruolo nella motilità, nella regolazione dei microtubuli, nella polarizzazione e nell'adesione cellulare. Si è, quindi, dimostrato che RILP controlla la velocità e l'adesione cellulare ma non la riorientazione dell'apparato di Golgi e la riorganizzazione dei microtubuli.

La scoperta del coinvolgimento di Rab7a e RILP nella migrazione cellulare potrebbe essere rilevante sia in condizioni fisiologiche che patologiche.

INTRODUCTION

1.1 Cell migration

Cell migration is the ability of a cell to actively move from one place to another and it is a relevant process in all organisms. It isn't important only during development but also during the lifetime as it participates in wound repair and immune responses (Etienne-Manneville, 2013; Raftopoulou and Hall, 2004). The general mechanism of cell migration involves the repetition of four basic steps: protrusion of the cell membrane, formation of new adhesions, contraction and retraction of the cell body (Etienne-Manneville, 2013; Vicente-Manzanares *et al.*, 2005).

During migration cells undergo several changes (Figure 1.1). When a cell receives migratory stimuli, several morphological modifications occur leading to the development of a polarized phenotype. First of all, cells are oriented towards the direction of migration presenting a protruding, leading front opposite to a retracting rear edge. Cell polarization refers to the presence of asymmetry within a cell that is generated by spatial differences in a variety of subcellular components. During migration, the polarized phenotype is identified by the extension of dynamic membrane protrusions at the leading edge, the formation and disassembly of focal adhesions (FAs), the reorganization of microtubules, actin and intermediate filaments, and the reorientation of the Golgi apparatus and of the microtubule organizing centre (MTOC) into the direction of the wound (Vicente-Manzanares *et al.*, 2005; Etienne-Manneville, 2013). In particular, proper microtubules organization is essential for the polarized structure. Microtubules are composed of α- and β-tubulin polymers and tubulin subunits are organized in a polar manner, with a fast-growing plus end which radiates toward the cell periphery and a slow-growing minus end which is attached to the MTOC, from which microtubules are generated (Muthuswamy and Xue, 2012). During migration, microtubules are oriented along the axis of migration and play an important role in establishing directionality by regulating actin polymerization and transporting membrane vesicles to the leading edge (Etienne-Manneville, 2013). Moreover, during cell polarization, the reorientation of the nucleus at the rear of migrating cells is required for cell polarization, by promoting correct MTOC localization and thus the establishment of front-rear polarity (Maninová *et al.*, 2013). In addition, other changes, such as in vesicular transport pathways and in gene transcription, occur during migration (Raftopoulou and Hall, 2004; Leduc and Etienne-Manneville, 2015). Cell polarity is essential for directional migration and enables the cell to turn intracellularly generated forces into net cell body translocation (Vicente-Manzanares *et al*, 2005; Lauffenburger and Horwitz, 1996).

All these events are essential for directed migration and several molecules coordinate both in space and time these processes (Vicente-Manzanares *et al*., 2005).

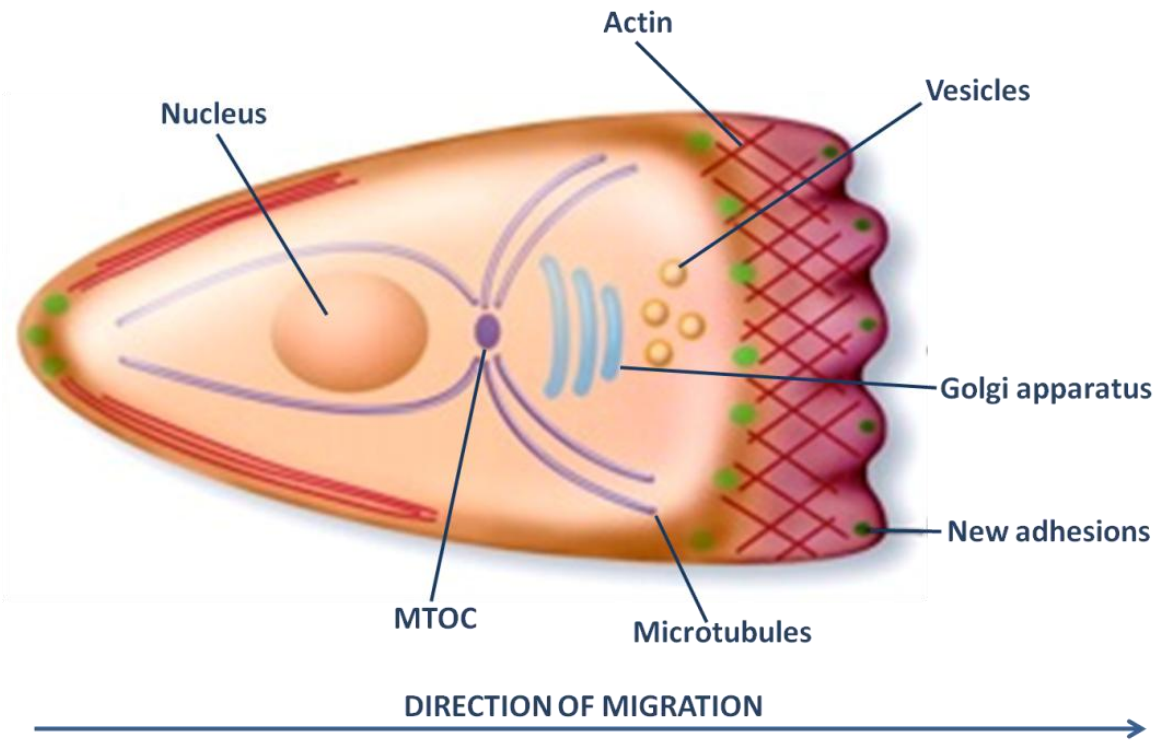

Figure 1.1 Cellular changes during migration. A polarized migrating cell shows reorganization of the cytoskeleton, Golgi apparatus and MTOC orientation, and the formation of protrusions and adhesion sites at the leading edge (adapted from Ridley *et al*., 2003).

1.2 Actin filaments and formation of protrusions

The actin cytoskeleton is an important player in cell migration as its reorganization influences cell shape and polarization, adhesions and contraction of the cell body. Actin filaments can organize into a variety of architectures that are responsible for the regulation of different aspects of cell migration (Figure 1.2). Lamellipodia are broad, flat, sheet-like structures composed of branched actin filaments which push the cell membrane by polymerizing against it. Instead, filopodia are thin, cylindrical, needle-like projections at the front of the cell and are composed of unbranched, bundled actin filaments oriented with their growning ends toward the membrane. Cytoplasmic organelles are excluded from lamellipodia and filopodia that are the main components driving motility (Lauffenburger and Horwitz, 1996; Blanchoin *et al.*, 2014). Contractile structures are represented by transverse arcs, focal adhesion-anchored stress fibers and cell cortex which ensure mechanical integrity and coherent movement of the cell as a whole. Transverse arcs and stress fibers are localized in all the cell except for the lamellipodia/filopodia region. Ventral stress fibers run approximately parallel to the direction of the movement, linking

focal adhesion sites, whereas transverse arcs run parallel to the leading edge, just behind the actin network forming the lamellipodia. Finally, cell cortex is a thin layer of actin which coats the plasma membrane at the back and sides of the cell and it is important for cell shape (Blanchoin *et al.*, 2014).

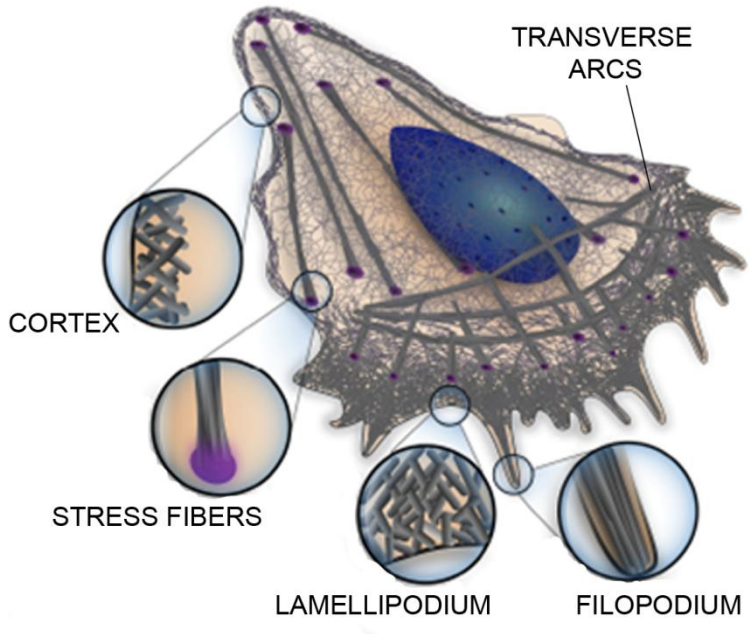

Figure 1.2 Actin filaments structures in migrating cells. Schematic representation of a migrating cell showing different actin architectures as indicated (adapted from Blanchoin *et al.*, 2014).

1.2.1 Filopodia protrusions and myosin X

Filopodia are fingerlike processes with a diameter of about 200 nm and length of several µm. They are dynamic structures that can show different modes of movement. The most common motions of filopodia are linear growth and retraction, whereas angular rotations around their anchor point are necessary to "scan" the area of the environment surrounding the cell. Filopodia are important in sensing the cell environment, initiating cell contacts, and transmitting cell-cell signals. Moreover, they exert pulling forces (Blanchoin *et al.*, 2014; Bornschlögl, 2013). The filopodial core is made up of 15-30 tightly packed actin filaments, which can exhibit a dense protein complex at the tip. Different proteins regulate filopodial formation, maintenance and dynamics. Among these, myosin X is a molecular motor that plays an important role in filopodial formation and is responsible for transporting various proteins, including transmembrane receptors, along actin filaments to the tips of filopodia to participate in filopodia maintenance and stabilization, and environment and cue sensing (Bornschlögl, 2013; Jacquemet *et al.*, 2015). In fact, myosin X overexpression induces an increase of the number of filopodia per cell,

whereas its silencing decreases endogenous filopodia. Myosin X binds β-integrin receptors through its tail domain. This interaction is hypothesized to allow myosin X to link the internal actin cytoskeleton with the extracellular matrix (Figure 1.3). In support of this, studies of cells expressing myosin X mutants lacking integrin binding have showed decreased filopodial adhesion. Moreover, myosin X over-expression leads to increased cell invasion, whereas its depletion inhibits cancer cell invasion. Myosin X is thought to drive cell invasion by transporting integrins to the tips of filopodia to tether the extra-cellular matrix (ECM). Myosin X undertakes its biological roles when activated by its dimerization (Courson and Cheney, 2015; Jacquemet *et al*., 2015).

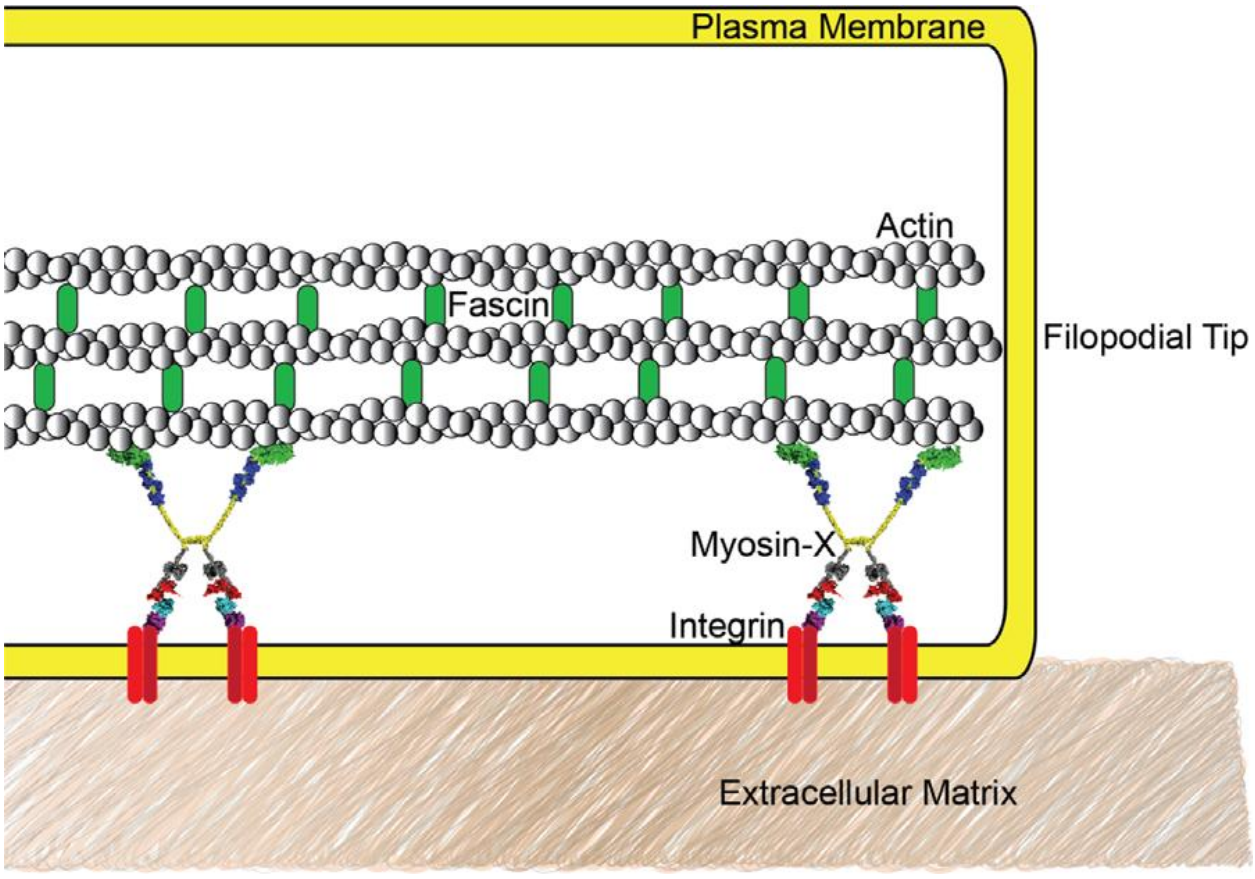

Figure 1.3 Myosin X localizes to the filopodial tip. Myosin X seems to be the molecular link between the actin cytoskeleton and integrin-based adhesions to the extracellular matrix in filopodia (Courson and Cheney, 2015).

1.3 Cell-matrix adhesions

Lamellipodia and filopodia are stabilized by adhesions that connect the actin cytoskeleton with the ECM. Cell-matrix adhesions are associated with actin microfilaments in the cytoplasm, whereas they establish tight connection with the substrate in the ECM. Adhesions regulate cell motility by assembling at the leading edge and disassembling at the rear edge in response to

extracellular cues. However, adhesions also disassemble at the front of the cell, and their components can be part of new adhesions that will form in the same region. This process is called adhesion turnover (Parsons *et al.*, 2010). Adhesions have been classified basing on their size, stability and localization in several subtypes: nascent adhesions, focal complexes and focal adhesions. They differ from each other in the levels of the protein components, however they seem to be in a *continuum* of structures rather than distinct adhesion types. The earliest detectable adhesions are the nascent adhesions, small, short-lived adhesions, which have origin in the lamellipodium just behind the leading edge. They can either disassemble in about a minute or mature to larger, dot-like adhesions called focal complexes. Focal complexes are localized at the lamellipodium-lamellum interface, therefore slightly further back from the leading edge. These adhesions are slightly larger in size (~1 μm in diameter) and persist for several minutes. Then, they mature in more stable structures that are referred to as focal adhesions. They are larger and elongated, in fact, their diameter is of about 2 μm whereas their length is of 3-10 μm. Focal adhesions reside at the ends of actin stress fibers (Figure 1.4). As the cell move forward, adhesions are disassembled and re-formed in a more advanced position. Continuous cycles of adhesion and retraction allow the translocation of the cell in the direction of migration (Parsons *et al.*, 2010).

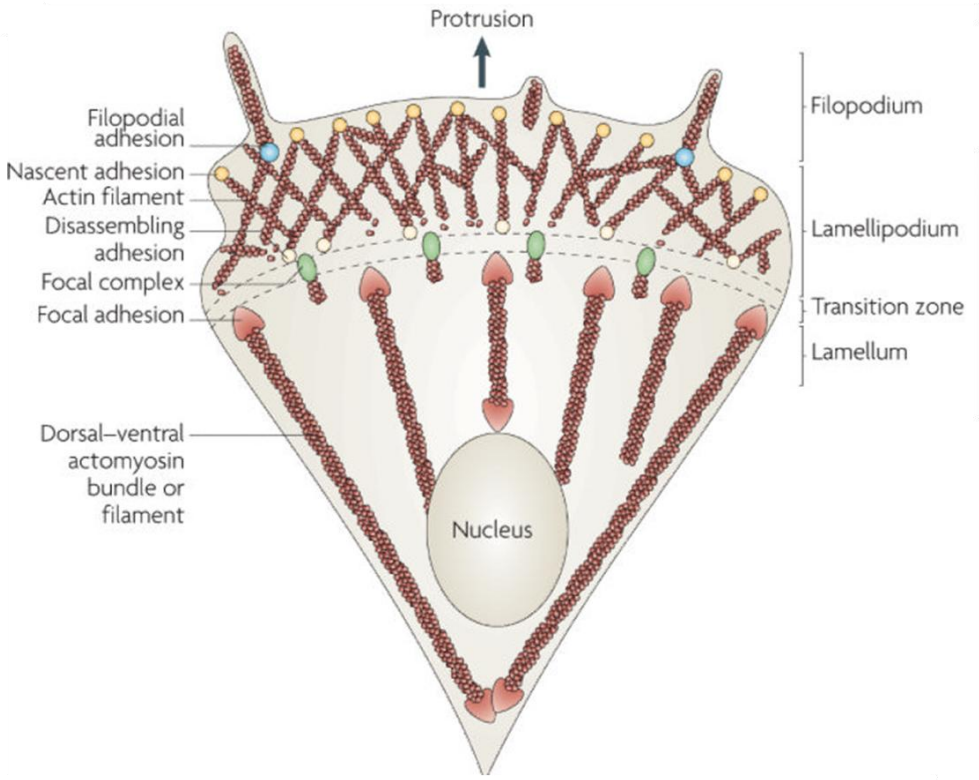

Figure 1.4 Nascent adhesions, focal complexes and focal adhesions localization sites. Nascent adhesions form in the lamellipodium. Nascent adhesion maturation gives origin to focal complexes, which are localized at the convergence of the lamellipodium and lamellum (the

transition zone). At the contrary, focal adhesions reside at the ends of actin stress fibers (adapted from Parsons *et al.*, 2010).

In addition to nascent adhesions, focal complexes and focal adhesions, fibrillar adhesions have been detected in fibroblasts grown in fibronectin-rich environments for extended time. These adhesions are highly elongated, have a long lifetime and are located towards the center of the cell. However, they are not prominent in rapidly migrating cells (Parsons *et al.*, 2010).
The formation, maturation and disassembly of adhesions are regulated by actin polymerization and actomyosin contraction. The most important components of these adhesions are the adhesive receptor integrins, but several adhesion components have been identified. Among them vinculin is recruited to the cytoplasmic tails of β integrins, through the interaction with talin, an actin-binding protein. Vinculin is important in stabilizing focal adhesions. In fact, cells lacking vinculin have fewer and smaller adhesions, whereas cells over-expressing vinculin show an increased number and size of focal adhesions compared to control cells. Moreover, cell motility is reduced in cells devoid of vinculin (Peng *et al.*, 2011; Parsons *et al.*, 2010).

1.3.1 Integrins

Integrins are a family of transmembrane cell surface heterodimeric molecules that constitute a major class of adhesion receptors. They are expressed in all cell types, erythrocytes excluded. In vertebrates, the assembly of 18 α-integrin and 8 β-integrin subunits within the endoplasmic reticulum leads to the formation of 24 different integrin heterodimers. They undergo further post-translational modification in the Golgi complex and then they localize as large, membrane-spanning proteins, at the cell surface linking ECM to the actin cytoskeleton in cell-matrix adhesions. In particular, their large extracellular domain binds to a variety of matrix ligands, whereas the short intracellular tail domain interacts with a number of adhesion components which mediate the association with actin filaments (De Franceschi *et al.*, 2015). Some integrin subunits appear only in a single heterodimer, while β1 subunit is part of twelve integrins and αV subunit of five (Humphries *et al.*, 2006). Integrins are differently expressed in tissues and exhibit a distinct binding affinity to ligands (Damianovich *et al.*, 1992; Humphries *et al.*, 2006). In addition, changes in the conformation of integrins and their clustering into oligomers can influence the binding of ligands. Integrins can exist in bent "closed" inactive conformation, intermediate extended conformations (also known as "primed") and extended "open" active conformation. These conformations reflect a low ability to bind ligand, an activated, and an activated and ligand-occupied integrin conformers, respectively (Figure 1.5). Instead, the formation of heterooligomers due to the interaction of integrin heterodimers is defined integrin

clustering. This event can be induced by binding of an extracellular ligand to different integrin extracellular domains at the same time (referred to as multivalent ligand), by inside-out signals that stimulate the recruitment of protein complexes that bind with several integrin cytoplasmic domains or by free diffusion of integrins in the plane of the membrane. Integrin clustering is important for triggering outside-in signalling, integrin recycling and mechanotransduction by focal complexes and focal adhesions (Shattil *et al.*, 2010).

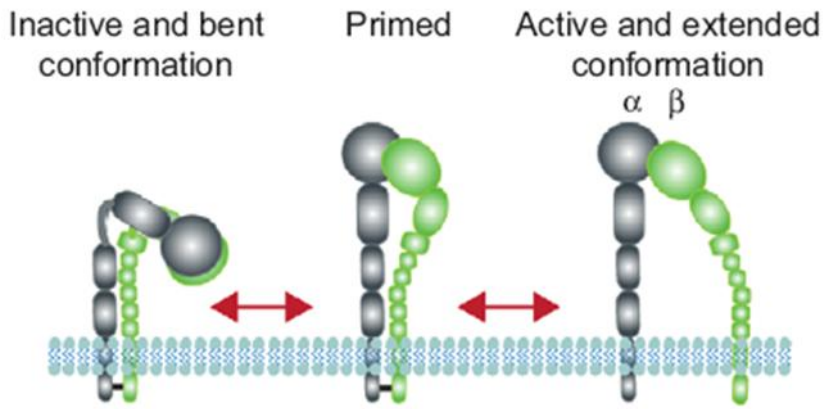

Figure 1.5 Schematic representation of integrin conformations. (adapted from De Franceschi *et al*., 2015).

Integrin signalling is bidirectional. During inside-out signalling, intracellular factors, such as talin, bind to β-integrin tails, leading to conformational changes that increase integrin affinity for extracellular ligands (primed conformation). Inside-out signalling regulates adhesion strength. During outside-in signalling, both the modulation of integrin conformation, due to the binding to extracellular ligands, and the clustering, caused by multivalent ligands, determines intracellular signals that control several biological aspects, such as cell polarity, cytoskeletal structure, gene expression, cell survival and proliferation (Shattil *et al.*, 2010). However, inside-out and outside-in signallings are closely linked. For instance, the primed integrin conformation caused by the binding of intracellular proteins (inside-out signalling) can lead to ligand binding, which in turn causes outside-in signalling (Shattil *et al.*, 2010).

Integrins function can also be regulated by the modulation of their trafficking through the endocytic system. In fact, integrins usually undergo cycles of endocytosis and recycling that control the availability of these receptors at the plasma membrane and therefore their function. Instead, their degradation is less frequent as it has been demonstrated that the half-life of surface integrin is of about 12-24 hours (Paul *et al*., 2015). Internalization of integrins regulates the turnover of focal adhesions and promotes adhesion formation at the front of migrating cells, thus regulating cell migration. Both inactive and active conformations of integrin heterodimers can be

internalised, but the binding of sorting nexins (SNX) 17 and 31 to β-integrins is determinant for their recycling, instead of being degraded (Paul *et al*., 2015). However, also autophagosomes seem to have a role in degradation of β1 integrins (Tuloup-Minguez *et al*., 2013). GTPases of the Rab and Arf families seem to be important for regulating integrin trafficking. In particular, it has been demonstrated that Rab5 and Rab21 are important for integrin endocytosis, whereas recycling from early endosomes occurs through the Rab4 short-loop pathway. Instead, perinuclear recycling of integrins is regulated by Rab11 through the long-loop pathway. Finally, Rab25 binds directly to the β1-integrin tail and regulates the trafficking of α5β1 integrin. Rab25 sorts inactive α5β1 integrin for recycling to the cell front, whereas it sorts the active form of this integrin back towards the cell body through late endosomes to chloride intracellular channel 3 (CLIC3)-positive lysosomes where CLIC3 prevents degradation of this integrin and promote its recycling back to the plasma membrane (Paul *et al*., 2015).

1.3.2 β1-integrin

β1-integrin is a protein of about 130 KDa. Several monoclonal antibodies have been developed to detect conformation-dependent epitopes of this integrin and used in experimental studies (Byron *et al*., 2009). Therefore, it has been demonstrated that inactive β1-integrin is mostly localized to the plasma membrane and protrusions. In fact, approximately 80% of surface β1-integrin is in the inactive form, whereas only 20% of cell surface β1-integrin is in the active conformation even if this conformation is more clustered than the inactive form. At the contrary, active β1-integrin is predominant in the cytoplasm (Tiwari *et al*., 2011; Arjonen *et al*., 2012). In addition to the particular localization, active and inactive β1-integrins show also different endocytosis. In fact, active β1-integrin is internalized together with the ligand and more efficiently than the inactive form. Both active and inactive β1 integrins were found in Rab5-, Rab4a-, Rab21- and Rab11-positive compartments. However, trafficking routes of the two conformations are distinct as only the active β1-integrin can localize to Rab7a-positive compartments, whereas inactive β1-integrin is recycled back through rapid F-actin and Rab4-dependent pathway to ARF6-positive protrusions on the plasma membrane (Figure 1.6) (Arjonen *et al*., 2012).

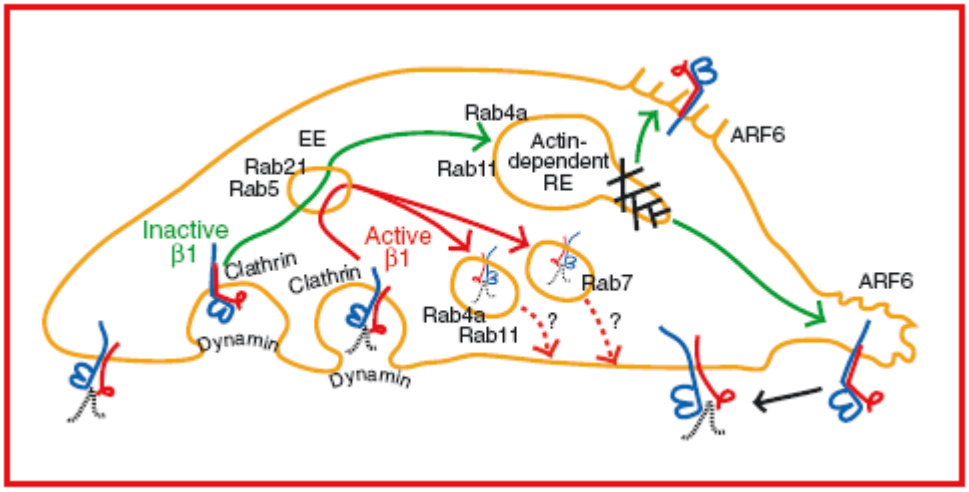

Figure 1.6 Model of trafficking routes of active and inactive β1-integrin. The trafficking routes of the two conformations of β1-integrin overlap in early endosomes, but show differences in the sequent steps. In fact, inactive β1-integrin is recycled through rapid F-actin and Rab4-dependent pathway to ARF6-positive protrusions on the plasma membrane, whereas the active β1-integrin recycling is less efficient, probably because the ligand, which is internalized together with the receptor, needs to be dissociated prior to receptor recycling. Moreover, only active β1-integrin is found in Rab7a-positive compartments (Arjonen *et al*., 2012).

1.4 Contraction and retraction

In order to translocate forward, several events must occur in a migrating cell. First of all, protrusive force is needed to extend lamellipodia and filopodia and it is mediated by actin polymerization. In addition, a contractile force is needed to move the cell body forward and it is dependent on the molecular motor protein myosin, by acting on the actin network. This induces contraction in the cell body and tension at adhesion sites, which are used as traction points for migration (Lauffenburger and Horwitz, 1996; Blanchoin *et al*., 2014). Then, adhesions at the rear are disassembled. Finally the trailing edge, devoid of integrin-cytoskeleton linkages and less supported by the cytoskeleton, retracts, avoiding that the tension rip the cell apart (Lauffenburger and Horwitz, 1996; Vicente-Manzanares *et al*., 2005).

1.5 Rac, Cdc42 and Rho are important regulators of cell migration

Several intracellular signalling molecules have been implicated in cell migration. In particular, Rac, Rho and Cdc42 GTPases are considered to be key regulator proteins of this process. It seems that they control some aspects of cell migration by integrating their action, but they also regulate specific events independently from each other. For instance, all three GTPases promote the assembly of integrin-based, cell-matrix adhesions and affect, even if in different ways, the microtubule cytoskeleton. Nevertheless, Rac and Cdc42 are required at the front of migrating cells where they regulate the polymerization of actin in the formation of lamellipodial and

filopodial protrusions, respectively, whereas Rho modulates the assembly of actomyosin filaments and controls cell body contraction and trailing edge retraction. In addition, Cdc42 is important for defining cell polarity (Raftopoulou and Hall, 2004).

1.6 Rab GTPases

Rab proteins (*Ras-related proteins in brain*) are small GTPases belonging to the Ras superfamily and regulate the trafficking among the different intracellular compartments (Schwartz *et al.*, 2007). Rab GTPases constitute the largest family of small GTPases with over 70 members in humans. Every Rab protein has a specific localization (Figure 1.7) (Bhuin and Roy, 2014).

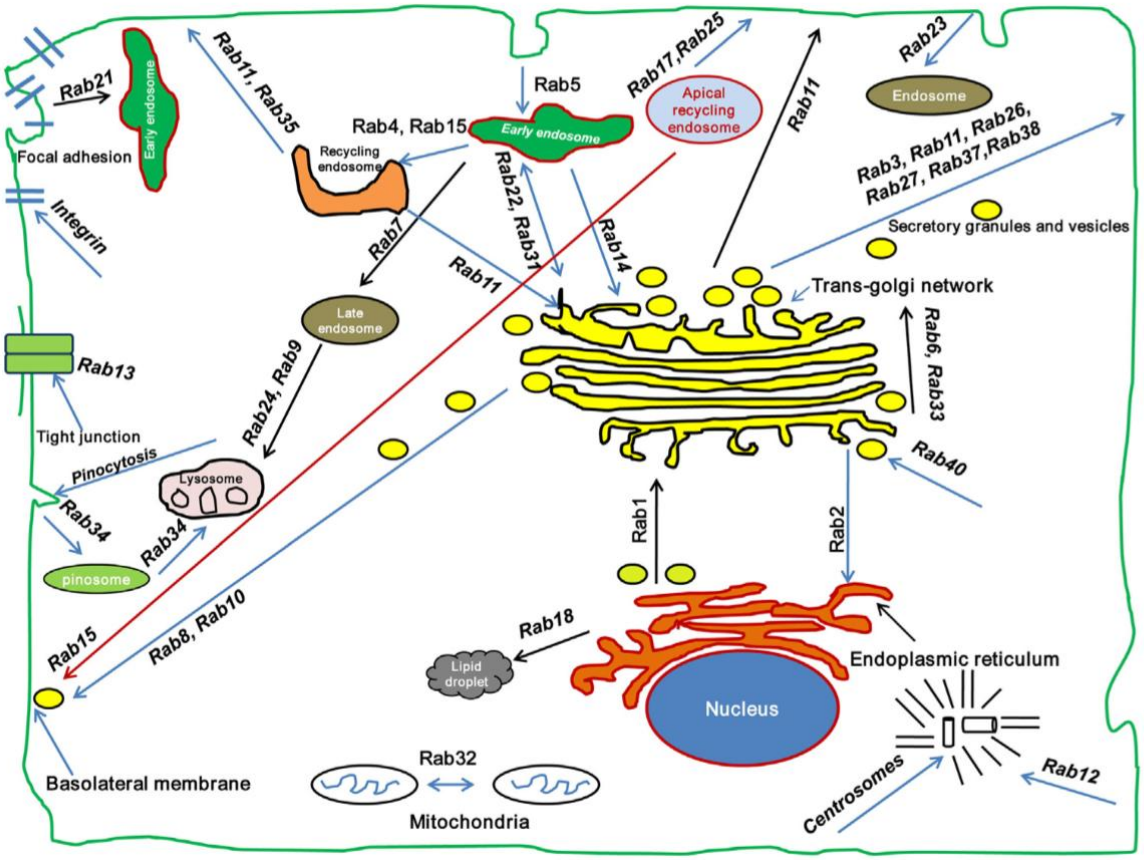

Figure 1.7 Rab GTPases subcellular localization. Rab GTPases control membrane trafficking at various steps and are localized to different compartments (Bhuin and Roy, 2014).

Rab GTPases work as molecular switches cycling between an active form, which binds GTP and is associated with membranes, and an inactive form, GDP-bound, which is citosolic. Active Rab proteins recruit specific effectors through which they regulate vesicle trafficking and fusion. Multiple regulatory proteins are available to modulate Rab proteins activity. Indeed, in the cytosol, prenylated Rabs can be found bound to a GDP-dissociation inhibitor (GDI) which recognizes inactive Rabs and covers up the prenyl groups. In order for a Rab to switch to the active GTP-bound state, the GDI has to be displaced, and this is done by the action of a GDI-

displacement factor (GDF). GDFs help Rabs attachment to specific membranes. Some proteins named Guanine nucleotide Exchange Factors (GEFs) catalyze the GDP/GTP exchange. Even though the Rabs have intrinsic hydrolytic activity towards GTP, the process of inactivation is catalyzed by GTPase activating proteins (GAPs), resulting in a renewed association with the GDI and in the recycling of the Rab GTPases back to the cytosol. Therefore, GEFs, GAPs and GDI play a critical role in the regulation of the activity of Rab proteins (Figure 1.8) (Bhuin and Roy, 2014).

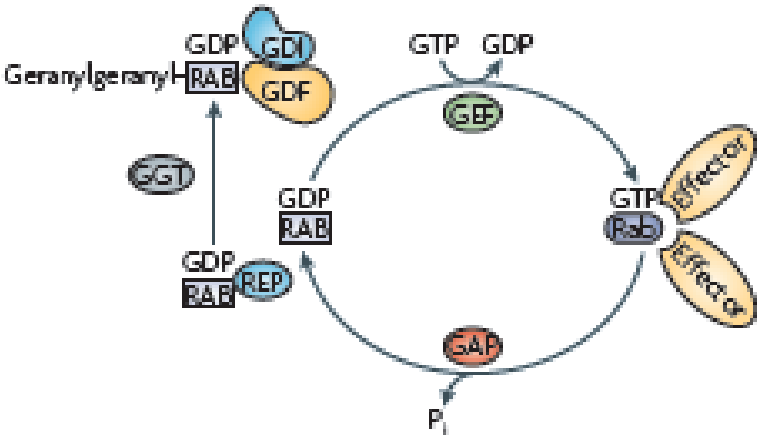

Figure 1.8 The Rab cycle. The newly synthesized Rab, in the GDP-bound form, associates with a Rab escort protein (REP). The REP presents the Rab to a Rab geranylgeranyl transferase (RabGGT), which geranylgeranylates the Rab. The Rab is then recognized by Rab GDP dissociation inhibitor (GDI), which regulates Rab membrane cycle. Targeting of the Rab-GDI complex to specific membranes is mediated by the interaction with a membrane-bound GDI displacement factor (GDF). Then, GDP-bound Rab is converted into the GTP-bound form through the exchange of GDP for GTP. This step is catalyzed by a guanine nucleotide exchange factor (GEF). The GTP-bound "active" Rab interacts with several Rab-specific effector proteins. Active Rab is converted back to the GDP-bound "inactive" form by interacting with a GTPase activating protein (GAP) which catalyzes the hydrolysis of GTP to GDP and the release of an inorganic phosphate (P_i). The Rab is then removed from the membrane by GDI (Stenmark, 2009).

Rab proteins are able to perform multiple roles ranging from transport, sorting, budding, tethering, fusion, motility and recruiting other effector proteins by cycling between the active GTP-bound state and the inactive GDP-bound state (Stenmark, 2009).

Recently, it has been demonstrated that some Rabs, such as Rab5, Rab7b, Rab11 and Rab25, have a role in cell migration (Borg *et al.*, 2014; Caswell *et al.*, 2007; Kessler *et al.*, 2012; Mendoza *et al.*, 2013). Rab5 activation promotes focal adhesion disassembly, migration and invasiveness in tumor cells, whereas Rab7b regulates actin remodeling and influences cell adhesion, polarization and migration (Mendoza *et al.*, 2013; Borg *et al.*, 2014). Rab25 interacts with β1-integrin and controls its localization by regulating integrin-recycling vesicles, while

Rab11 promotes cell migration by modulating basal long-distance transport from the rear end to the front of the migrating cell (Caswell *et al*., 2007; Kessler *et al*., 2012).

1.7 Rab7a

Rab7a is a small GTPase of the Rab family. It is ubiquitously expressed and localizes mainly to late endosomes. Rab7a regulates vesicular transport to late endosomes and lysosomes in the endocytic pathway, and biogenesis of lysosomes, phagolysosomes and autolysosomes (Bucci *et al.*, 2000; Harrison *et al.*, 2003; Wang *et al*., 2011; Hyttinen *et al*., 2013; Vanlandingham and Ceresa, 2009). Moreover, it is required for channel trafficking, growth factor-independent survival and apoptosis (Seebohm *et al.*, 2008; Romero Rosales *et al*., 2009; Edinger *et al*., 2003). In addition, Rab7a controls the endocytic trafficking of the complex EGF-EGFR, regulating its lysosomal degradation (Ceresa and Bahr, 2006). Further studies have proved that Rab7a controls also the retrograde axonal transport of neurotrophine receptors which are required for neurotrophine signalling, neuronal differentiation, plasticity and survival (Saxena *et al.*, 2005; Deinhardt *et al.*, 2006). Moreover, it has been recently demonstrated that Rab7a interacts and recruits protrudin, a protein which promotes protrusion and neurite outgrowth, on late endosomes compartments (Shirane and Nakayama, 2006; Raiborg, 2015). In addition, Rab7a-dependent lysosomal degradation disturbs the terminal translocation at the final phase of migration of immature neurons during the development of cerebral cortex *in vivo* (Kawauchi *et al*., 2010; Kawauchi, 2011).

Rab7a exerts its functions through the interaction with several effectors (Wang *et al.*, 2011). Some of Rab7a interactors suggest that the functions of this small GTPase are closely connected to cytoskeletal elements.

One of the Rab7a interactors is RILP (Rab-interacting lysosomal protein), an important downstream effector of Rab7a, which can be recruited to membrane from cytosol by Rab7a to regulate late endosome and lysosome traffic, phagosome and autophagosome maturation and signalling receptor degradation (Cantalupo *et al*., 2001; Jordens *et al*., 2001; Harrison *et al*., 2003; Progida *et al*., 2007). RILP is required also for the formation of multivesicular bodies (MVB) (Progida *et al*., 2007). RILP is a protein of 401 amino acids and contains two coiled-coil domains (aminoacids 140-180 and 245-280), whereas the truncated form of RILP (amino acids 207-401), named RILP-C33, retains the second half of the protein but lacks the N-terminal domain (Cantalupo et al, 2001). The first half of RILP is required for dynein/dynactin motor recruitment, whereas its C-terminal domain binds to activated Rab7a on late endosomes and lysosomes, therefore both RILP and RILP-C33 interact with the GTP bound form of Rab7a, but

only RILP binds to the dynein/dynactin complex (Jordens *et al.*, 2001). Overexpression of RILP induces late endosome/lysosome enlargement and clustering to the perinuclear region by regulating microtubule minus-end directed transport through the interaction with the dynactin/dynein complex. Instead, cells over-expressing RILP-C33 show dispersed lysosomes (Cantalupo *et al*., 2001; Jordens *et al.*, 2001). ORP1L (OSBP (oxysterol-binding protein) related protein) is another important interactor of Rab7a which modulates dynein motor recruitment by Rab7a-RILP-dynactin complex (Wang *et al*., 2011). Moreover, Rab7a interacts with FYCO1 (FYVE and coiled-coil domain containing 1), which controls plus-end directed transport of autophagosomes (Pankiv *et al.*, 2010). Therefore, Rab7a controls vesicles movement along microtubule tracks by interacting with different effectors.

A connection between Rab7a and actin filaments comes from the interaction between Rab7a and Rac1, which is a fundamental regulator of actin cytoskeleton (Sun *et al.*, 2005; Bosco *et al*., 2009). In fact, it has been demonstrated that Rab7a interacts and colocalizes with Rac1 at the fusion zone of the ruffled border in bone-resorbing osteoclasts where Rab7a is involved in the formation of late endosomal-like compartments localized in the plasma membrane. This interaction may mediate late endosomal transport between microtubules and microfilaments in order to regulate ruffled border formation in osteoclasts (Sun *et al*., 2005). A functional link of the Rac1-Rab7a association has been proved by Frasa and colleagues. In fact, they demonstrated that active Rac1 is responsible for the recruitment of its effector Armus which, in turn, deactivates Rab7a and that the integration of Rac1 and Rab7a activities regulates E-cadherin turnover and stability of cell-cell contacts (Frasa *et al*., 2010). Finally, coordination between Rab7a and Rac1 functions seems to be important in integrating autophagy with intracellular trafficking and signalling (Carroll *et al*., 2013).

Rab7a regulates also intermediate filament (IF) proteins. In fact, Rab7a directly interacts with vimentin (Cogli *et al*., 2013a). Vimentin is one of the most abundant type III IF protein and it is mainly expressed in mesenchymal cells. This IF protein contains an N-terminal head region, a central rod domain and a C-terminal tail (Figure 1.9). The rod domain is a highly conserved α-helical region that is composed by four helical segments (1A, 1B, 2A, 2B), divided by three non-helical linker regions (L1, L1-2, L2). Vimentin filaments assembly occurs through the association of two monomers forming a dimer, which in turn associates in an antiparallel manner with another dimer, creating a tetramer, which is the fundamental subunit of IFs. Multiple tetramers assemble to form an elongated filament. IFs undergo extensive reorganization upon phosphorylation. In fact, this post-translational modification controls vimentin assembly and disassembly (Figure 1.10) (Dave and Bayless, 2014).

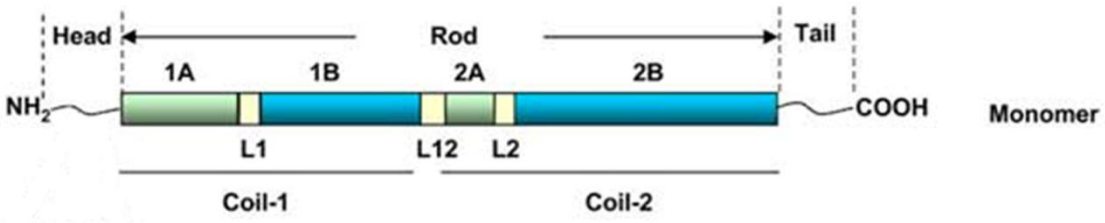

Figure 1.9 Structure of vimentin monomer. The structure of vimentin consists of an N-terminal "head" domain, a C-terminal "tail" domain, and a central rod domain. Three linkers referred to as L1, L12 and L2 divide the rod domain in coil1A, coil1B, coil2A and coil2B (adapted from Tang, 2008).

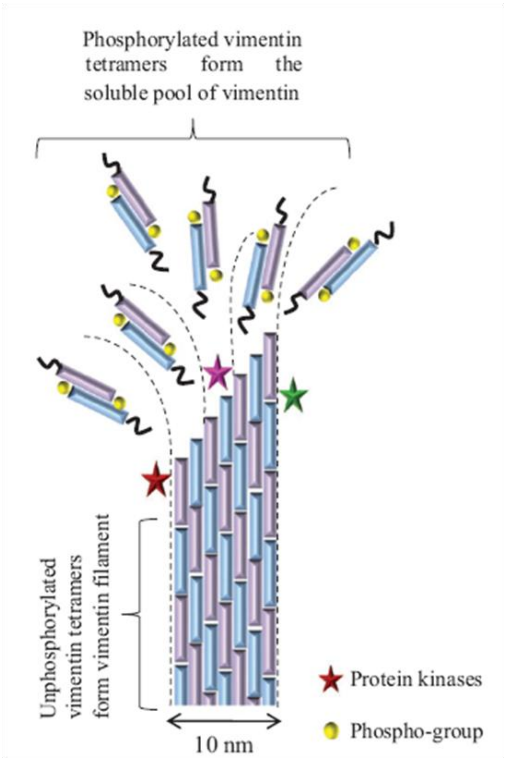

Figure 1.10 Phosphorylation-mediated disassembly of vimentin. Vimentin depolymerization is triggered by the action of several protein kinases (adapted from Dave and Bayless, 2014).

Several phosphorylation sites are located in the N-terminal head domain of vimentin and phosphorylation mediated by protein kinases on these sites determines disassembly of the IFs, as phosphorylation of the head region increases the distance between two head groups of a dimer, altering tetramer ability to assemble into a filament (Dave and Bayless, 2014). Rab7a regulates vimentin filament assembly. In fact, overexpression of Rab7a increases vimentin phosphorylation and causes redistribution of vimentin in the soluble fraction. Accordingly, Rab7a-depletion induces a decreased phosphorylation of vimentin head domain, thus increasing the amount of filamentous vimentin (Figure 1.11). Rab7a is able to interact with both soluble and filamentous vimentin (Cogli *et al.*, 2013a).

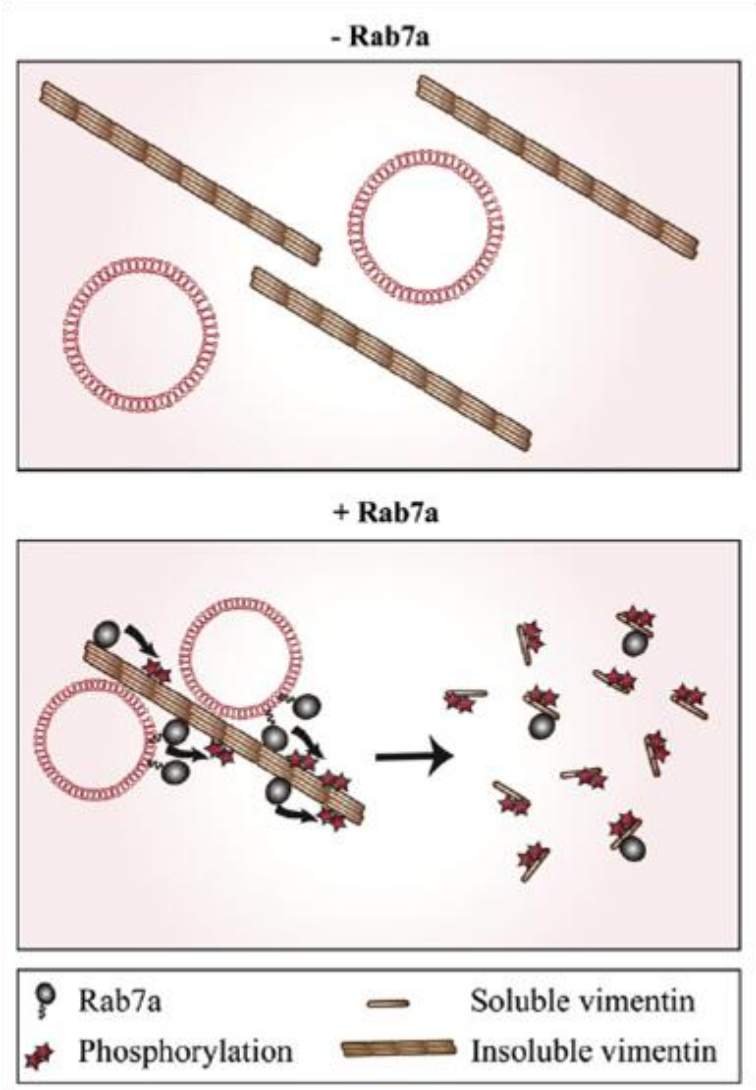

Figure 1.11 Rab7a regulates vimentin assembly/disassembly. Rab7a induces vimentin phosphorylation at the head domain causing vimentin disassembly (Cogli *et al*., 2013a).

In addition to mechanical stabilization of cells, vimentin functions include the regulation of cell adhesion, motility and signalling. Moreover, altered actin cytoskeleton and spatial organization of focal adhesion proteins were observed in fibroblasts lacking vimentin (Dave and Bayless, 2014).

Finally, Rab7a interacts and regulates the assembly of peripherin, another IF protein that shares the same structure and assembly of vimentin (Cogli *et al*., 2013b).

1.7.1 Rab7a and the Charcot-Marie-Tooth type 2B disease

Mutations in the RAB7A gene have been identified as causative of the Charcot-Marie-Tooth type 2B (CMT2B) disease. The CMT2B disease is an autosomal dominant axonal neuropathy which is clinically characterized by prominent sensory loss, marked distal weakness, normal or near-normal nerve conduction velocities and frequent foot ulcers due to deformities. The disease

onset is generally in the second or third decade of life (Bucci and De Luca, 2012). The CMT2B-associated Rab7a mutations target very conserved amino acid residues in the Rab7a protein. In particular five are the amino acidic substitutions responsible for the onset of the neuropathy: L129F, K157N, N161T, N161I, V162M (Meggouh *et al.*, 2006; Houlden *et al.*, 2004; Verhoeven *et al.*, 2003; Wang *et al.*, 2014). GTPases have a GTP-binding and hydrolysis site which is characterized by four conserved motifs that in the three-dimensional structure of the protein form a pocket able to accommodate the nucleotide and Mg^{2+}. *In silico* analysis of CMT2B-disease Rab7a mutated proteins predicted important conformational changes (Bucci and De Luca, 2012). CMT2B-associated Rab7a mutants have been biochemically and functionally characterized. It has been demonstrated that CMT2B mutants exhibited higher nucleotide exchange rates, hydrolyzed GTP slower than the wild-type protein and bound prevalently GTP (Spinosa *et al*., 2008; De Luca *et al*., 2008). Nevertheless, CMT2B-associated mutants were able to bind the Rab7a effector RILP and to rescue Rab7a function after silencing, suggesting that activated forms of Rab7a were responsible for the onset of the neuropathy (Spinosa *et al*., 2008; De Luca *et al*., 2008). Moreover, CMT2B-disease Rab7a mutants inhibited neurite outgrowth in PC12 cells and in Neuro2A cells as proved by the impaired up-regulation of growth-associated protein 43 (GAP43) and of the nuclear neuronal differentiation marker NeuN, respectively. This effect was similar to that induced by the constitutively active Rab7a mutant, confirming that active Rab7a mutants are responsible for CMT2B (Cogli *et al*., 2010). The inhibition of neurite outgrowth was probably due to the phosphorylation of nerve growth factore receptor TrkA by CMT2B-associated Rab7a mutants. In fact, the mutant proteins significantly enhanced the phosphorylation of TrkA in response to brief NGF stimulation, affecting Erk1/2 downstream signalling pathway (BasuRay *et al*., 2010). In addition, CMT2B-disease Rab7a mutants interacts stronger with peripherin and vimentin than the wild type protein and affect more the assembly of these IF than the wild type protein (Cogli *et al*., 2013a; Cogli *et al*., 2013b).

AIM OF THE PROJECT

Cell migration is an important event during the lifetime of all organisms and it is characterized by cell polarization, protrusion of the cell membrane, formation of new adhesions, contraction and retraction of the cell body. All these events are essential for migration and are coordinated by several proteins.

Rab7a, a small GTPase of the Rab family, localizes to late endosomes and lysosomes and regulates vesicular transport to these compartments. Among Rab7 effector proteins, there are Rac1, a key regulator of actin cytoskeleton and a fundamental player in cell migration, and vimentin, an intermediate filament protein, which is important in cell adhesion and motility. Another Rab7a interactor is RILP that regulates, together with Rab7a, late endosomal and lysosomal trafficking controlling Rab7-positive vesicle movement along microtubule tracks.

Given the link between Rab7a and RILP with cytoskeleton components and in particular with key proteins in cell migration, the aim of the project is to clarify the role of Rab7a and RILP in cell migration by studying several aspects of this process, such as motility, formation of protrusions, adhesion with components of the extracellular matrix, cell polarization and cytoskeleton rearrangements. For this purpose, we have used three different approaches: (i) modulating expression of Rab7a to study its role in the various steps of cell migration; (ii) expressing constitutively active, dominant negative and CMT2B-causing Rab7a mutant proteins to study the impact of these mutants on cell migration; (iii) modulating expression of RILP to establish its role in cell migration.

MATHERIAL AND METHODS

3.1 Cryopreservation of *E. coli* DH5α stocks

In a tube, 0,4 ml of a sterile 50% glycerol solution was added to 0,6 ml of a *E. coli* DH5α bacterial culture cultivated overnight (O/N) in LB medium to give a final concentration of 20% glycerol. The tube was put in liquid nitrogen before being stored at -80°C. To revive the bacteria, the surface of the culture was rapidly scraped using a sterile inoculation loop and streaked onto a LB agar plate which was incubated O/N at 37°C.

3.2 Competent *E. coli* cells preparation

E. coli competent cells have been made by using the Inoue method (Inoue *et al*., 1990). This protocol differs from other procedures in that the bacterial culture is grown at 18°C rather than the conventional 37°C and this leads to a higher efficiency of transformation. The lower temperature likely affects the composition or the physical characteristics of bacterial membranes synthesized at 18°C that are more favourable for uptake of DNA. The term "Transformation Efficiency" is defined as the number of colony-forming units (cfu) produced by 1 µg of plasmid DNA and it is used as a parameter to evaluate the quality of the competent *E. coli* cells preparation.

Protocol: *E. coli* DH5α cells from a glycerol stock solution were plated onto a LB agar plate and incubated O/N at 37°C. A single bacterial colony was then aseptically transferred to a 10 ml tube containing 5 ml of sterile LB medium and placed O/N in a shaking incubator (37°C, 250 rpm). 1 ml was then used to inoculate a 1 L shake flask containing 250 ml of SOB medium and placed O/N on a shaker at a temperature of 18°C to achieve an OD_{600} = 0,6. When the appropriate OD_{600} value was reached, the culture was put on ice for 10 minutes, and kept cold for the rest of the procedure. The culture was then centrifuged for 10 minutes (2500g, 4°C). The supernatant was discarded and the pellet resuspended in 80 ml of ice-cold TB solution. The resuspension was left on ice for 10 minutes before being centrifuged again as described above. The supernatant was discarded and the pellet gently resuspended in 20 ml of TB solution. 1,4 ml of 100% DMSO was then added to give a final concentration of 7% DMSO (which is important in protecting the cells upon freezing). The solution was left on the ice for 10 minutes. Aliquots of 500µl were made into microcentrifuge tubes and immediately put into liquid nitrogen until frozen. The tubes were then stored at -80°C for later use.

To establish the transformation efficiency of the competent cells, a control transformation reaction, using a known amount of circular plasmid DNA, was performed.

Reagents:

SOB medium	
Bacto Tryptone	20 g/L
Yeast Extract	5 g/L
NaCl	10 mM
KCl	2,5 mM
$MgCl_2$	10 mM
$MgSO_4$	10 mM

Adjust pH to 6.7-7.0 with NaOH

SOC medium	
SOB	
Glucose	20 mM

TB solution	
Pipes	10 mM
$MnCl_2$	55 mM
$CaCl_2$	15 mM
KCl	250 mM

Adjust pH to 6.7 with 5N KOH prior to adding the $MnCl_2$. The solution was filter-sterilised and stored at 4°C for immediate use.

3.3 Bacterial transformation

Transformation is a technique by which bacterial cells take up naked DNA more readily than by natural mechanisms. Transformation of bacteria with plasmids is important not only for studies in bacteria but also because bacteria are used as the means for replicating plasmids. Because of this, also plasmids designed for use in mammalian cells carry both a bacterial origin of replication and an antibiotic resistance gene to be used as a selectable marker in bacteria.

Protocol: Competent DH5α cells were thawed on ice. Cells were mixed gently by flicking the bottom of the tube with finger and 200µl of cells were aliquoted for each transformation into 1,5 ml tubes. Then 10-100 ng DNA (for preparation of DNA solution to be used in mammalian cells) or 5-10µl DNA (in case of ligation products) were added to bacterial cells. Tubes were incubated on ice for 30 minutes and each transformation was then subjected to heat shock by placing the tube into a 42°C water bath for 45 seconds and subsequently on ice for 2 minutes. 800µl of SOC were added to each tube which was then placed in 37°C shaker for 1 hour. This outgrowth step allowed the bacteria to generate the antibiotic resistance proteins encoded on the plasmid so that they will be able to grow once plated on the antibiotic-containing agar plate. Indeed, after 1 hour of incubation, 200µl of each transformation are plated on LB-agar containing ampicillin (75

μg/ml) or kanamycin (30 μg/ml), depending on the resistance that the plasmid conferred to bacteria. Plates were incubated inverted at 37°C O/N to let the transformed colony appear.

Reagents:

LB medium	
Bacto Tryptone	10 g/L
Yeast Extract	5 g/L
NaCl	10 g/L

Add distilled water to final volume.

LB-agar medium	
Bacto Tryptone	10 g/L
Yeast Extract	5 g/L
NaCl	10 g/L
Agar	15 g/L

Add distilled water to final volume.

3.4 Preparation of plasmidic DNA

A plasmidic preparation is a method used to extract and purify plasmidic DNA. Many methods have been developed to purify plasmidic DNA from bacteria. These methods invariably involve three steps: growth of bacteria transformed with the plasmid, harvesting and lysis of the bacteria, and purification of plasmid DNA. Kits are available from varying manufacturers to purify plasmidic DNA, which are named by size of bacterial culture and corresponding plasmid yield. In increasing order, there are the miniprep, midiprep, maxiprep, megaprep and gigaprep. We used the QIAGEN Plasmid Maxi Kit (for maxi-preparation of plasmidic DNA) and the Wizard Plus Midipreps DNA Purification System from Promega (for midi-preparation of plasmidic DNA) according to the manufacturer's instructions in order to obtain DNA solutions to be used in mammalian cells. Mini-preparation of DNA was performed according to the "Boiling prep" method as described below. This is a rapid method for small-scale isolation of plasmidic DNA from bacteria. Mini-preparations were used in the process of molecular cloning to analyze bacterial clones.

3.4.1 Mini-preparation of DNA

Protocol: after transformation of bacteria with plasmid, a single colony growth on the plate was touched gently with an inoculation loop and bacteria were transferred to a 10 ml tube containing 5 ml of sterile LB medium containing the appropriate antibiotic. The tube was then placed O/N in a shaking incubator (37°C, 250 rpm). 1,5 ml of culture was then centrifuged for 2 minutes (13000 rpm, 4°C) and the supernatant was discarded. 50μl of 25% sucrose (prepared in distilled

water) were added. The sample was then swirled for 30 seconds and 300µl of M-STET solution were added. The sample was swirled for 10 seconds and 25µl of 10 mg/ml lysozime (dissolved in TE buffer) was added. The tube was put at 100°C for 45 seconds and rapidly in ice. Then it was centrifuged for 15 minutes (13000 rpm, 4°C) and pellet was removed. 40µl of 3M sodium acetate (pH 5.2) and 270 µl of isopropanol were added to the supernatant, which was mixed for inversion. After 1 minute of incubation at room temperature the sample was centrifuged for 15 minutes (13000 rpm, room temperature) and the supernatant was removed. Pellet was washed with 250 µl of 70% cold ethanol and then air-dried. Pellet was finally resuspended in 40µl of 100µg/ml RNAsiA solution (dissolved in TE buffer).

Reagents:

STET solution	
Triton X-100	5%
EDTA (pH 8.0)	50 mM
Tris-HCl (pH 8.0)	50 mM
Sucrose	80 g/L

TE buffer	
Tris (pH 7.5)	10 mM
EDTA (pH 8.0)	1 mM

3.5 Molecular cloning

Molecular cloning is a set of experimental methods in molecular biology that are used to assemble recombinant DNA molecules and replicate them, using *in vivo* systems, for further processing. The essential steps of molecular cloning are the production of the nucleic acid fragment of interest, ligation (incorporating the fragment in an appropriate vector), transformation (incorporating the vector system/fragment of interest into an appropriate host), selection (obtaining hosts with the correct vector system/fragment of interest), amplification (manipulating the host to create multiple copies of the vector/fragment of interest), and isolation (isolate the vector/fragment of interest).

3.5.1 Primer design

All the plasmids generated in this study contain fragments that were PCR-amplified from either pcDNA3 2xHA-tagged Rab7a wt or pCMV6-ENTRY Myc-tagged vimentin wt plasmids. DNA

fragments were amplified using the primers (DNA oligonucleotides) indicated in Table 3.1 and designed according to the following criteria: primers length should be of 18-30 nucleotides, they should contain a sequence of 16-18 nucleotides complementary to the target region, the GC content should be between 40% and 60% with the 3' of the primer ending in C or G to promote binding, the melting temperature should be similar for pairs of primers and around 60°C-65°C, primers should be designed so that self-complementation and formation of secondary structures are avoided. All oligonucleotides contained restriction sites on the ends to allow easier downstream cloning. Restriction sites for AsiSI or EcoRV enzymes were included in forward primers used for vimentin and Rab7a amplifications, respectively. Restriction sites for MluI or NotI enzymes were included in reverse primers used for vimentin and Rab7a amplifications, respectively. Insertion of the vimentin and Rab7a fragments will occur at the same restriction sites situated on the acceptor plasmids.

DNA fragment	Primers (Forward/Reverse)	Template
Vimentin 1-256	5'-TCTGCCGCCGCGATCGCCATGTCCACCAGG-3'	pCMV6-ENTRY Myc-tagged vimentin wt
	5'-CGTACGCGTGATTTGGACATGCTGTTC-3'	
Vimentin 92-256	5'-ATAGCGATCGCCATGATCAACACCGAG-3'	pCMV6-ENTRY Myc-tagged vimentin wt
	5'-CGTACGCGTGATTTGGACATGCTGTTC-3'	
Vimentin 256-411	5'-ATAGCGATCGCCATGATCGATGTG-3'	pCMV6-ENTRY Myc-tagged vimentin wt
	5'-CGTACGCGTAATCCTGCTCTCCTC-3'	
Vimentin 256-466	5'-ATAGCGATCGCCATGATCGATGTG-3'	pCMV6-ENTRY Myc-tagged vimentin wt
	5'-CCGCGTACGCGTTTCAAGGTCATC-3'	
Vimentin 1-141	5'-TCTGCCGCCGCGATCGCCATGTCCACCAGG-3'	pCMV6-ENTRY Myc-tagged vimentin wt
	5'-CTGATTACGCGTTTGGCCCTTGAGCTGCTC-3'	
Rab7a 11-207	5'-CCACGGGATATCCATGGTTATCATCCTGGGAGATTCTGGAG-3'	pcDNA3 2xHA-tagged Rab7a wt
	5'-ATAAGAATGCGGCCGCTCACTGCCCCTTCAGCAACTGC-3'	
Rab7a 1-176	5'-CGGGATATCCATGACCTCTAGGAAGAAAG-3'	pcDNA3 2xHA-tagged Rab7a wt
	5'-ATAAGAATGCGGCCGCTCACTGTTTAAGTGCATTCCT-3'	

Table 3.1 List of primers used to amplify DNA fragments. DNA fragments produced, the pairs of primers and the plasmids (templates) used in the PCR reactions are shown.

3.5.2 Polymerase Chain Reaction (PCR)

DNA fragments were PCR-amplified from plasmidic DNA as indicated in Table 3.1 by using *Taq* polymerase. This DNA polymerase assembled a new DNA strand from nucleotides by using single-stranded DNA as a template and primers which are required for initiation of DNA synthesis. Cycles of repeated heating and cooling of the reaction for DNA melting and enzymatic replication of the DNA generated new DNA. As PCR progressed, the new DNA was itself used as a template for replication so that DNA was exponentially amplified.

The mixture was prepared as follows:

Reaction buffer	1X
DMSO	0-5%
Forward primer	2 pM
Reverse primer	2 pM
dNTPs	200 µM
Template DNA	40 µg
Taq DNA polymerase	0,05U/µl
H_2O	up to 25 µl

DMSO was added as additive for the amplification of vimentin fragments in order to aid in the denaturing of the GC-rich template.

The following PCR profile was used:

First denaturation step	94 °C	7 minutes	
Denaturation step	94 °C	1 minute	30 cycles
Annealing step	50 °C	30 seconds	
Elongation step	72 °C	45 seconds	
Final elongation step	72 °C	7 minutes	
End	4 °C	∞	

3.5.3 Purification of PCR products

Qiaquick PCR purification kit (Qiagen) and GenElute Gel Extraction kit (Sigma) were used according to the manufacturer's instructions for PCR product purification and to extract DNA fragments from agarose gels in order to remove primers, salts, agarose, ethidium bromide and other impurities. The PCR purification kit was preferred when no aspecific PCR products were

generated during the amplification reaction, otherwise samples were loaded on agarose gel and Gel Extraction kit was used by gel-extracting bands of the expected size.

3.5.4 Digestion of amplified products and acceptor plasmids

In order to clone the DNA fragments in the proper plasmids, compatible ends on both fragments and plasmids (pcDNA3 2xHA-tagged Rab7a wt; pCMV6-ENTRY Myc-tagged vimentin wt) were created by digesting them with appropriate restriction endonucleases.

Protocol: 1 g of DNA was digested with 3 U of each enzyme (AsiSi and MluI for cloning of vimentin mutants, whereas EcoRV and NotI for cloning of Rab7a deleted mutants) in the buffer suggested by the manufacturer for 2 hours at 37°C. The reaction volume was 10 times the volume of enzymes used to dilute the glycerol of the enzyme storage buffer. Therefore, Rab7a wt and vimentin wt fragments were removed from pcDNA3 2xHA-tagged Rab7a wt and pCMV6-ENTRY Myc-tagged vimentin wt, respectively. At the end of the digestion step, enzymes activity was heat-inactivated.

3.5.5 Gel extraction and purification

GenElute Gel Extraction kit (Sigma) was used according to the manufacturer's instructions for digestion products purification by extracting DNA fragments of the expected size from the agarose gel were they were loaded and removing salts, agarose, ethidium bromide and other impurities.

3.5.6 Agarose gel electrophoresis of DNA

Conventional agarose gel electrophoresis was used to analyze DNA fragments. The electrophoretic mobility of DNA fragments mainly depends on the fragment size and to a lesser extent on the conformation of the DNA, type and concentration of agarose used as well as applied voltage and electrophoresis buffer used.

Protocol: gels containing 1% (w/v) of agarose in TAE buffer were used for the separation of DNA fragments. Ethidium bromide, an intercalating agent, was added to gels to the final concentration of 0,5 μg/ml for later visualization of the DNA bands. Before the loading, DNA samples were mixed with 1/6 volume of 6x loading buffer. 1 Kb DNA Ladder (Cat. 15615-024, Invitrogen) was used as a molecular weight standard. The electrophoresis was performed in TAE buffer. Finally, ethidium bromide-DNA complexes were visualized under UV transilluminator due to their bright red-orange fluorescence.

Reagents:

Loading buffer	
Bromophenol blue	0,5%
Xylene cyanol	0,5%
Glycerol	30%

Ladder	
1 Kb DNA Ladder (1 µg/µl)	100 µl
Loading buffer	150 µl
TE buffer	643,5 µl
5M NaCl	6,5 µl

TAE	
Tris	2 M
Acetic acid glacial	5,71%
0,5M EDTA (pH 8.0)	50 mM

3.5.7 Ligation

For cloning of DNA inserts into plasmids, a ligation reaction was set up for each vimentin and Rab7a mutant. Suitable controls without inserts, to check the amount of undigested or single-site digested plasmid, were included.

Protocol: amount of the used acceptor plasmid DNA varied from 25 to 50 ng. For the ligation reaction, plasmid and insert DNA were generally taken in the molar ratio 1:10. The amount of insert to use, having a certain amount of vector, is given by the formula:

$$ng_{insert} = \frac{ng_{plasmid} \cdot Kb_{insert}}{Kb_{plasmid}} \cdot molar\ ratio \frac{insert}{plasmid}$$

The ligation reaction was performed in a 20 µl final volume comprising plasmid and insert DNA, ligation buffer and T4 DNA Ligase (1U, Invitrogen). Ligation was carried out O/N at 16°C. The ligation reaction was then used for bacterial transformation.

3.5.8 Amplification of the new plasmids

Competent bacterial cells were transformed with the products of ligation in order to amplify the new plasmids generated. Several bacterial colonies from each sample were then singularly transferred to different 10 ml tubes containing 5 ml of sterile LB medium each and placed O/N in a shaking incubator (37°C, 250 rpm). Both LB-agar and LB medium contained the appropriate antibiotics to select the transformed bacteria. These cell cultures were used for mini-preparation of plasmidic DNA, which were then screened by digestion and analyzed by agarose gel

electrophoresis to identify positive bacterial colonies with the plasmids of interest containing the desired inserts. Plasmids that corresponded to the expected size after digestion with the enzymes used for cloning the insert inside the plasmid were sequenced to ensure an absence of PCR-introduced mutations. Finally, maxi-preparation or midi-preparations of plasmidic DNA was performed.

3.6 Site-directed mutagenesis

In vitro site-directed mutagenesis is an invaluable technique for creating plasmid modifications and studying protein structure-function relationships. This technique was used to make point mutations in a DNA sequence and switch amino acids in the relative protein. Pfu DNA Polymerase, synthetic oligonucleotide primers containing the desired mutation and a temperature cycler were used.

3.6.1 Primer design

The plasmid used as a template for site-directed mutagenesis was pcDNA3 2xHA-tagged Rab7a wt. In order to create pcDNA3 2xHA-tagged plasmids containing a set of nucleotides coding for mutated Rab7a proteins, pairs of complementary oligonucleotides containing the desired mutation, flanked by unmodified nucleotide sequence, were designed (Table 3.2).

Rab7a mutants to generate	Primers (Forward/Reverse)
Rab7a N30A	5'-CACTCATGAACCAGTATGTGGCCAAGAAATTCAGTAATCAG-3'
	5'-CTGATTACTGAATTTCTTGGCCACATACTGGTTCATGAGTG-3'
Rab7a S34I	5'-GTGAACAAGAAATTCATTAATCAGTACAAAGC-3’
	5’-GCTTTGTACTGATTAATGAATTTCTTGTTCAC-3’
Rab7a S111G	5’-CTCATCCAGGCCAGGCCCCGGGATCC-3’
	5’-GGATCCCGGGGCCTGGCCTGGATGAG-3’
Rab7a N117A	5’-GCCAGTCCCCGGGATCCTGAAGCCTTCCCTTTCGTTGTGTTGGG-3’
	5’-CCCAACACAACGAAAGGGAAGGCTTCAGGATCCCGGGGACTGGC-3’
Rab7a K175E	5’-GCAAGGAATGCACTTGAACAGGAAACAGAGG-3’
	5’-CCTCTGTTTCCTGTTCAAGTGCATTCCTTGC-3’

Table 3.2 List of primers used to generate plasmids coding for Rab7a mutated proteins. Rab7a mutants and primers used to generate them in the site-directed mutagenesis experiments are listed. Codons that contains point mutations (underlined) and that code for different amino acids are highlighted in yellow.

3.6.2 PCR reaction

The procedure utilized a supercoiled double-stranded DNA plasmid with an insert of interest (pcDNA3 2xHA-tagged Rab7a wt) and two synthetic oligonucleotide primers containing the desired mutation. The oligonucleotide primers, each complementary to opposite strands of the plasmid, were extended during temperature cycling by using Pfu DNA polymerase, which replicated both plasmid strands with high fidelity. Incorporation of the oligonucleotide primers generated a mutated plasmid containing staggered nicks.

The mixture was prepared as follows:

Reaction buffer	1X
Primer #1	2,5 ng/µl
Primer #2	2,5 ng/µl
dNTPs	50 µM
Template DNA	0,2 ng/µl
Pfu DNA polymerase	0,05U/µl
H_2O	up to 50 µl

The following PCR profile was used:

First denaturation step	95 °C	1 minute	
Denaturation step	95 °C	50 seconds	18 cycles
Annealing step	60 °C	50 seconds	
Elongation step	68 °C	1 minute/Kb of plasmid length	
Final elongation step	68 °C	7 minutes	
End	4 °C	∞	

3.6.3 DpnI digestion

Following temperature cycling, the PCR product was treated with DpnI endonuclease, which is specific for methylated and hemimethylated DNA. It was used to digest the parental DNA template, which had the nucleotides sequence coding for the wild type protein, and to select for mutation-containing synthesized DNA. In fact, the plasmid used as a template was dam methylated given that it was isolated by *E. coli* DH5α strain as indicated in paragraph 3.3.

Protocol: 10 U of DpnI endonuclease were added to each sample. Subsequently, incubation for 1hour at 37°C was conducted.

3.6.4 Amplification of the plasmids

Competent bacterial cells were transformed with the new nicked plasmids generated in order to amplify them. Several bacterial colonies from each sample were then singularly transferred to different 10 ml tubes containing 5 ml of sterile LB medium each and placed O/N in a shaking incubator (37°C, 250 rpm). Both LB-agar and LB medium contained the appropriate antibiotic to select the transformed bacteria. These cell cultures were used for mini-preparations of plasmidic DNA, which were then screened by digestion and analyzed by agarose gel electrophoresis to verify the presence of the plasmids of interest. Plasmids that corresponded to the expected size after digestion with appropriate enzymes were sequenced to ensure the presence of the desired mutation and the absence of random mutations. Finally, maxi-preparation or midi-preparation of plasmidic DNA was performed.

3.7 Cell culture

Cell culture is the process by which cells are grown outside of their natural environment, in an incubator, under controlled conditions, such as medium, temperature, humidity and gas mixture.
NCI H1299 and HeLa cells were maintained at 37°C in 5% CO_2 atmosphere in Dulbecco's Modified Eagle's Medium (DMEM, Sigma) supplemented with 10% fetal bovine serum (FBS, Gibco), 2 mM L-glutamine (Sigma), 100 U/ml penicillin (Sigma) and 10 mg/ml streptomycin (Sigma). NCI H1299 and HeLa cells are human epithelial cancerous cells of the lung and the cervix, respectively. Both of them are able to grow in adhesion to a substrate. When cells are confluent, they need to be subcultured to dilute and avoid to interrupt their growth.
Protocol: proper sterile technique, sterile solutions and equipment, and a laminar flow hood were used. Spent cell culture medium was removed and discarded. Cells were washed using PBS (Phosphate Buffer Saline), a balanced salt solution without calcium and magnesium, in order to remove any traces of serum, calcium, and magnesium that would inhibit the action of the following dissociation reagent. Wash solution was then gently removed. A sufficient amount to cover the cell layer of trypsin solution was used as dissociation reagent. Cells were then incubated in the incubator for few minutes, then observed under the microscope to verify the detachment of the cells from the substrate. Therefore, new complete growth medium was dispersed by pipetting over the cell layer surface several times. Cell suspension was diluted to the desired seeded density and plated into a new cell culture vessel, labelled with the passage

number, date and cell type. Cells were then returned to incubator. Cells were subcultered for a maximum of 20 passages. Then, a new vial of cells was thawed.

Reagents:

DMEM medium supplemented with:	
FBS	10%
L-glutamine	2 mM
Penicillin	100 U/ml
Streptomycin	10 µg/ml

Tryspsin solution	
Trypsin	0,05%
EDTA	0,02%

PBS (pH 7,4)	
NaCl	8 g/L
KCl	0,2 g/L
Na_2HPO_4	1,44 g/L
KH_2PO_4	0,24 g/L

3.8 Mammalian cell transfection

Transfection is a procedure that introduces foreign nucleic acids (DNA and RNA) into cells to produce genetically modified cells. This technique is a powerful analytical tool for studying genes and proteins functions. The introduced genetic materials can exist in cells either stably or transiently depending on their nature. The ideal method of transfection should have high efficiency, low cell toxicity, minimal effects on normal physiology, be reproducible and easy to use. Several transfection methods are available (Kim and Eberwine, 2010).

3.8.1 Transfection of DNA plasmids

Transfection was performed using DNA plasmids isolated as described in paragraph 3.3 and Metafectene Pro (Biontex) or Lipofectamine 2000 (Invitrogen) as reagents. Cells were then analyzed after 24 hours from transfection.

Protocol (Metafectene Pro): Cells to be transfected were well proliferating and their confluence was around 70-80%. Transfection solutions were prepared as follows:

		Culture plate diameter (mm)			
		16	**35**	**60**	**100**
Solution A	**Suspension volume (ml)**	50	100	100	700
	DNA amount (µg)	0,5	4	6	14
Solution B	**Suspension volume (ml)**	50	100	100	700
	Metafectene Pro amount (µl)	2	8	13	32

Serum- and antibiotic-free medium was used. Solution A was suddenly mixed with solution B and the combined solution was incubated at room temperature for 20 minutes. After incubation time, DNA-lipid complexes were added in a dropwise manner to the cells previously incubated with serum- and antibiotic-free medium. After three hours, medium was removed and discarded. Complete medium was added to cells. After 24 hours cells were subjected to further analyses.

Protocol (Lipofectamine 2000): Cells to be transfected were well proliferating and their confluence was around 70-80%. Transfection solutions were prepared as follows:

		Culture plate diameter (mm)	
		16 (24-well plate)	**35 (6-well plate)**
Solution A	**Suspension volume (ml)**	50	200
	DNA amount (µg)	0,5	2
Solution B	**Suspension volume (ml)**	50	200
	Lipofectamine 2000 amount (µl)	0,7	2,8

Optimem medium was used. Solutions were incubated at room temperature for 10 minutes. Then, solution A was mixed with solution B and the combined solution was incubated at room temperature for 20 minutes. After incubation time, the final solution was added to the cells previously incubated with antibiotic-free medium. After four hours, medium was removed and discarded. Complete medium was added to cells. After 24 hours cells were subjected to further analyses.

3.8.2 RNA interference

Transfection of cells with siRNA was performed using Lipofectamine RNAiMAX (Invitrogen) or Metafectene SI (Biontex). siRNAs were purchased from MWG-Biotech and are reported in Table 3.3.

Target	siRNAs (Sense/Antisense)
Control RNA	5'-ACUUCGAGCGUGCAUGGCUTT-3'
	5'-AGCCAUGCACGCUCGAAGUTT-3'
Rab7a siRNA	5'-GGAUGACCUCUAGGAAGAATT-3'
	5'-UUCUUCCUAGAGGUCAUCCTT-3'
Vimentin siRNA	5'-ACACCGAGUUCAAGAACACTT-3'
	5'-GUGUUCUUGAACUCGGUGUTT-3'
RILP siRNA	5'-GAUCAAGGCCAAGAUGUUATT-3'
	5'-UAACAUCUUGGCCUUGAUCTT-3'

Table 3.3 List of siRNAs. Control RNA, and Rab7a, vimentin and RILP siRNAs used in the experiments are indicated.

Protocol (RNAiMAX): The day before transfection, 10^5 were seeded in 3,5 cm diameter dishes and incubated with antibiotic-free medium. The day of transfection, solutions were prepared as follows:

		Culture plate diameter (mm)	
		16 (24-well plate)	**35 (6-well plate)**
Solution A	**Suspension volume (ml)**	50	200
	siRNA final concentration (nM)	12	60
Solution B	**Suspension volume (ml)**	50	200
	Lipofectamine RNAiMAX amount (µl)	0,8	4

Serum- and antibiotic-free medium was used. Solution A was suddenly mixed with solution B and the final solution was incubated at room temperature for 20 minutes. After incubation time, final solutions were added in a dropwise manner to the cells. After five hours, medium was removed and discarded. Complete medium was added to cells. After 24 hours cells were subjected to further analyses.

Protocol (Metafectene SI): 10x SI buffer was diluted to 1x SI buffer with sterile water (suitable for cell culture). Then, a cell suspension with complete cell culture medium with a concentration of 0,8 * 10^5 cells was prepared. Transfection solutions were prepared as follows:

	Culture plate diameter (mm)	
	60	**100**
1x SI buffer (µl)	180	360
Metafectene SI (µl)	12	24
siRNA (pmol)	180	360

Solutions were incubated at room temperature for 20 minutes. After incubation time, solution was added in a dropwise manner to the well. A proper volume of the cell suspension (2 ml in 60mm diameter dishes and 6 ml in 100mm diameter dishes) was added to the plate containing the transfection solution. Cells were subjected to further analyses after 48-72 hours from transfection.

3.9 Cell lysis

To prepare proteic samples for further analyses, cells need to be lysed to release proteins of interest.

Protocol: all the steps were conducted on ice. Culture medium was removed from the cell culture plate and cells were rinsed with pre-chilled PBS buffer. PBS was then removed and lysis buffer, supplemented with protease inhibitor, was added to cells. Cells were detached with a rubber policeman and transferred into a 1,5 ml microcentrifuge tube. Then, they were incubated for 10 minutes on ice and centrifuged for 10 minutes (12000 rpm, 4°C). The supernatant was transferred in a new microcentrifuge tube and stored at -20°C.

Reagents:

Lysis buffer	
NaCl	150 mM
NP-40	1%
Sodium deoxycholate	0,5%
SDS (sodium dodecyl sulfate)	0,1%
Tris HCl (pH 8.0)	50 mM
Complete™ protease inhibitor cocktail tablets (Roche)	1x

Lysis buffer (for co-immunoprecipitation assay)	
NaCl	100 mM
NP-40	0,5%
Tris HCl (pH 7.5)	25 mM
Complete™ protease inhibitor cocktail tablets (Roche)	1x

3.10 SDS-PAGE

Protein samples were separated on mini SDS-PAGE (Sodium Dodecyl Sulphate-PolyAcrylamide Gel Electrophoresis) gels. In this system, proteins denatured in the presence of SDS and DTT as reducing agent acquired a rod-like shape and a uniform charge-to-mass ratio proportional to their molecular weights. Gels were made of 5% stacking gel and 8%, 10% or 12% separating gel, depending on the proteins of interest.

Protocol: the protein samples were prepared in a 1:1 ratio with 2x Laemmli buffer (without DTT in the case of non-reducing conditions), boiled for 5 minutes and centrifuged briefly before loading onto the gel. The run was performed in running buffer at 100 V for about 2 hours.

Reagents:

2x Laemmli buffer	
Tris HCl (pH 6,8)	100 mM
SDS	4%
Bromophenol blue	0,2%
Glycerol	20%
DTT (add just before use)	200 mM

1 M DTT	
DTT	150 g/L
0,01 M sodium acetate (pH 5,2)	Up to final volume

	Separating gel (10 ml)		
Solution components (ml)	8%	10%	12%
H_2O	4,6	4,0	3,3
30% acrylamide mix	2,7	3,3	4,0
1,5 M Tris (pH 8,8)	2,5	2,5	2,5
10% SDS	0,1	0,1	0,1
APS (ammonium persulfate)	0,1	0,1	0,1
TEMED (N,N,N',N'- tetramethyletylenediamine)	0,006	0,004	0,004

Solution components (ml)	5% Stacking gel (5 ml)
H_2O	3,4
30% acrylamide mix	0,83
1,0 M Tris (pH 6,8)	0,63
10% SDS	0,05
APS	0,05
TEMED	0,005

Running buffer	
Tris	3 g/L
Glycine	14,4 g/L
SDS	0,05%
H_2O	Up to final volume

3.11 Western blotting

Western blotting is used in order to detect specific proteins from a complex mixture of proteins extracted from cells.

Protocol: proteins were separated by SDS-PAGE and subsequently electrophoretically transferred from the gel onto polyvinylidene fluoride (PVDF) membrane (Millipore) using a transfer buffer. The transfer took place at 400mA for 1 hour or 80mA O/N. Incubation with primary antibody was performed for 2 hours at room temperature in 2% milk in PBS. The primary antibodies that were used in the experiments and their concentration are listed in Table 3.4. After incubation, the membrane was washed with PBS/0,1% Tween-20 for three times, 5 minutes each. Subsequently the membrane was incubated for 1 hour at room temperature with the HRP-conjugated secondary antibody at a 1:5000 dilution in 2% milk in PBS. A list of the secondary antibodies that were used is represented in Table 3.5. The membrane was again washed as described above. Antibodies bound to the target protein were detected by using western blot Luminol Reagent (Santa Cruz) or WesternBright ECL kit (Advansta). The signal was captured on a film (Kodak).

Antibody	Dilution
Mouse monoclonal anti-Rac1, ARC03 (Cytoskeleton)	1:500
Mouse monoclonal anti-β1-integrin, sc18887 (Santa Cruz)	1:100
Mouse monoclonal anti-active β1-integrin, sc59827 (Santa Cruz)	1:3000
Goat polyclonal anti-EEA1, sc6415 (Santa Cruz)	1:100
Mouse monoclonal anti-Rab7a, sc376362 (Santa Cruz)	1:500
Mouse monoclonal anti-vimentin, sc6260 (Santa Cruz)	1:1000
Mouse monoclonal anti-HA, sc7392 (Santa Cruz)	1:500
Mouse monoclonal anti-myc, sc40 (Santa Cruz)	1:500
Rabbit polyclonal anti-myosin X, 22430002 (Novus biologicals)	1:100
Mouse monoclonal anti-tubulin, T5168 (Sigma-Aldrich)	1:10000
Mouse monoclonal anti-vinculin, V9131 (Sigma-Aldrich)	1:15000
Rabbit polyclonal anti-RILP (Cantalupo *et al*., 2001)	1:100

Table 3.4 List of primary antibodies and their working dilution.

Antibody	Dilution
Goat anti-rabbit-HRP (Invitrogen)	1:5000
Goat anti-mouse-HRP (Invitrogen)	1:5000
Donkey anti-goat-HRP (Invitrogen)	1:2000

Table 3.5 List of secondary antibodies. Information about secondary antibodies used for western blotting experiments.

Reagents:

Transfer buffer	
Tris	3 g/L
Glycine	14,4 g/L
Methanol	20%
H_2O	Up to final volume

3.12 Co-immunoprecipitation assay

Co-immunoprecipitation (Co-IP) is an important technique to identify physiologically relevant protein-protein interactions by using target protein-specific antibodies to indirectly capture proteins that are bound to this specific target protein. Ezview™ Red Anti-HA Affinity Gel (Sigma-Aldrich) was used in co-IP experiments. The affinity resin contains anti-HA monoclonal antibody covalently attached to crosslinked agarose beaded particles.

Protocol: All the centrifugation steps were performed at 10000 rpm (4°C). The affinity resin was carefully mixed and 10 µl of it were added into a clean 1,5 ml microcentrifuge tube on ice. Beads were equilibrated in Buffer A by adding 250 µl of buffer A to the tube, vortexing for 15 seconds and centrifuging. The supernatant was removed and beads were equilibrated a second time. Lysate was added to the resin, mixed by inversion and then incubated with gentle mixing for 1 hour at 2-8 °C to allow HA-tagged proteins to bind to the anti-HA Affinity Gel. After incubation, the sample was centrifuged and the supernatant was removed. The immunoprecipitate was washed three times with Buffer A. For each time 250 µl of Buffer A was added, the sample was mixed by inversion and incubated for 5' gentle mixing at 2-8 °C. Then, it was centrifuged and supernatant was removed. A last wash with ice-cold Buffer B was performed before precipitate was boiled in Laemmli buffer and subjected to SDS-PAGE.

Reagents:

Buffer A	
NaCl	150 mM
NP-40	0,1%
Tris HCl (pH 7.5)	25 mM
Complete™ protease inhibitor cocktail tablets (Roche)	1x

Buffer B	
Tris HCl (pH 7.5)	10 mM
Complete™ protease inhibitor cocktail tablets (Roche)	1x

3.13 Immunofluorescence

Immunofluorescence utilizes fluorescent-labeled antibodies to detect specific cellular target antigens. Different protocols were used depending on the proteic target to be visualized.

Protocol: after washing with PBS cells were either permeabilized for 2 minutes in Pipes buffer containing 0,25% saponin and subsequently fixed for 20 minutes with 3% PFA or first fixed and then permeabilized with 0,1-0,25% saponin/PBS (for 10 minutes) or 0,2% Triton X-100/PBS

(for 15 minutes). Subsequently, cells were washed with PBS and incubated with 50mM NH_4Cl/PBS for 10 minutes. Cells were then washed with PBS. The primary antibody solution (Table 3.6) was added to the cells. After 40 minutes of incubation at room temperature, cells were washed three times with PBS for 5 minutes each time. Cells were then incubated with the secondary antibodies for 20 minutes. After 1 washing with PBS, cells were stained for 5 minutes with either DAPI or Hoechst DNA dye. Samples were washed twice with PBS. Then cells were, either directly or after mounting with mowiol, observed at the appropriate microscope.

Antibody	Dilution
Rat monoclonal anti-inactive β1-integrin, 552828 (BD Biosciences)	1:1000
Mouse monoclonal anti-active β1-integrin, sc59827 (Santa Cruz)	1:50
Goat polyclonal anti-EEA1, sc6415 (Santa Cruz)	1:50
Mouse monoclonal anti-vimentin, sc6260 (Santa Cruz)	1:100
Rabbit polyclonal anti-HA, ab9110 (Abcam)	1:500
Rabbit polyclonal anti-giantin, ab24586 (Abcam)	1:1000
Rat monoclonal anti-tubulin, ab6161 (Abcam)	1:100

Table 3.6 List of primary antibodies and their working dilutions.

Secondary antibodies conjugated to fluorochromes (1:200) were from Invitrogen.

Reagents:

Pipes solution (pH 6.8)	
Pipes	80 mM
EGTA	5 mM
$MgCl_2$	1 mM
H_2O	Up to final volume

3.14 Wound-healing assay

The wound-healing assay permits to study cell migration by making a wound on a confluent monolayer of cells.

Protocol: after 24 hours from transfection, NCI H1299 cells were confluent and were subjected to wound-healing assay. In particular, confluent monolayers of cells were scratched by a pipette tip, medium was removed and cells were washed twice to eliminate detached cells. Fresh medium was added to the cells. Samples were used for several analyses or procedures.

Cell motility analyses: Imaging medium (DMEM without phenol red) was added to cells. Cells were imaged for a period of 9 hours with a 20X objective on an Olympus Fluoview 1000 IX-81 inverted confocal laser scanning microscope. During the observation cells were maintained at 37°C under 5% CO_2. Images were acquired every 30 minutes. Cells were then lysed to verify the transfection. Images were used to make movies and cell nuclei were tracked along the slices by using the Manual Tracking plugin of ImageJ software (National Institutes of Health). The data collected were analyzed by using the Chemotaxis and Migration Tool software (Ibidi) in order to calculate several migratory parameters, such as cell velocity, directness, accumulated and euclidean distances.

TIRF analyses of integrins: wound-healing assay was performed on cells previously seeded on MatTek glass-bottomed dishes. Cells were fixed for 20 minutes with 3% PFA and then permeabilized with 0,2% Triton X-100/PBS. Cells were then incubated with anti-β1-integrin antibodies and Rhodamine-conjugated phalloidin. Samples were observed with a Leica DMI600B system with a 63x objective (NA 1.47). The TIRF evanescent field depth was set to 110nm for all the excitation wavelengths.

Golgi apparatus orientation assay: wound-healing assay was performed on cells previously seeded on round coverslips. Cells were incubated for 3 hours after the start of the wound-healing assay at 37°C under 5% CO_2. Then, cells were fixed with 3% PFA, permeabilized with 0,25% saponin/PBS and stained with Rhodamine-conjugated phalloidin, anti-giantin antibody and Hoechst 33258. Cells were observed with a 63X PlanApo NA 1.42 objective on an Olympus FluoView FV1000 microscope with the FV1000 software. Cells with the Golgi in the 1/3 of the cell facing the wound were considered to be polarized.

Vimentin filaments reorientation assay: wound-healing assay was performed on transfected cells. Cells were incubated for 3 hours after the start of the wound-healing assay at 37°C under 5% CO_2. After 3 hours from the start of the assay, a new scratch was performed in each sample, 90 degrees rotated compared to the first scratch. Cells were subsequently permeabilized, fixed and stained with anti-vimentin antibody and Hoechst. Cells that were migrating towards the scratch made at the start of the wound-healing assay were considered to be migrating cells, whereas cells at the edge of the scratch performed right before fixation (after 3 hours from the start of wound-healing assay) were considered non-migrating cells. Cells were observed with a 63X PlanApo NA 1.42 objective on an Olympus FluoView FV1000 microscope with the FV1000 software. Vimentin filaments in the area between the nucleus and the leading edge of migrating cells were considered to be oriented.

Microtubules reorientation assay: after wound-healing assay, cells were incubated for 3 hours at 37°C under 5% CO_2. Then, cells were fixed with 3% PFA, permeabilized with 0,25%

saponin/PBS and stained with anti-tubulin antibody and Hoechst 33258. Cells were observed with a 63X PlanApo NA 1.42 objective on an Olympus FluoView FV1000 inverted microscope with the FV1000 software. Microtubules in the area between the nucleus and the leading edge of migrating cells were considered to be oriented.

3.15 Adhesion assay

The adhesion assay is a useful method to evaluate the ability of cells to adhere to a specific surface.

Protocol: After 24 hours of transfection, control and transfected cells were seeded onto fibronectin-coated coverslips (BD Biosciences). 30 minutes later cells were fixed with 3% PFA and permeabilized with 0,25% saponin/PBS. Staining was performed with Rhodamine-conjugated phalloidin, Hoeschst 33258 and anti-HA antibody. Coverslips were then mounted and observed by using an Olympus FluoView FV1000 microscope. Cell areas were determined by using ImageJ software.

3.16 EEA1 and active β1-integrin colocalization assay

Protocol: NCI H1299 cells were transfected with control RNA and Rab7a siRNA. Cells were then fixed and permeabilized with 0,1% saponin/PBS. Cells were stained for active β1-integrin and EEA1. Coverslips were then mounted and observed with a Zeiss LSM 700 confocal microscope. The level of EEA1 colocalizing with active β1-integrin was quantified by using the Zeiss software and normalized against active β1-integrin abundance.

3.17 Rac1 activation assay

Rac1 activity was tested by using the Rac1 Pull-down Activation Assay Biochem Kit (BK035, Cytoskeleton) according to the manifacturer's protocol. The Rac1 Activation assay uses the Cdc42/Rac Interactive Binding (CRIB) region (also called PBD) of the Cdc42/Rac effector protein, p21 activated kinase I (PAK). This motif binds specifically to the GTP-bound form of Rac and/or Cdc42 proteins. The PAK-PBD provided by the kit is in the form of a GST fusion protein which allows to “pull-down” the PAK-PBD/GTP-Rac complex with glutathione affinity beads. Therefore, GTP-bound Rac1 was immunoprecipitated from cell lysates with GST-Pak-PBD using glutathione affinity beads. After washing, the beads were subjected to western blot analysis using anti-Rac1 antibody to detect GTP-bound Rac1. Total amount of Rac1 was detected by immunoblotting of the whole cell lysates.

3.18 Live imaging

Protocol: NCI H1299 cells were grown on MatTek glass-bottomed dishes, washed with PBS and then incubated in DMEM without phenol red at 37°C under 5% CO_2. Cells were imaged with a 63X PlanApo NA 1.42 objective on an Olympus IX-71 microscope equipped with a CSU22 spinning-disk confocal unit (Yokogawa), an Ixon EMCCD camera (Andor) and the Andor iQ1.8 software.

3.19 Statistical analyses

Data were statistically analyzed using Student's *t*-test (GraphPad Prism4 software) (*$p<0.05$, **$p<0.01$ and ***$p<0.001$). Error bars represent s.e.m. or s.d. as indicated. Experiments were performed at least in triplicate.

RESULTS

4.1 RAB7A REGULATES CELL MIGRATION THROUGH RAC1 AND VIMENTIN

The small GTPase Rab7a regulates vesicular transport to late endosomes and lysosomes in the endocytic pathway, and biogenesis of lysosomes, phagolysosomes and autolysosomes (Bucci *et al.*, 2000; Harrison *et al.*, 2003; Wang *et al.*, 2011; Hyttinen *et al.*, 2013; Vanlandingham and Ceresa, 2009). Rab7a exerts its functions by interacting with several proteins, some of which are strictly connected with cytoskeletal elements. In particular, it directly interacts with Rac1, an important regulator of actin cytoskeleton, which has a fundamental role in orchestrating some aspects of cell migration (Bosco *et al.*, 2009; Sun *et al.*, 2005) and with vimentin, an intermediate filament protein which has been involved in cell migration (Cogli *et al.*, 2013a; Dave and Bayless, 2014). Considering these interactions and the fact that Rac1 and vimentin are key factors for cellular motility, we investigated the possible role of Rab7a in cell migration.

4.1.1 Depletion of Rab7a alters cell motility

In order to investigate the role of Rab7a on cell migration we performed a wound-healing assay on confluent monolayers of NCI H1299 control and Rab7a-depleted cells. Indeed, we transfected NCI H1299 cells with control RNA or siRNA against Rab7a. After 24 hours of transfection confluent monolayers of cells were scratched with a pipette tip and the cells migrating toward the wound were imaged at time intervals of 30 min over a 9 hour time period. Movies were then analyzed. The effective silencing of Rab7a was checked by western blot of control and Rab7a-depleted cells lysates (Figure 4.1). As shown in Figure 4.1, Rab7a abundance was strongly reduced.

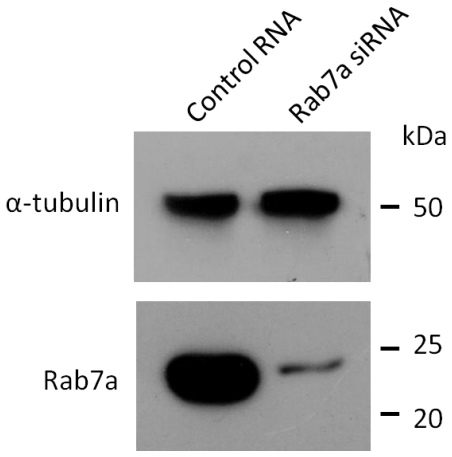

Figure 4.1 Rab7a abundance is reduced after silencing. NCI H1299 control and Rab7a-depleted cells were lysed and lysates were subjected to western blotting analysis using anti-Rab7a and anti-tubulin antibodies. Tubulin serves as loading control. The migration of protein molecular weight size markers is indicated.

Interestingly, analysis of the movies showed that Rab7a-depleted cells migrated slower than control cells (Movie 1; Figure 4.2).

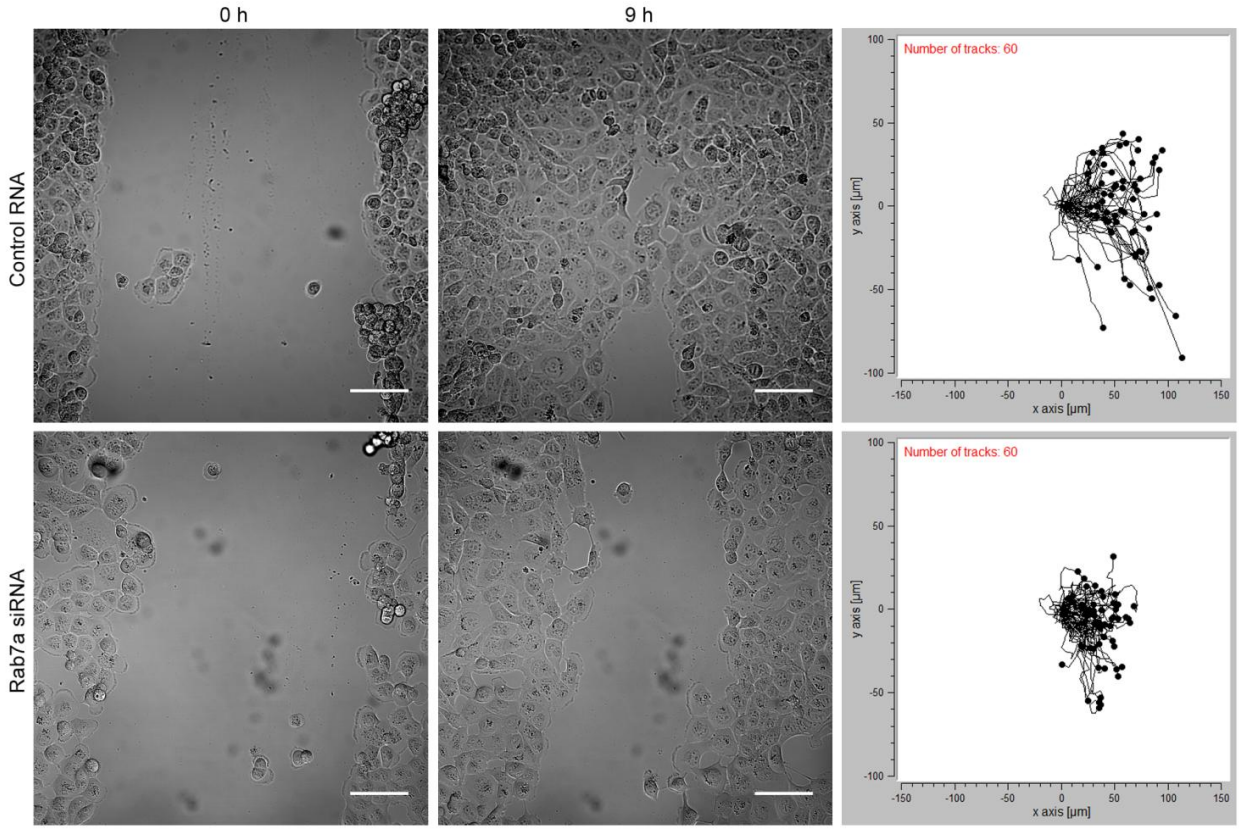

Figure 4.2 Rab7a delays wound closure. NCI H1299 cells transfected with either control RNA or Rab7a siRNA were imaged during a wound-healing assay. Images were taken every 30 min over a 9 hours period. Images referring to the initial time point (0 hours) or after the closure of the wound (9 hours) are shown. On the right panel the migratory tracks of some representative cells obtained by tracking the nuclei of migrating cells are shown for control and Rab7a-depleted cells. Individual tracks are shown so that each starts at the origin (0,0). Scale bars = 50 µm.

Tracking of the nuclei was performed by using the "Manual tracking" plugin distributed by ImageJ and data were analyzed by using the "Chemotaxis and Migration" tool distributed by Ibidi. Migration parameters such as accumulated distance, Euclidean distance, cell velocity and directness were analyzed. Accumulated distance is the total distance that the cell travelled in a certain amount of time. Euclidean distance measures the distance along straight-line path between the positions of the cell at the initial (0h) and final (9h) points. Directness measures the

ability of a cell to move persistently along its migratory path and it is calculated by comparing the Euclidean distance and the accumulated distance (Figure 4.3).

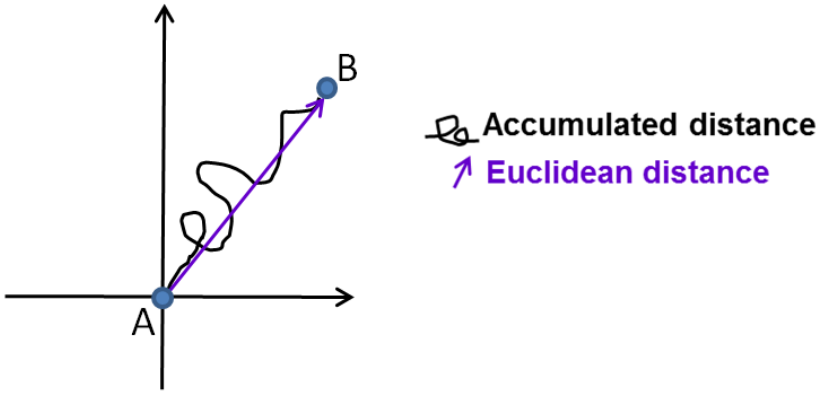

Figure 4.3 Scheme illustrating the path of an hypothetic cell during migration. Cell moves from an initial point (marked with A) to the final point (marked with B). The arrows, in black and violet, indicate the accumulated and Euclidean distance, respectively.

Interestingly, accumulated distance, Euclidean distance and cell velocity were strongly decreased in Rab7a-depleted cells compared to control cells (Figure 4.4 A-C). In particular, velocity and accumulated distance were decreased of ~40% in Rab7a-depleted cells compared to control cells, whereas Euclidean distance was ~50% lower upon silencing of Rab7a (Figure 4.4 A-C). Importantly, also directness was affected in cells silenced for Rab7a with a reduction of about 20% (Figure 4.4 D).

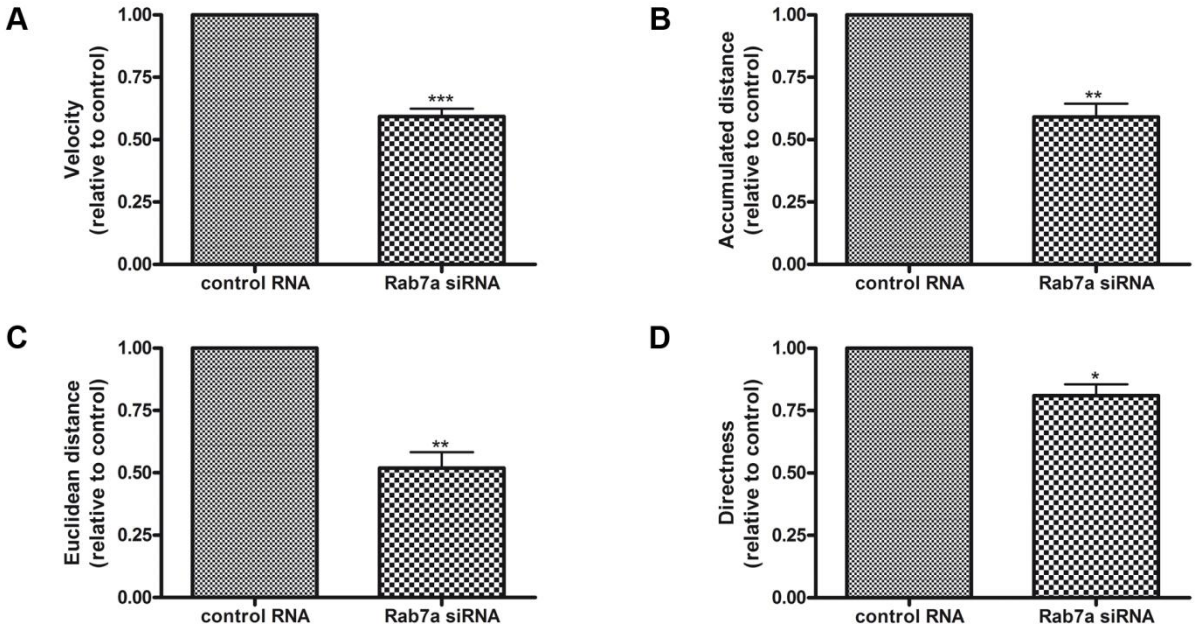

Figure 4.4 Loss of Rab7a affects several migratory parameters. Migration velocity (A), accumulated distance (B), Euclidean distance (C) and directness (D) have been quantified by using the "Chemotaxis and Migration" tool distributed by Ibidi. Data represents the mean ± s.e.m. of four independent experiments (n=60).

4.1.2 Rab7a silencing does not influence Golgi apparatus reorientation

We then evaluated a possible role of Rab7a on cell polarization by measuring the orientation of the Golgi complex into the direction of the wound during migration. We performed a wound healing assay in control and Rab7a-depleted cells and after three hours of migration, cells were fixed and stained against giantin (a protein localized at the Golgi apparatus), actin (by using Rhodamine-conjugated phallodin) and nuclei (by using Hoechst). Images were taken with a confocal microscope and were subsequently analyzed (Figure 4.5 A). Cells with the Golgi apparatus in the 1/3 of the cell facing the wound were considered to be polarized (Figure 4.5 B). Quantitative analysis showed that in the majority of Rab7a-depleted cells the Golgi apparatus was correctly oriented in the direction of the wound similarly to control cells and differences were not statistically significative (Figure 4.5 C). Therefore, depletion of Rab7a did not interfere with Golgi orientation.

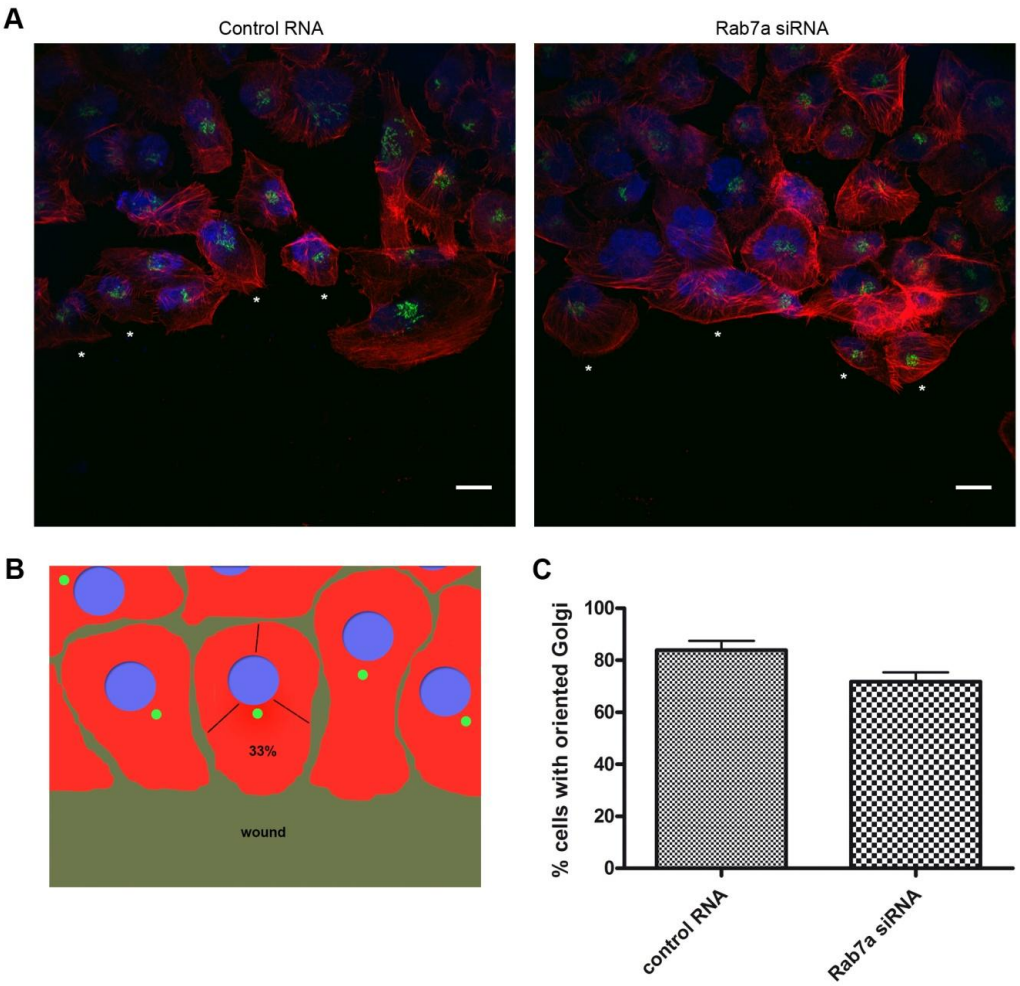

Figure 4.5 Golgi complex orientation is not impaired by Rab7a. (A) NCI H1299 cell were transfected with either control RNA or siRNA against Rab7a and were subsequently subjected to wound-healing assay. After three hours from the start of the assay, cells were stained with anti-giantin antibody (green), Rhodamine-conjugated phalloidin (red) and Hoechst (blue). * indicates a polarized cell with Golgi apparatus oriented into the direction of the wound. (B) Model representing a polarized cell. Cell is considered to be polarized only if the Golgi complex is oriented in the 1/3 of the cell facing the wound. (C) Quantification of NCI H1299 control or Rab7a-depleted cells with oriented Golgi apparatus after three hours of migration. Data represent the mean ± s.e.m. of three indipendent experiments (n=50). Scale bars = 10 μm.

4.1.3 Rab7a alters filopodia formation

Another important event occurring during migration is the formation of protrusions (Vicente-Manzanares *et al.*, 2005). Therefore we investigated whether Rab7a could affect the formation of filopodia. We performed a wound healing assay in control and Rab7a-depleted cells. After three hours from the start of the assay cells were fixed, permeabilized and stained with Rhodamine-conjugated phalloidin. Images were taken and subsequently analyzed (Figure 4.6 A). Quantitative analysis of the formation of filopodia in control cells and in cells silenced for Rab7a demonstrated that the formation of these protrusions was strongly affected upon Rab7a-depletion (Figure 4.6 B). In particular, we observed 64% of control cells having filopodia, whereas only

37% of cells silenced for Rab7a had filopodia. Thus, Rab7a depletion caused a ~40% reduction of cells with filopodia at the leading edge compared to control cells (Figure 4.6 B).

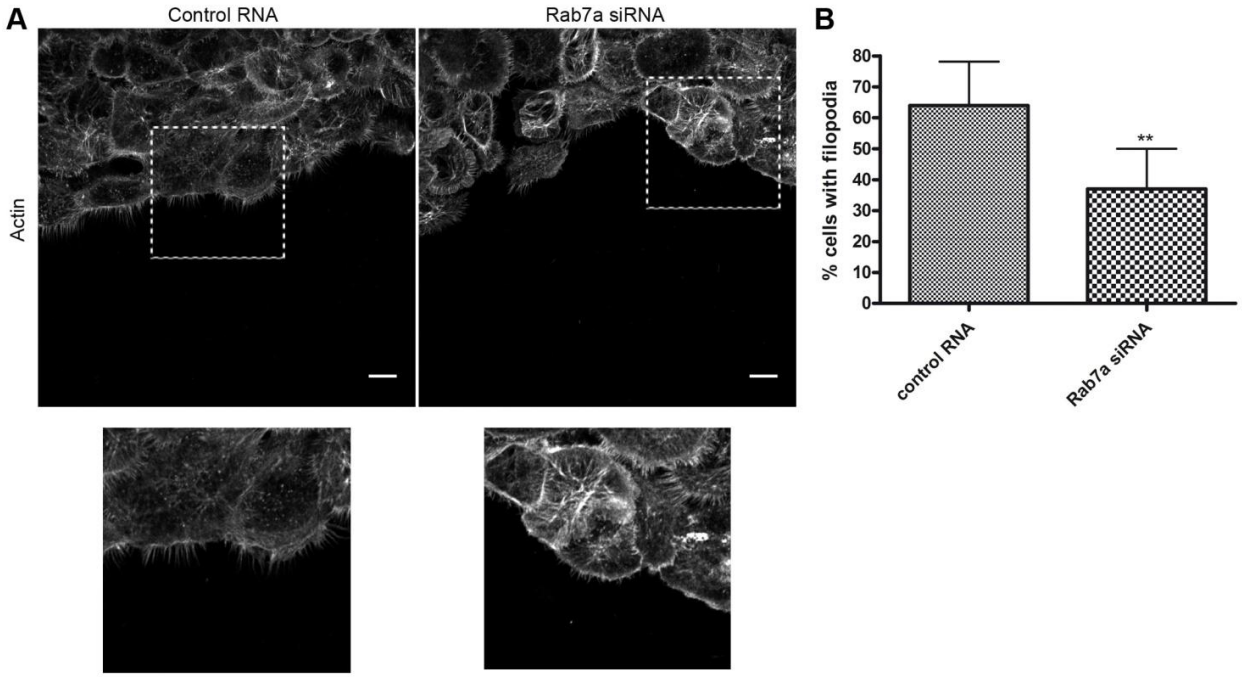

Figure 4.6 Rab7a depletion impairs filopodia formation. (A) Confocal microscopy of NCI H1299 cells transfected with either control RNA or siRNA against Rab7a and subjected to wound healing assay. Cells were subsequently stained with Rhodamine-conjugated phalloidin. Enlargements of the indicated areas are shown. (B) Quantification of control and Rab7a-depleted cells showing well-structured filopodia at the leading edge. Data represent the mean ± s.e.m. of three different experiments (n=50). Scale bar = 10 μm.

4.1.4 Rab7a impairs myosin X localization to filopodia tips

Given that we observed a decrease in the number of filopodia in Rab7a-depleted cells compared to control cells, we investigated whether Rab7a could have a role on myosin X function, which is responsible for promoting filopodia formation (Bohil, 2006; Zhang, 2004). Therefore, we overexpressed mCherry-Rab7a and GFP-myosin X in NCI H1299 cells and we performed live imaging experiments. We could detect that GFP-myosin X was localized to filopodia tips. Nevertheless, a fraction of myosin X localized also intracellularly on Rab7a-positive endosomes (Fig. 4.7). Interestingly, these endosomes transported myosin X to the cell periphery, where then the Rab7a coat was lost (Fig. 4.7, Movie 2).

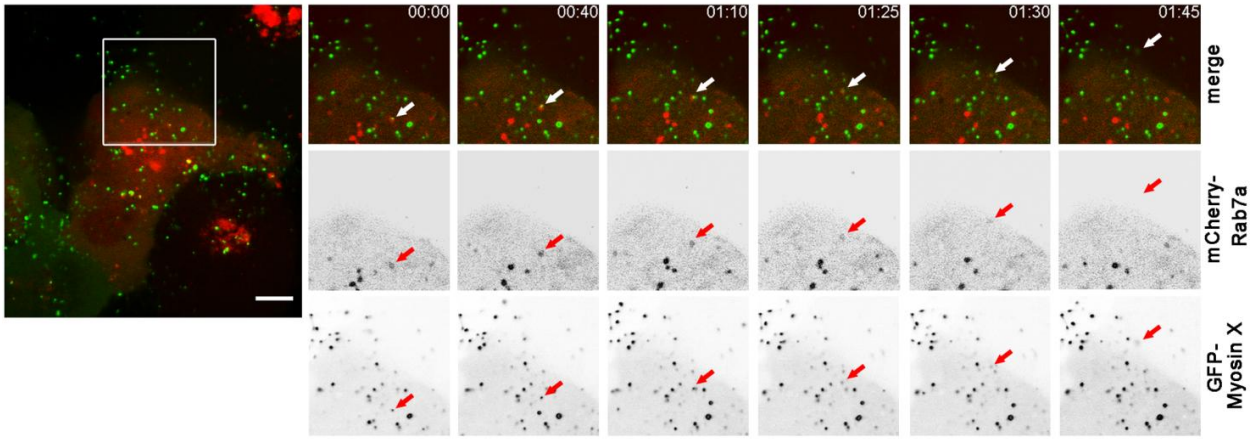

Figure 4.7 Myosin X is transported to cell periphery in Rab7a-positive compartments. NCI H1299 cells were co-transfected with GFP-myosin X and mCherry-Rab7a and imaged using a spinning-disk confocal microscope at the indicated time points. The red and white arrows indicate a vesicle positive for both GFP-myosin X and mCherry-Rab7a moving toward the cell periphery. Scale bar = 10 µm.

We then evaluated whether the decreased number of filopodia in Rab7a-depleted cells could be a consequence of altered myosin X transport. We therefore investigated the GFP-myosin X localization in cells silenced for Rab7a. Thus, we transfected NCI H1299 cells with control RNA or Rab7a siRNA, we subsequently overexpressed GFP-myosin X in both samples and then we imaged them using a spinning-disk confocal microscope (Figure 4.8 A). Interestingly, while in about 80% of the control cells myosin X localized mostly at the filopodia tip, in 50% of the cells transfected with siRNA against Rab7a, myosin X was predominantly intracellular and not present at the filopodia tip (Fig. 4.8 B). We excluded that the increase of intracellular myosin X after Rab7a silencing could be caused by an increase in the total amount of myosin X by western blot of either overexpressed (Fig. 4.9 A-B) or endogenous myosin X (Fig. 4.10 A-B) showing that Rab7a depletion did not affect myosin X total abundance.

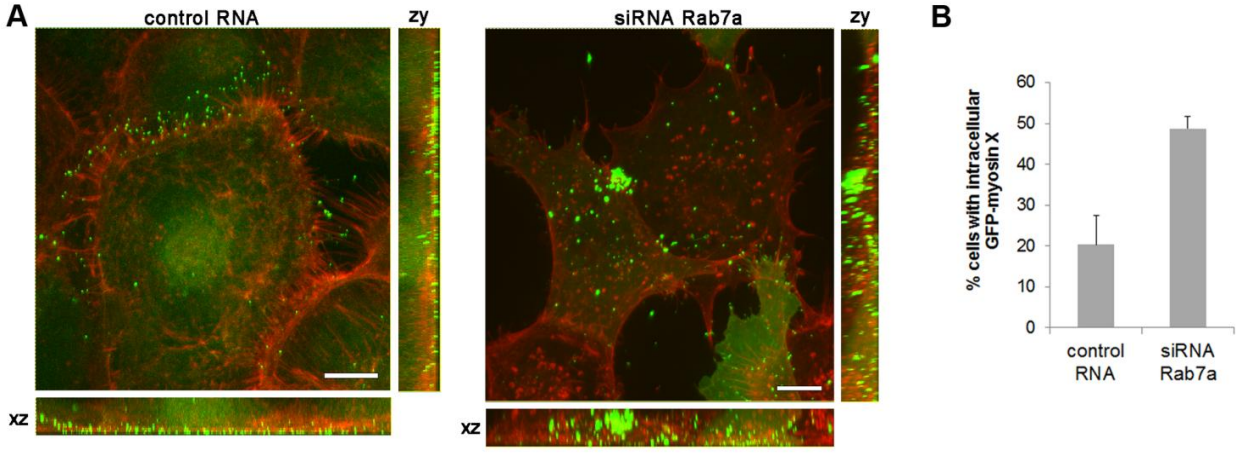

Figure 4.8 Loss of Rab7a impairs myosin X localization. (A) NCI H1299 cells were transfected with control RNA or siRNA against Rab7a and subsequently with GFP-myosin X.

Samples were fixed and stained with Rhodamine-conjugated phalloidin. xy (large image), xz and yz maximum intensity projections of confocal images are shown. Scale bar = 10 µm. (B) Quantification of the percentage of cells with intracellular GFP-myosin X in control and Rab7a-depleted cells. Data represents the mean ± s.e.m. of three independent experiments (n = 50).

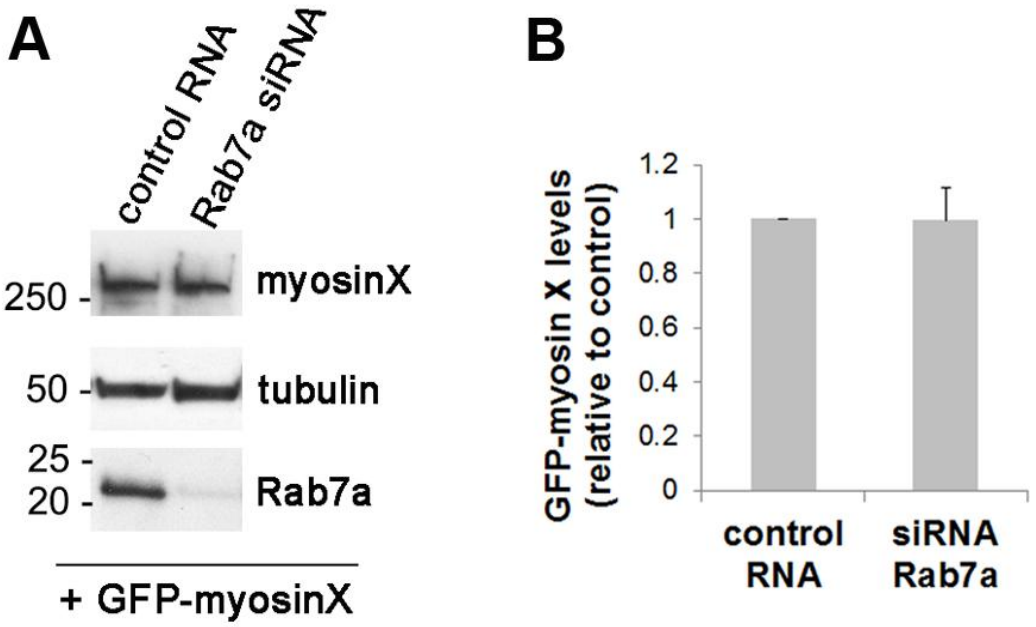

Figure 4.9 Overexpression of GFP-myosin X does not alter myosin cellular abundance. (A) NCI H1299 cells were transfected first with control RNA or with siRNA against Rab7a and subsequently with GFP-myosin X. Cell lysates were analyzed by western blotting against myosin X, Rab7a and tubulin (serving as a loading control). (B) Quantification of myosin X abundance in cells transfected with GFP-myosin X. The intensities of the bands were quantified by densitometry, normalized against the amount of tubulin, and plotted relative to the intensities obtained in cells transfected with control RNA. The values represent the mean ± s.d. of three independent experiments.

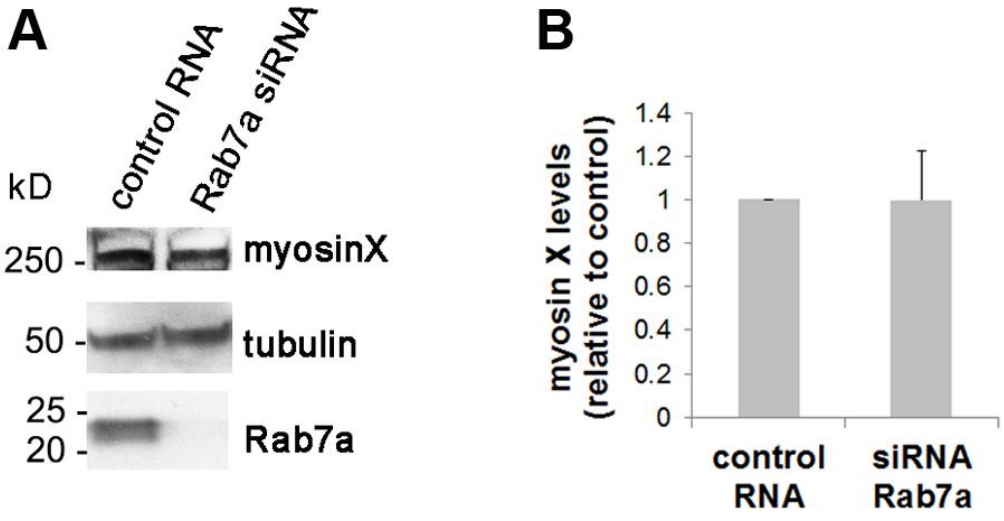

Figure 4.10 Silencing of Rab7a does not impair myosin X abundance. (A) NCI H1299 were transfected with either control RNA or with siRNA against Rab7a. Cell lysates were analyzed by

western blotting against myosin X, Rab7a and tubulin (serving as a loading control). (B) Quantification of the endogenous myosin X abundance. The intensities of the bands were quantified by densitometry, normalized against the amount of tubulin, and plotted relative to the intensities obtained in cells treated with control RNA. The values represent the mean ± s.d. of three independent experiments.

4.1.5 Loss of Rab7a reduces cell adhesion

Having observed that Rab7a affects cell motility and the formation of protrusions, we further evaluated whether Rab7a could be important also for cell adhesion. In particular, we investigated the ability of control and Rab7a-depleted cells to spread out on fibronectin-coated coverslips. We seeded cells on these coverslips and after 30 min cells were fixed, permeabilized and stained by using Rhodamine-conjugated phalloidin in order to look at the actin cytoskeleton. Interestingly, Rab7a-depleted cells showed lower ability to spread compared to control cells (Figure 4.11 A). In particular, the average cell area of Rab7a-depleted cells was of 90 μm^2, about 60% lower than the average cell area of control cells, which showed an average cell area of ~220 μm^2 (Figure 4.11 B). To confirm that the inability of Rab7a-depleted cells to spread onto fibronectin-coated dishes was specifically due to Rab7a depletion, we also performed rescue experiments. Transient expression of HA-tagged Rab7a wt in Rab7a-depleted cells was sufficient to re-induce, although partially, cell spreading onto fibronectin. Quantification of the average cell area resulted in about 50% recovery of spreading in Rab7a-silenced cells expressing HA-tagged Rab7a wt compared to Rab7a-silenced cells (Figure 4.11 B), confirming the role of Rab7a in adhesion (Figure 4.11). Moreover, we demonstrated that active Rab7a is necessary for cell adhesion as transient expression of HA-tagged Rab7a Q67L, the constitutively active Rab7a mutant, in Rab7a-depleted cells re-induced, although partially, cell spreading onto fibronectin. Quantification of the average cell area resulted in about 50% recovery of spreading in Rab7a-silenced cells expressing HA-tagged Rab7a Q67L compared to Rab7a-silenced cells, similarly to the transient expression of HA-tagged Rab7a wt (Figure 4.11 B). In contrast, as expected, expression of the dominant negative HA-tagged Rab7aT22N mutant in Rab7a-depleted cells was not able to recover spreading onto fibronectin (Fig. 4.11 B).

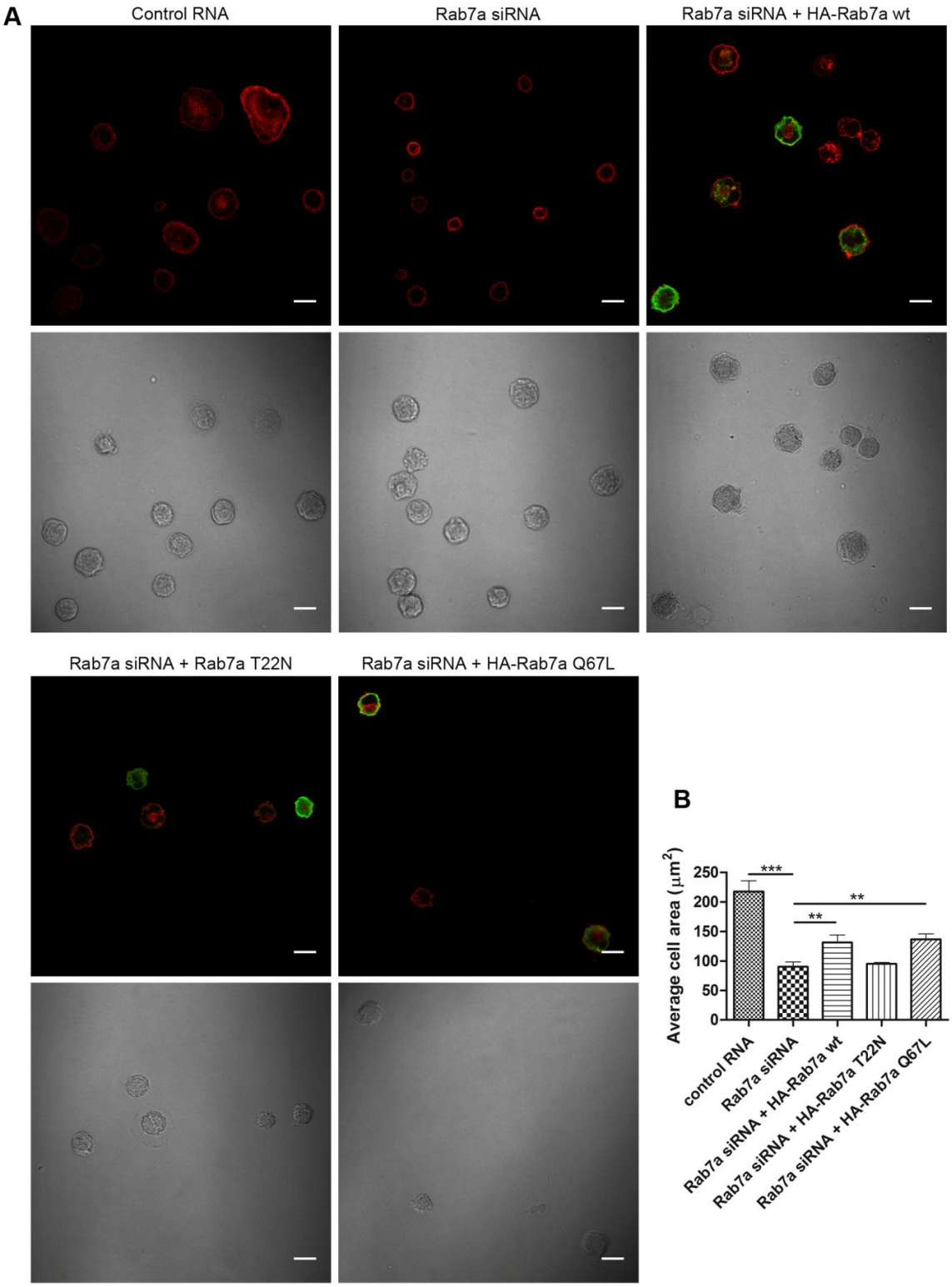

Figure 4.11 Rab7a is required for cell adesion. (A) NCI H1299 cells transfected with control RNA, siRNA against Rab7a, or silenced and transfected afterward with HA-Rab7a wt, HA-Rab7a T22N or HA-Rab7a Q67L were plated on fibronectin-coated coverslips and left to adhere for 30 minutes. Samples were subsequently fixed, permeabilized and stained with Rhodamine-conjugated phalloidin and anti-HA antibody. Confocal images and the relative transmission images are shown. (B) Quantification of the average area (in μm^2) of NCI H1299 cells transfected as described in A after 30 minutes of adhesion on fibronectin. Data represent the mean ± s.e.m. of at least three different experiments (n=50). Scale bar = 10 μm

4.1.6 Rab7a alters β1-integrin localization and activation

As β1-integrin is important for cell adhesion to fibronectin and we have demonstrated that in Rab7a-depleted cells adhesion to fibronectin is impaired, we next investigated whether there was a link between Rab7a and β1-integrin. First of all, we co-transfected NCI H1299 cells with GFP-β1-integrin and mCherry-Rab7a and we observed a high degree of colocalization between β1-integrin and Rab7a. Indeed, about 40% of β1-integrin was colocalizing with Rab7a. In addition, we could observe Rab7a vesicles positive for β1-integrin in live cells, suggesting that intracellular transport of β1-integrin is mediated by Rab7a (Figure 4.12; Movie 3).

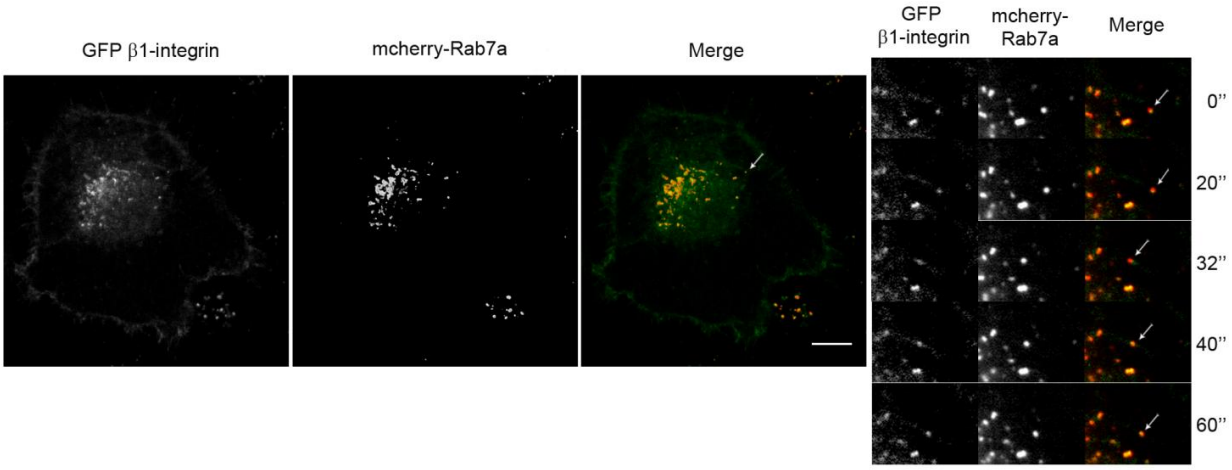

Figure 4.12 Rab7a and β-1 integrin colocalize. NCI H1299 cells co-transfected with GFP β1-integrin and mcherry-Rab7a were imaged with a Spinning Disk confocal microscope. Merged double fluorescence is shown. Enlargement of the area surrounding the vesicle indicated by the arrow at different time points is shown in the right panel.

Integrins exist in different conformational states which have different localization. In particular, inactive β1-integrin is mainly localized to the plasma membrane and protrusions and it represents about 80% of cell surface β1-integrin, whereas only 20% of cell surface β1-integrin is in the active conformation, which is predominant in the cytoplasm (Arjonen *et al*., 2012; Tiwari *et al*., 2011). Only active β1-integrin has been previously reported to localize to Rab7a-positive compartments (Arjonen *et al.*, 2012). Therefore, we used specific antibodies able to recognize and discriminate the active and inactive forms of β1-integrin in immunofluorescence experiments. First of all we confirmed the localization of active and inactive β1-integrin in NCI H1299 cells, thus proving that the antibodies used were able to discriminate the two forms of the receptor (Figure 4.13).

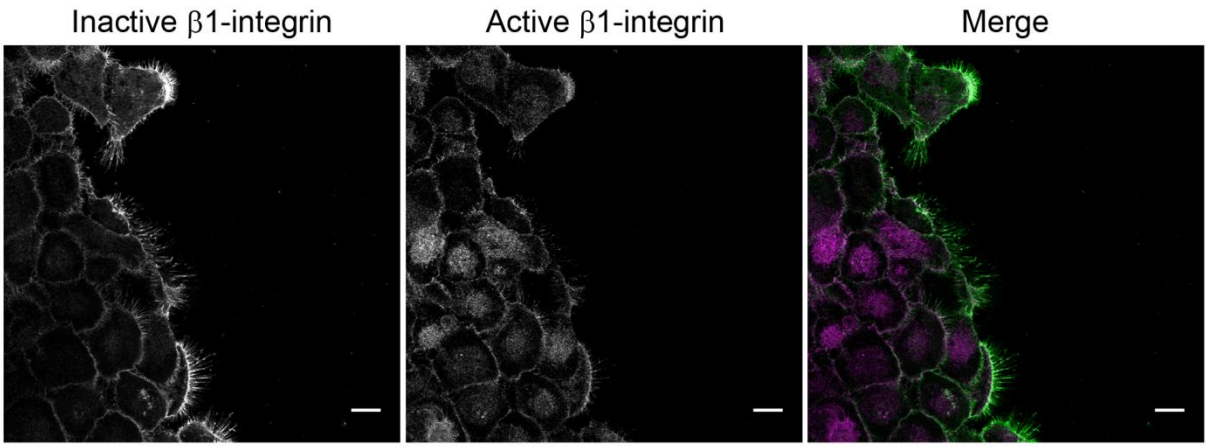

Figure 4.13 Localization of active and inactive β1-integrin. Confocal microscopy of NCI H1299 cells subjected to wound healing assay. Cells were subsequently stained with antibodies able to detect active and inactive β1-integrin as indicated. Merge of the two channel is shown in the right panel (green, inactive β1-integrin; magenta, active β1-integrin). Scale bar = 10 μm.

Then, we investigated the localization of the active and the inactive forms of β1-integrin in control and Rab7a-depleted migrating cells by total internal reflection fluorescence (TIRF) microscopy in order to detect differences of receptor localization at the leading edge (Figure 4.14).

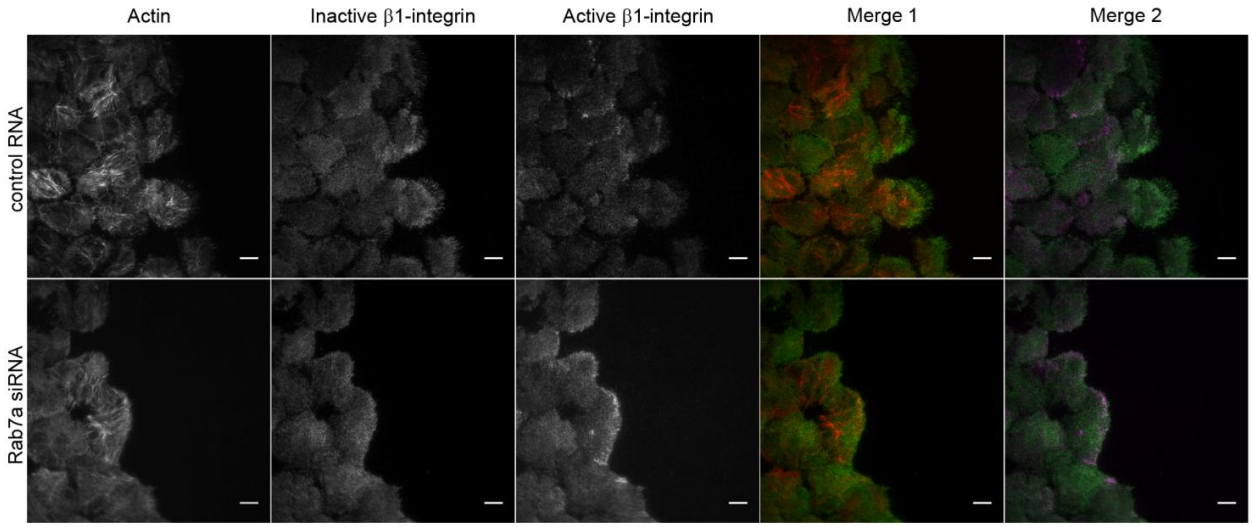

Figure 4.14 Rab7a depletion alters localization of active β-1 integrin during wound healing. TIRF images of migrating NCI H1299 cells transfected with either control RNA or siRNA against Rab7a and stained with Rhodamine-conjugated phalloidin in order to detect actin and antibodies against inactive and active β-1 integrin. Merge of actin (red) and inactive β-1 integrin (green) is shown (Merge 1). Merge of inactive β-1 integrin (green) and active β-1 integrin (magenta) is shown (Merge 2). Images were taken at 110 nm depth.

TIRF analysis of migrating cells stained for β1-integrin confirmed that Rab7a depletion inhibits filopodia formation as documented by the decrease of about 50% of the number of cells with β1-integrin-rich filopodia (Figure 4.15 A). Furthermore, we detected an increase of about 80% of the number of Rab7a-depleted cells with the active form of β1-integrin at the level of the plasma membrane facing the wound, compared to control cells (Figure 4.15 B).

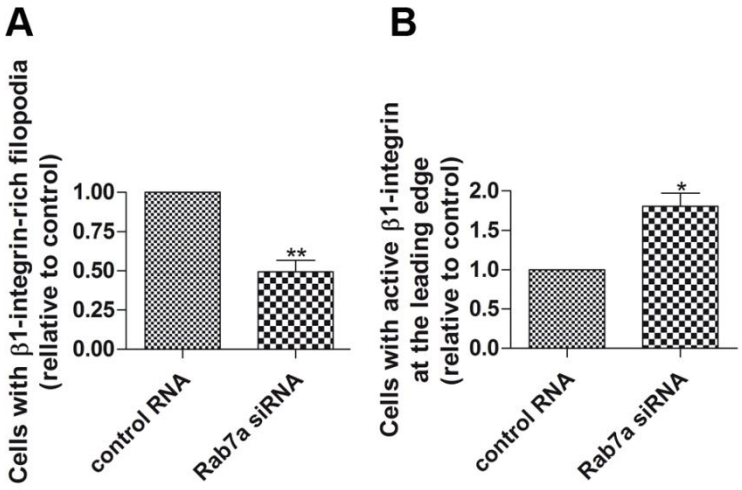

Figure 4.15 Loss of Rab7a alters the localization of β1-integrin at the leading edge. (A) Quantification of the number of control and Rab7a-depleted cells showing well-formed filopodia localization of inactive β-1 integrin in migrating cells. Data represent the mean ± s.e.m. of four different experiments (n=50). (B) Quantification of the number of cells showing active β-1 integrin accumulation at the leading edge of migrating cells. Data represent the mean ± s.e.m. of three different experiments (n=50).

Given that only active β1-integrin associates with Rab7a-positive vesicles (Arjonen *et al*., 2012) and that we saw an altered localization of this form of integrin, we further investigated whether Rab7a affected β1-integrin activation. We evaluated by western blotting analyses the abundance of total and active β1-integrin. The total amount of integrin was similar in control cells and in cells silenced for Rab7a cells, whereas Rab7a-depletion caused a decrease of active β1-integrin (Figure 4.16 A). In fact, the amount of active β1-integrin was 25% lower in cells depleted for Rab7a compared to control cells (Figure 4.16 B).

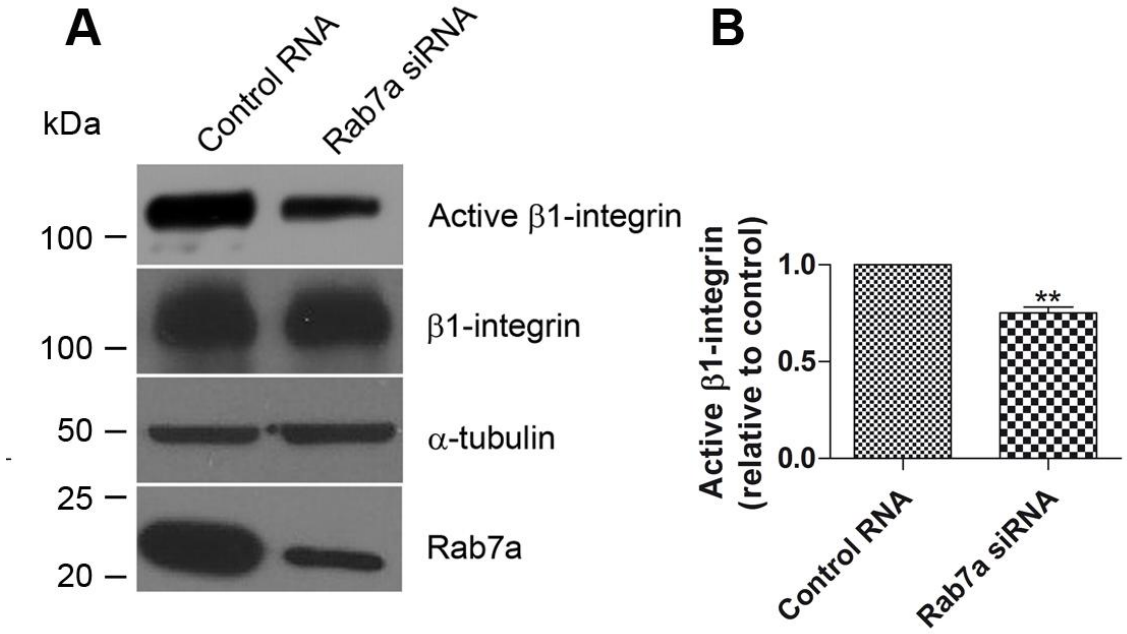

Figure 4.16 Activation state of β1-integrin is altered after Rab7a depletion. (A) Lysates of NCI H1299 cells transfected with control RNA or siRNA against Rab7a were subjected to western blot analysis under non-reducing conditions using anti-active β1-integrin, anti-β1-integrin, anti-Rab7a and anti-tubulin antibodies. The migration of protein molecular weight size markers is indicated. (B) Quantification of active β1-integrin abundance. The intensities of the bands were quantified by densitometry, normalized against the amount of β1-integrin, and plotted relative to the intensities obtained in cells treated with control RNA. Data represent the mean ± s.e.m. of four independent experiments.

Usually inactive β1-integrin is mostly localized at the plasma membrane while active β1-integrin seems to be more cytoplasmic (De Franceschi *et al.*, 2015). Thus, we evaluated the abundance of active β1-integrin in the cytoplasm of NCI H1299 cells treated with control RNA or Rab7a siRNA by immunofluorescence analysis. We found that active β1-integrin was less abundant in the cytoplasm after Rab7a depletion but the staining was more vesicular (Figure 4.17).

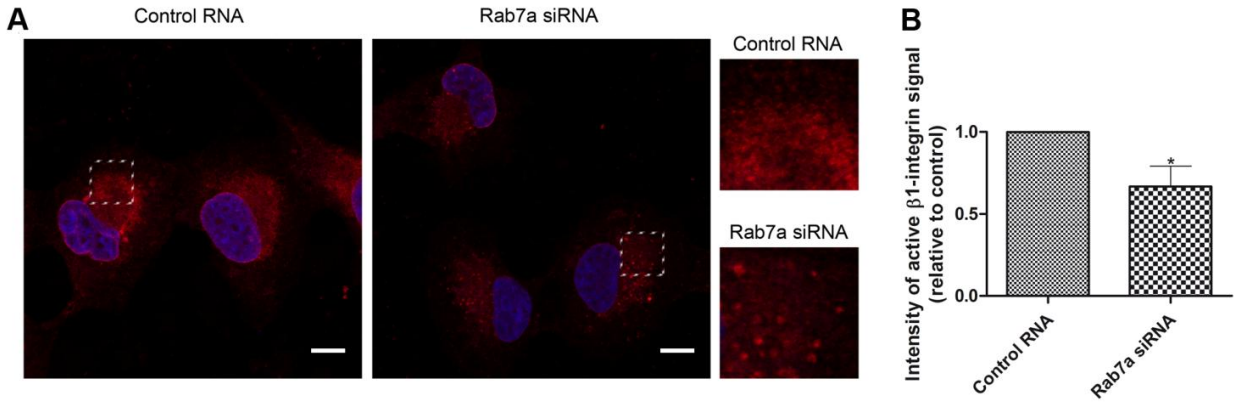

Figure 4.17 Cytoplasmic active β1-integrin localization is impaired in Rab7a-depleted cells. (A) Confocal images of NCI H1299 cells transfected with control RNA or siRNA against Rab7a were stained with anti-active β1-integrin antibody (red) and DAPI (blue). Enlargements of the indicated areas are shown. (B) Quantification of active β1-integrin intensity. Data represent the mean ± s.e.m. of four independent experiments (n=50). Scale bar = 10 µm.

Moreover, we analyzed the colocalization between the early endosomal marker EEA1 and active β1-integrin by staining control and Rab7a-depleted cells with antibodies against active β1-integrin and EEA1 (Figure 4.18 A). We found that this value was four times higher in Rab7a-depleted cells compared to control cells (Figure 4.18 B).

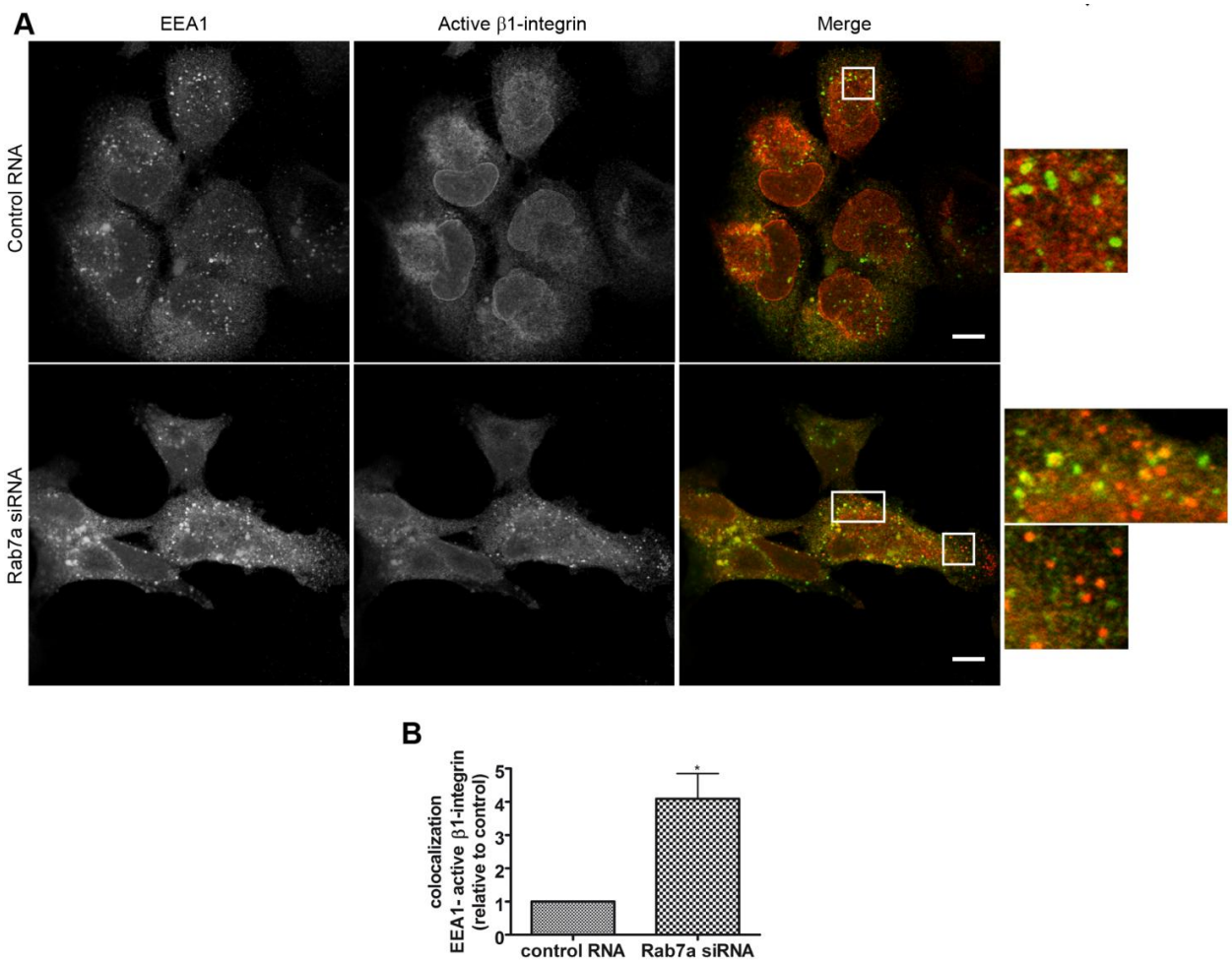

Figure 4.18 Colocalization between EEA1 and active β1-integrin is higher in Rab7a-depleted cells. (A) NCI H1299 cells were transfected with control RNA or siRNA against Rab7a and then stained with anti-EEA1 antibody (green) and anti-active β1-integrin antibody (red). Enlargements of the indicated areas are shown. (B) Quantification of colocalization between EEA1 and active β1-integrin. Data were normalized against active β1-integrin abundance and represent the mean ± s.e.m. of three independent experiments (n=50). Scale bar = 10 µm.

We excluded that the increase in colocalization between EEA1 and active β1-integrin could be affected by a modulation in the total amount of EEA1 in control and Rab7a-depleted cells by western blot (Figure 4.19 A). We found that EEA1 abundance was unchanged after Rab7a depletion (Figure 4.19 B).

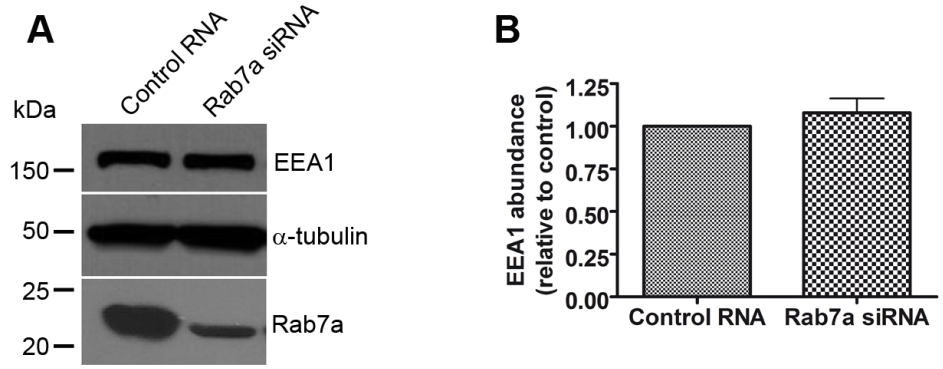

Figure 4.19 EEA1 abundance is not affected by the lack of Rab7a. (A) Lysates of NCI H1299 cells transfected with control RNA or siRNA against Rab7a were subjected to western blot analysis using anti-EEA1, anti-Rab7a and anti-tubulin antibodies. The migration of protein molecular weight size markers is indicated. (B) Quantification of EEA1 abundance. The intensities of the bands were quantified by densitometry, normalized against the amount of tubulin, and plotted relative to the intensities obtained in cells treated with control RNA. Data represent the mean ± s.e.m. of three independent experiments.

4.1.7 Rab7a does not impair vinculin abundance

Given that Rab7a alters cell adhesion and the localization, activity and trafficking of β1-integrin and β1-integrin is a component of cell-matrix adhesions where it associates with vinculin, we investigated whether Rab7a silencing could impair vinculin abundance. Therefore, we transfected NCI H1299 cells with control RNA or Rab7a siRNA. Cells were lysed and lysates were subjected to western blotting analyses (Figure 4.20 A). As shown in Figure 4.20 B, we did not detect any difference in vinculin abundance in Rab7a-depleted cells compared to control cells.

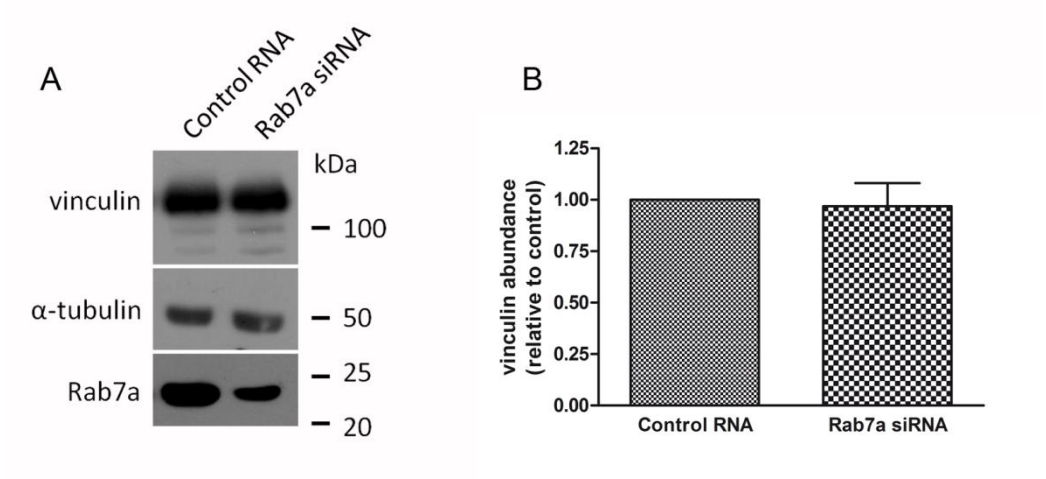

Figure 4.20 Lack of Rab7a does not influence vinculin abundance. (A) Lysates of NCI H1299 cells transfected with control RNA or siRNA against Rab7a were subjected to western blot analysis using anti-vinculin, anti-Rab7a and anti-tubulin antibodies. The migration of protein molecular weight size markers is indicated. (B) Quantification of vinculin abundance. The intensities of the bands were quantified by densitometry, normalized against the amount of tubulin, and plotted relative to the intensities obtained in cells treated with control RNA. Data represent the mean ± s.e.m. of three independent experiments.

4.1.8 Loss of Rab7a does not impair Rac1 abundance

Rab7a interacts with Rac1, a regulator of actin cytoskeleton and cell migration (Bosco *et al.*, 2009; Sun *et al.*, 2005). Given that we demonstrated that Rab7a has a role in migration, we investigated whether, in our system, modulation of Rab7a expression affected Rac1 abundance. Therefore we transfected cells with control RNA or Rab7a siRNA but we couldn't detect any differences in Rac1 protein amount upon silencing of Rab7a by western blot analysis (Figure 4.21). Then we transfected cells with HA-tag or HA-tagged Rab7a and also in this case we did not detect any differences in Rac1 protein amount (Figure 4.21).

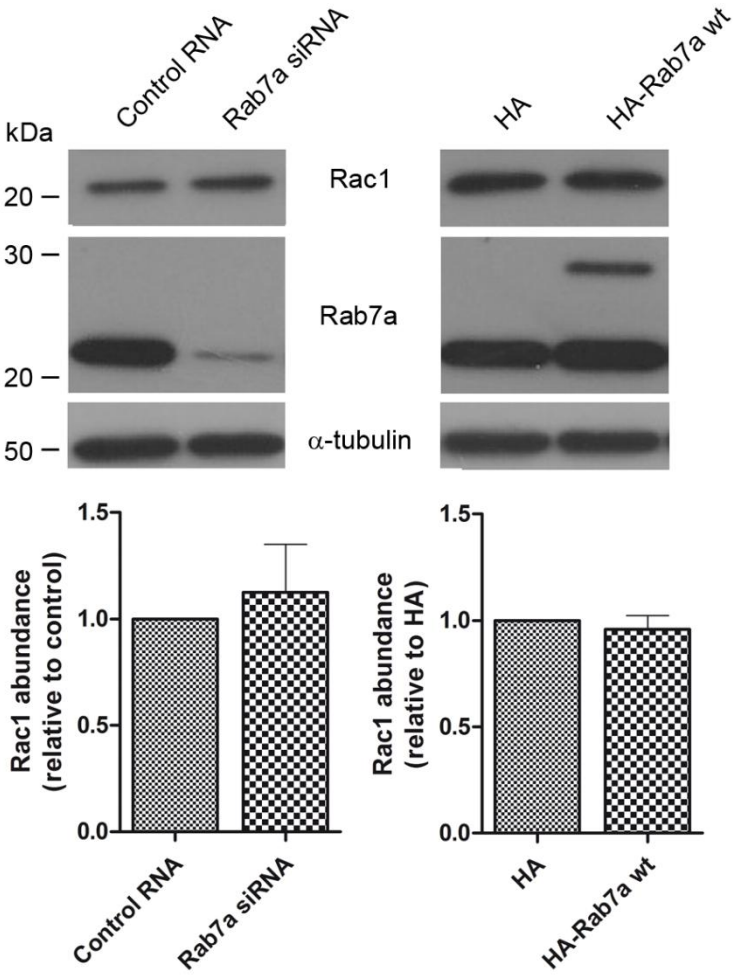

Figure 4.21 Rab7a does not alter Rac1 abundance. Lysates of control NCI H1299 cells or of cells either overexpressing or silenced for Rab7a were subjected to western blot analysis using anti-Rac1, anti-Rab7a and anti-tubulin antibodies. The migration of protein molecular weight size markers is indicated. Quantification of Rac1 abundance is shown. The intensities of the bands were quantified by densitometry, normalized against the amount of tubulin, and plotted relative to the intensities obtained in cells treated with control sample. Data represent the mean ± s.e.m. of at least three independent experiments.

Then, we studied the localization of Rac1 and Rab7a using live microscopy. We found that Rac1 and Rab7a co-localize on the same vesicles and move together in the cell (Figure 4.22; Figure 4.23; Movie 4). Furthermore, Rab7a co-localized with Rac1 in proximity of the plasma membrane and Rac1 was localized also at filopodia (Figure 4.22; Figure 4.23; Movie 4).

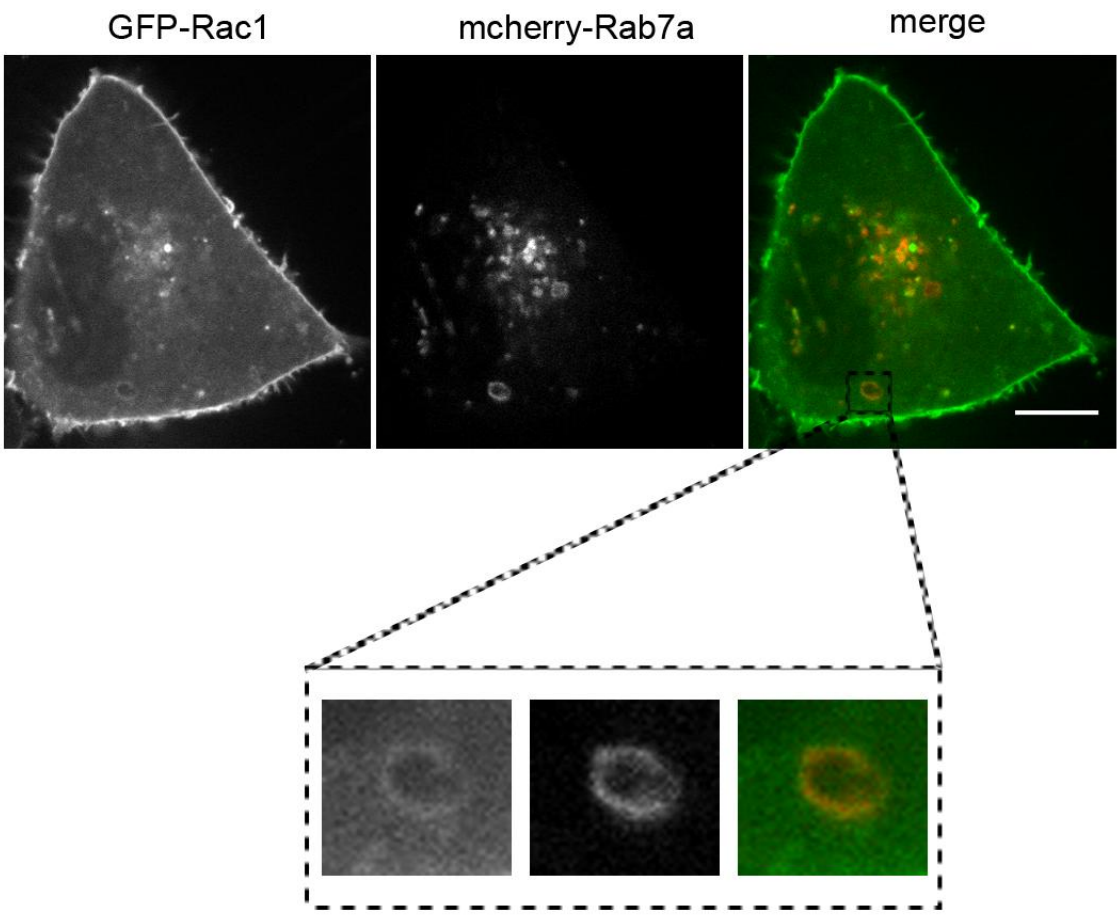

Figure 4.22 Rab7a and Rac1 overlap on the same vesicles. NCI H1299 cells co-transfected with GFP-Rac1 and mcherry-Rab7a were imaged with a Spinning Disk confocal microscope and enlargements of the indicated area are shown. Scale bar = 10 μm.

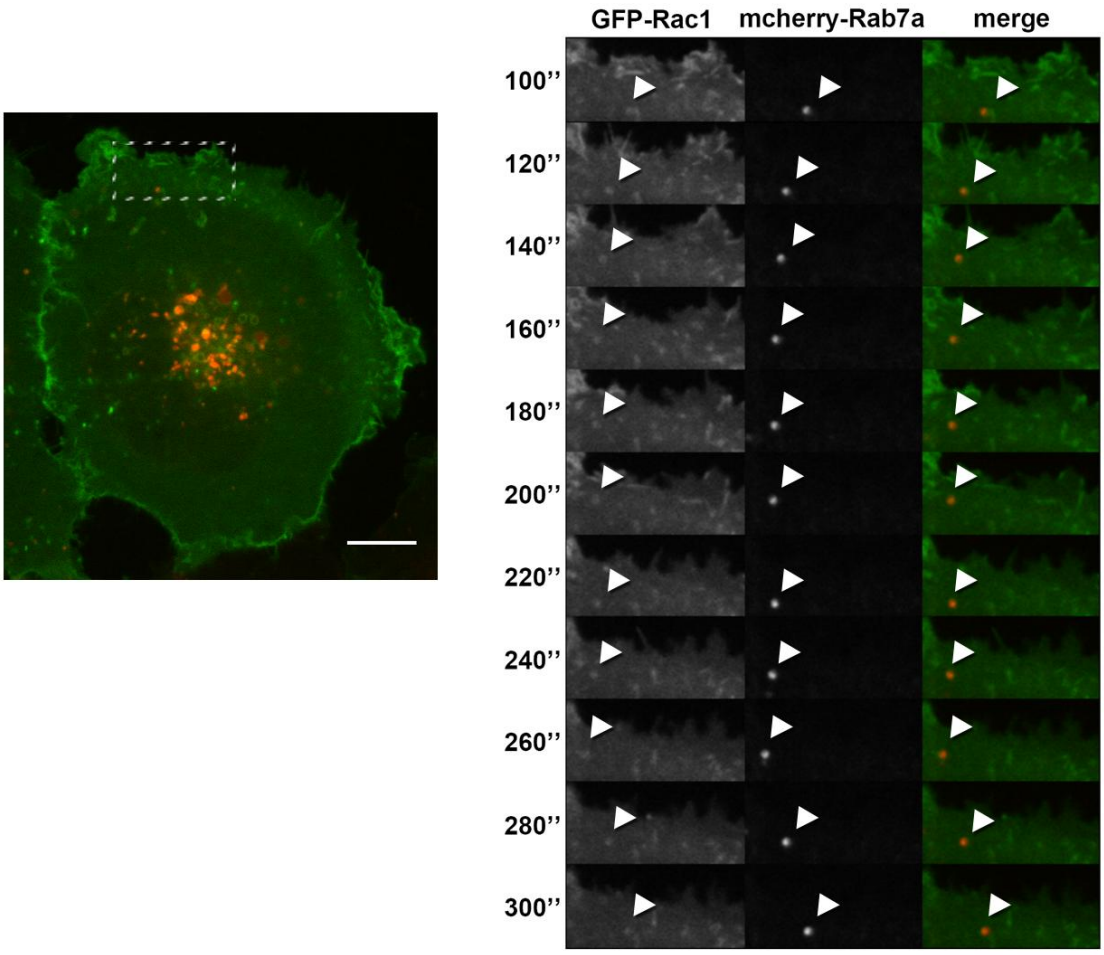

Figure 4.23 Rab7a and Rac1 move together. NCI H1299 cells co-transfected with GFP-Rac1 and mcherry-Rab7a were imaged with a Spinning Disk confocal microscope and enlargements of the indicated area are shown. Subsequent frames for the two channels and the merge are shown in the right panel. Scale bar = 10 μm.

4.1.9 Loss of Rab7a influences Rac1 activation state

Given that in β1-integrin-null nerves and Schwann cells Rac1 activation is impaired (Nodari *et al.*, 2007), we evaluated whether Rab7a could affect Rac1 activation through the regulation of β1 integrin trafficking. Therefore, we transfected NCI H1299 cells with control RNA or Rab7a siRNA and then we evaluated the amount of active Rac1 by performing a Rac1 activation assay. Interestingly, we detected lower levels of Rac1-GTP in Rab7a-depleted cells (Figure 4.24 A). Indeed, the amount of active Rac1 decreased of about 65% upon Rab7a silencing (Figure 4.24 B).

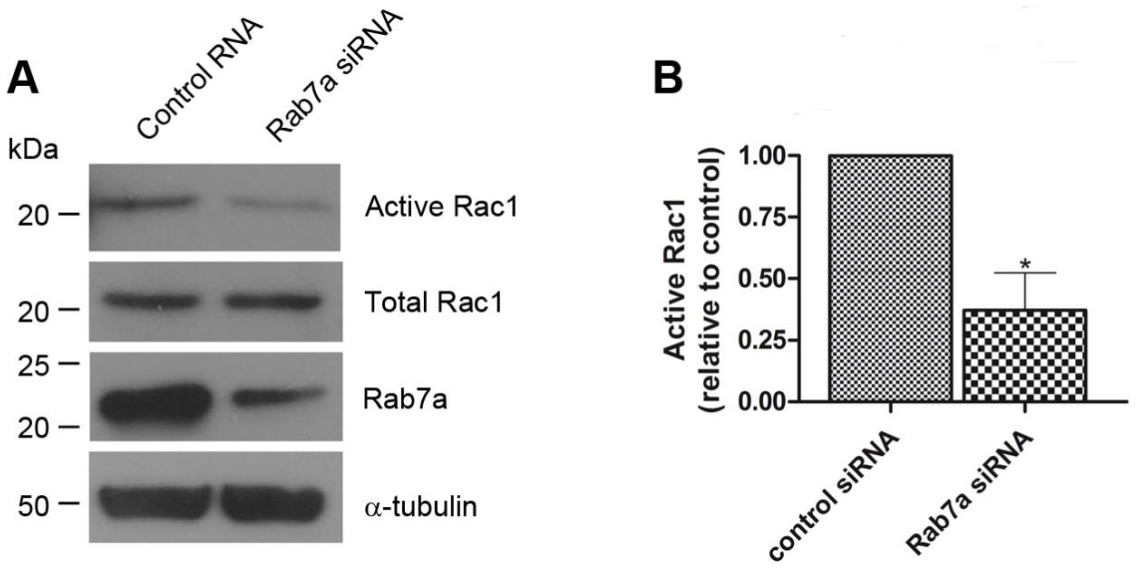

Figure 4.24 Rab7a modulates Rac1 activation state. (A) Lysates of NCI H1299 control or Rab7a-depleted cells were subjected to Rac1 activation assay and then subjected to western blot analysis using anti-Rac1, anti-Rab7a and anti-tubulin antibodies. The migration of protein molecular weight size markers is indicated. (B) Quantification of Rac1-GTP in control or Rab7a-depleted cells. The intensities of the bands were quantified by densitometry, normalized against the amount of total Rac1 and plotted relative to the intensities obtained in cells treated with control sample. Data represent the mean ± s.e.m. of three independent experiments.

4.1.10 Characterization of the interaction between Rab7a and vimentin

It has been previously shown that Rab7a interacts with vimentin and that depletion of Rab7a determined a lower phosphorylated state of the head domain of vimentin and a higher abundance of vimentin in the insoluble, filamentous fraction (Cogli *et al.*, 2013a). In addition, several reports showed a role of vimentin in cell migration (Gilles *et al.*, 1999; Bershadsky *et al.*, 1987; Homan *et al.*, 1998; Gonzales *et al.*, 2001; Sutoh Yoneyama *et al.*, 2014), therefore we investigated deeper the meaning of the interaction between Rab7a and vimentin by making deleted mutants of vimentin and studying its domain of interaction with Rab7a, and analyzing the role of Rab7a on vimentin and vice versa.

4.1.10.1 Construction of vimentin deleted mutants

Deleted mutants of vimentin were cloned in order to investigate the domain of interaction between Rab7a and vimentin. Based on the known structure of human vimentin protein, we decided to clone sequence fragments corresponding to one or two domains of the wild type protein: the N-terminal domain (head domain) plus the coil1 domain, the coil1 domain, the coil2 domain, the coil2 domain plus the C-terminal domain (tail domain), the head domain plus only the first coil that compose the coil1 domain (coil1A) (Table 4.1).

DELETED MUTANTS OF VIMENTIN	DOMAINS RETAINED IN THE MUTANT
VIMENTIN 1-256	HEAD - COIL1
VIMENTIN 92-256	COIL1
VIMENTIN 256-411	COIL2
VIMENTIN 256-466	COIL2 - TAIL
VIMENTIN 1-141	HEAD - COIL1A

Table 4.1 List of mutants of vimentin created and brief information on the amino acids and domains composing them.

These mutants were cloned into pCMV6-ENTRY Myc-tagged vector (Figure 4.25 A) by removing the fragment coding vimentin wt in pCMV6-ENTRY Myc-tagged vimentin wt plasmid (Figure 4.25 B) and adding the fragments coding the several vimentin deleted mutants.

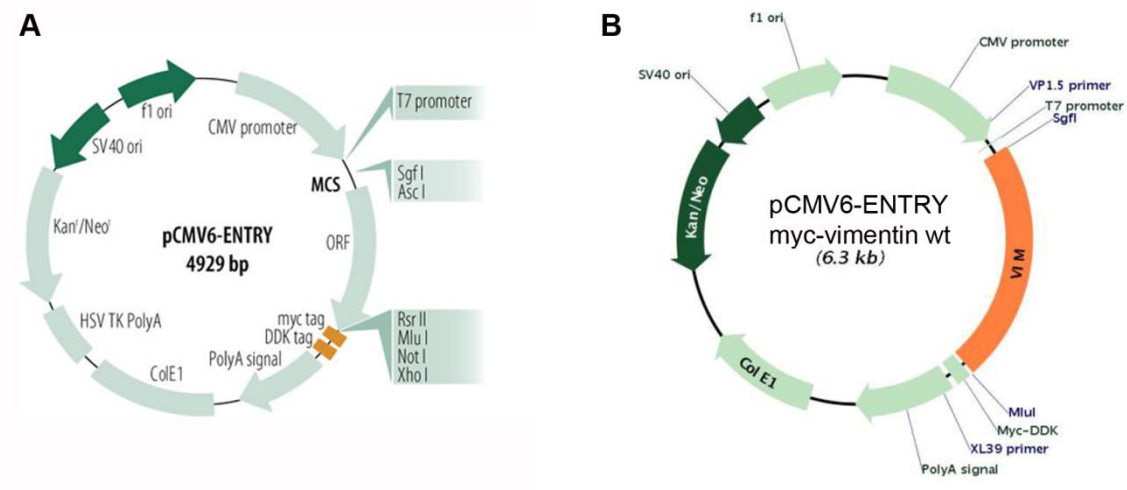

Figure 4.25 Map of the plasmid used in the cloning experiments. (A) Map of the pCMV6-ENTRY Myc-tagged vector. (B) Map of the pCMV6-ENTRY Myc-tagged vimentin wt plasmid which differs from (A) for the fragment encoding vimentin wt between the cloning sites AsiSI (a SgfI isoschizomer) and MluI. Both plasmids are characterized by a CMV promoter and a Kozak consensus sequence which drive protein expression in mammalian cells, a Myc- and DDK-tagged C-terminus of the ORF, and an antibiotic selection cassette (Neo^r/Kan^r) that confers resistance to kanamycin in *E. coli* and neomycin analogs in mammalian cells.

The coding regions of vimentin deleted mutants were amplified by PCR using synthetic oligonucleotides containing the AsiSI/MluI restriction sites, suitable for cloning into pCMV6-ENTRY Myc-tagged vimentin wt plasmid after removing of the vimentin wt fragment. PCR products were then purified as described in "Matherial and Methods". Figure 4.26 shows the cloning strategy for the deleted mutants of vimentin and the PCR products separated on 1% agarose gel (Figure 4.26 A-B). After digestion with the restriction enzymes, the PCR products were purified from impurities and inserted into the AsiSI/MluI linearized pCMV6-ENTRY Myc-tagged plasmid (obtained from pCMV6-ENTRY Myc-tagged vimentin wt plasmid which lost the vimentin wt fragment during digestion and purified as the PCR products) (Figure 4.26 C).

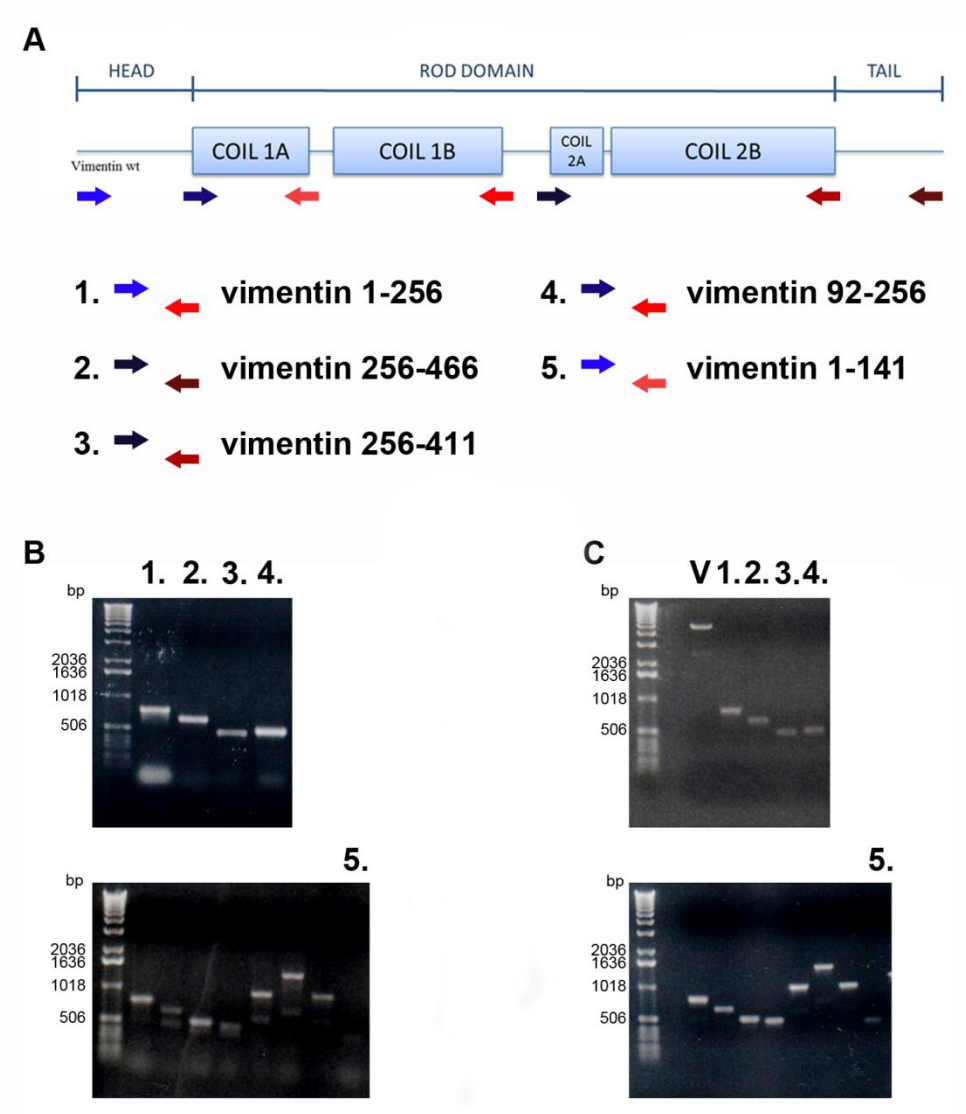

Figure 4.26 Cloning strategy for human vimentin deleted mutants. (A) Scheme of the cloning strategy used. (B) The PCR products are shown in the 1% agarose gels prior to purification. PCR products refers to vimentin deleted mutants as indicated in A. (C) The PCR

products are shown in the 1% agarose gels after purification. PCR products refers to vimentin deleted mutants as indicated in A. V is the linearized vector.
After digestion, PCR products were ligated to the linearized vector in order to have the plasmids coding for the vimentin deleted mutants. Ligation products were used to transform *E. coli* DH5α. Colony screening and DNA sequencing provided the final products (Figure 4.27).

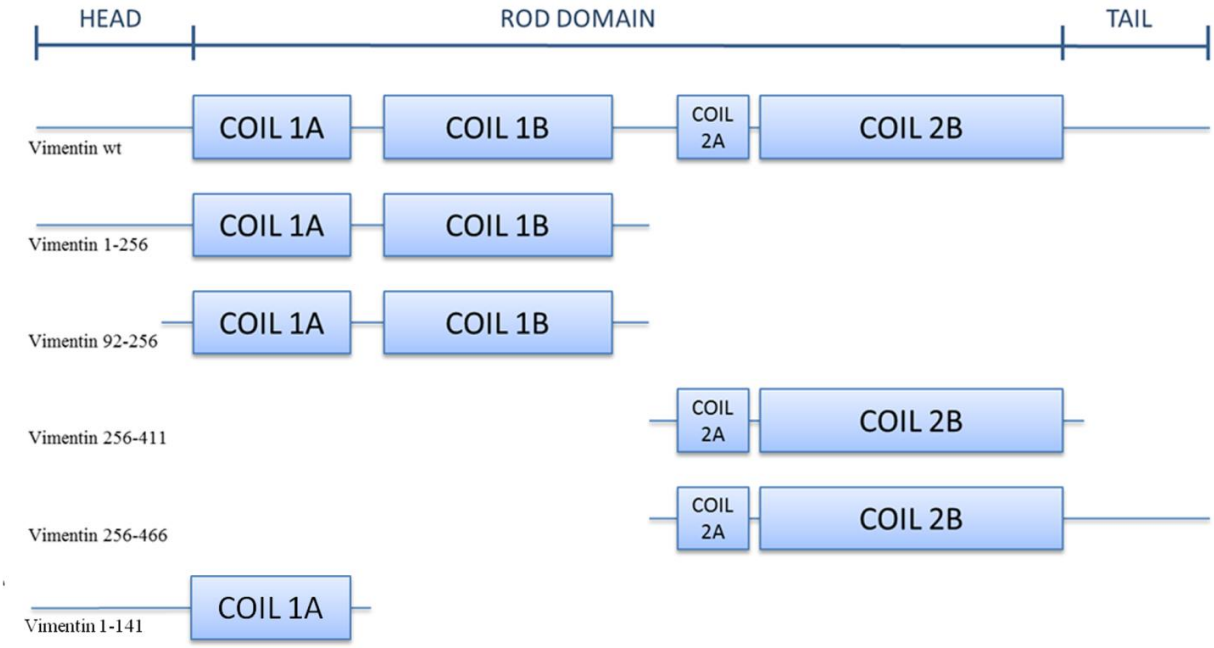

Figure 4.27 Scheme representing the vimentin mutants created. Vimentin 1-256 mutant contains the head domain plus the coil1 domain, vimentin 92-256 mutant contains only the coil1 domain, vimentin 256-411 mutant is composed by only the coil2 domain, vimentin 256-466 mutant contains the coil2 domain plus the tail domain, vimentin 1-141 mutant is composed by the head domain plus coil1A domain.

4.1.10.2 Rab7a interacts with coil1A vimentin domain

In order to investigate the vimentin domain of interaction with Rab7a co-immunoprecipitation assays were performed. HeLa cells were co-transfected with HA-tagged Rab7a wt and myc-tagged wt or mutated vimentin. Cells were lysed after 24 hours of transfection and lysates were subjected to co-immunoprecipitation assay by using anti-HA monoclonal antibody covalently attached to crosslinked agarose beads. Samples were then used for SDS-PAGE and western blotting analysis. The membrane was incubated with antibodies against myc and HA tags. We found that Rab7a interacts with vimentin 1-466 (wt), vimentin 1-256 and vimentin 92-256, but not with vimentin 256-411 and vimentin 256-466. Therefore, we demonstrated that Rab7a interacts with coil1 of vimentin (Figure 4.28, left panel). We investigated whether Rab7a was able to interact with another mutant of vimentin (1-141) which lacks the second half of coil1. As

shown in the right panel of the Figure 4.28, Rab7a interacted also with vimentin 1-141, proving that the vimentin domain which interact with Rab7a is coil1A (Figure 4.28).

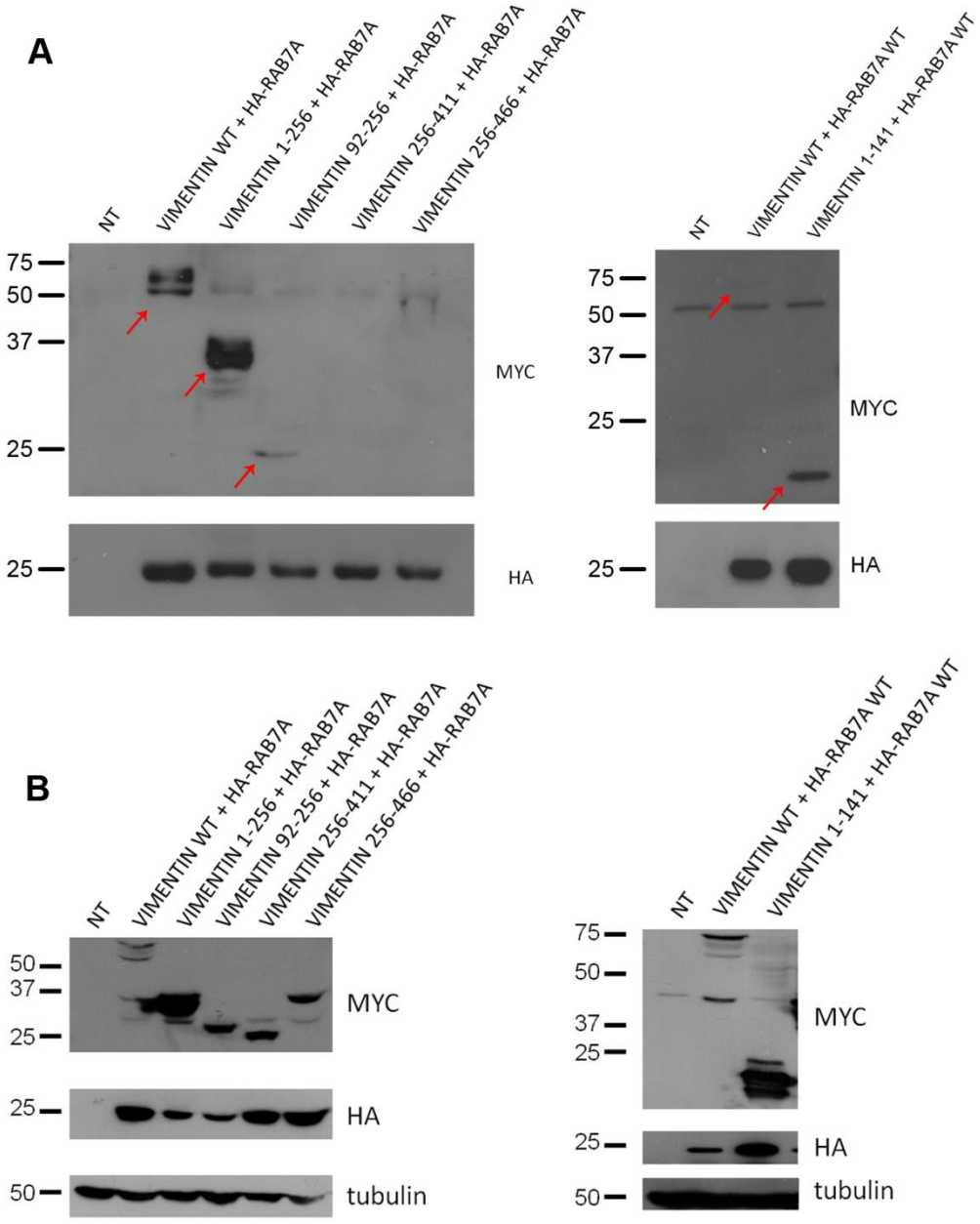

Figure 4.28 Rab7a interacts with coil1A of vimentin. Lysates of HeLa cells overexpressing HA-Rab7a and wt or mutated myc-vimentin as indicated in the picture were subjected to co-immunoprecipitation assay. Samples were then loaded on acrylamide gel. Proteins were transferred onto PVDF membrane and incubated with antibodies against HA and myc tags. (A) IP. (B) WB.

4.1.10.3 Vimentin depletion affects Rab7a abundance

Given that Rab7a interacts with coil1A domain of vimentin and that depletion of Rab7a alters the phosphorylation state and assembly of vimentin, we investigated whether vimentin could have a role on Rab7a abundance. Therefore we evaluated whether depletion of vimentin could affect

Rab7a abundance. NCI H1299 control cells or cells silenced for vimentin were lysed after 72 hours from transfection and lysates were subjected to western blot analysis using anti-vimentin, anti-tubulin and anti-Rab7a antibodies (Figure 4.29 A). Vimentin siRNA efficiency in silencing was proved (Figure 4.29 B). After depletion of vimentin, Rab7a abundance decreased (Figure 4.29 C), proving that vimentin is able to modulate the levels of Rab7a protein.

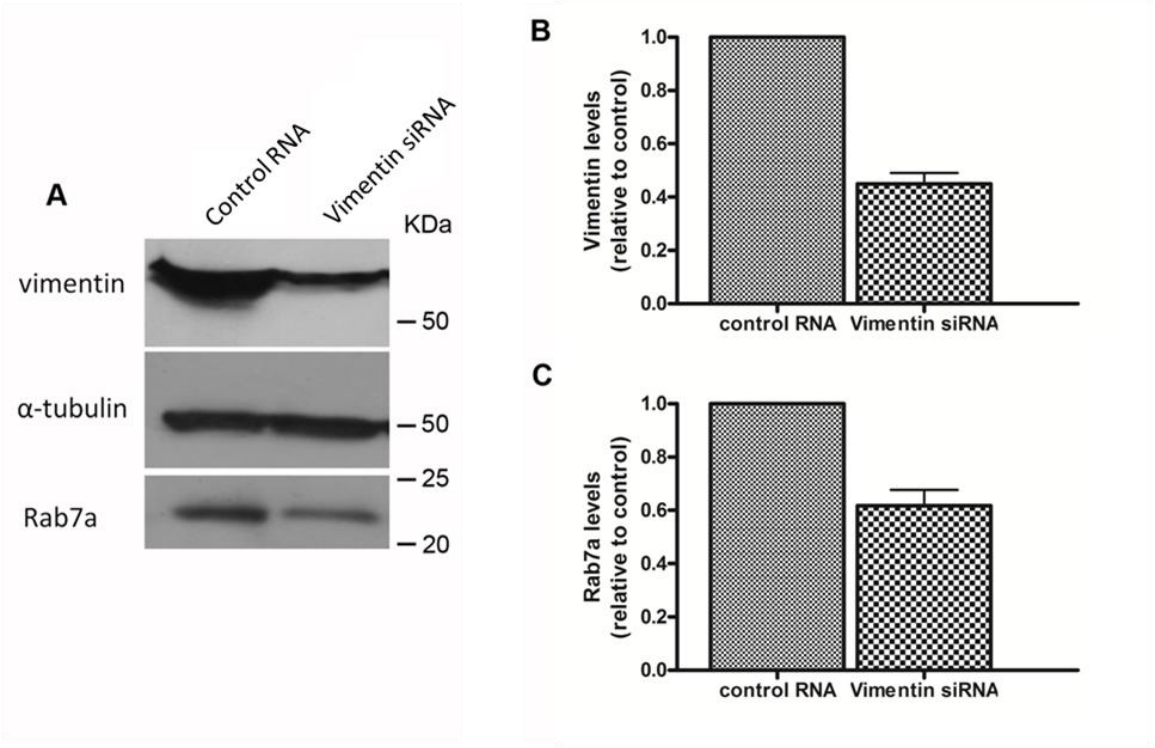

Figure 4.29 Vimentin depletion alters Rab7a abundance. (A) Lysates of NCI H1299 transfected either with control RNA (scr) or vimentin siRNA (siRNA VIM) were subjected to western blot analysis using anti-vimentin, anti-Rab7a and anti-tubulin antibodies. The migration of protein molecular weight size markers is indicated. (B) Quantification of vimentin abundance is shown. The intensities of the bands were quantified by densitometry, normalized against the amount of tubulin, and plotted relative to the intensities obtained in cells treated with control RNA. Data represent the mean ± s.e.m. of three independent experiments. (C) Quantification of Rab7a abundance is shown. The intensities of the bands were quantified by densitometry, normalized against the amount of tubulin, and plotted relative to the intensities obtained in cells treated with control RNA. Data represent the mean ± s.e.m. of three independent experiments.

4.1.11 Rab7a regulates vimentin filaments orientation during cell migration

We proved that Rab7a interacts with coil1A domain of vimentin and that vimentin modulates Rab7a protein levels. Moreover, Rab7a regulates vimentin phosphorylation state and assembly (Cogli *et al.*, 2013a). Furthermore, it has been demonstrated that vimentin regulates Rac1 activation whereas activation of Rac1 induces vimentin phosphorylation and disassembly (Havel

et al., 2015; Meriane *et al.*, 2000; Lee *et al.*, 2001; Helfand *et al.*, 2011). As both Rab7a and Rac1 regulate vimentin assembly and since it has previously been shown that vimentin filaments are re-oriented towards the leading edge during migration (Sakamoto *et al.*, 2013), we investigate whether vimentin filament orientation was impaired in Rab7a-depleted cells in a wound healing assay. Thus, we transfected NCI H1299 cells with either control RNA or Rab7a siRNA and after 24 hours from transfection, cells were confluent and therefore subjected to wound-healing assay. After three hours from the start of the assay a new scratch was made (to be considered as initial time point when cells are not migrating yet) and cells were permeabilized, fixed and stained with anti-vimentin antibody and Hoechst (Figure 4.30 A). We observed that in control non-migrating cells there was about 50% of cells showing vimentin facing the wound, whereas after 3 hours about 85% of cells had vimentin oriented towards the leading edge. Therefore, there was an increment of about 60% of the number of cells with vimentin facing the wound compared to the cells before migration. Interestingly, this value was much lower in Rab7a-depleted cells, where only 66% of migrating cells (after 3 hours) showed oriented vimentin compared to the 55% of Rab7a-depleted cells at the initial time point (0 hours). The increment of the number of cells with vimentin facing the wound was ~ 25% in cells silenced for Rab7a (Figure 4.30 B). These data demonstrate that Rab7a is important for vimentin filaments re-orientation during migration.

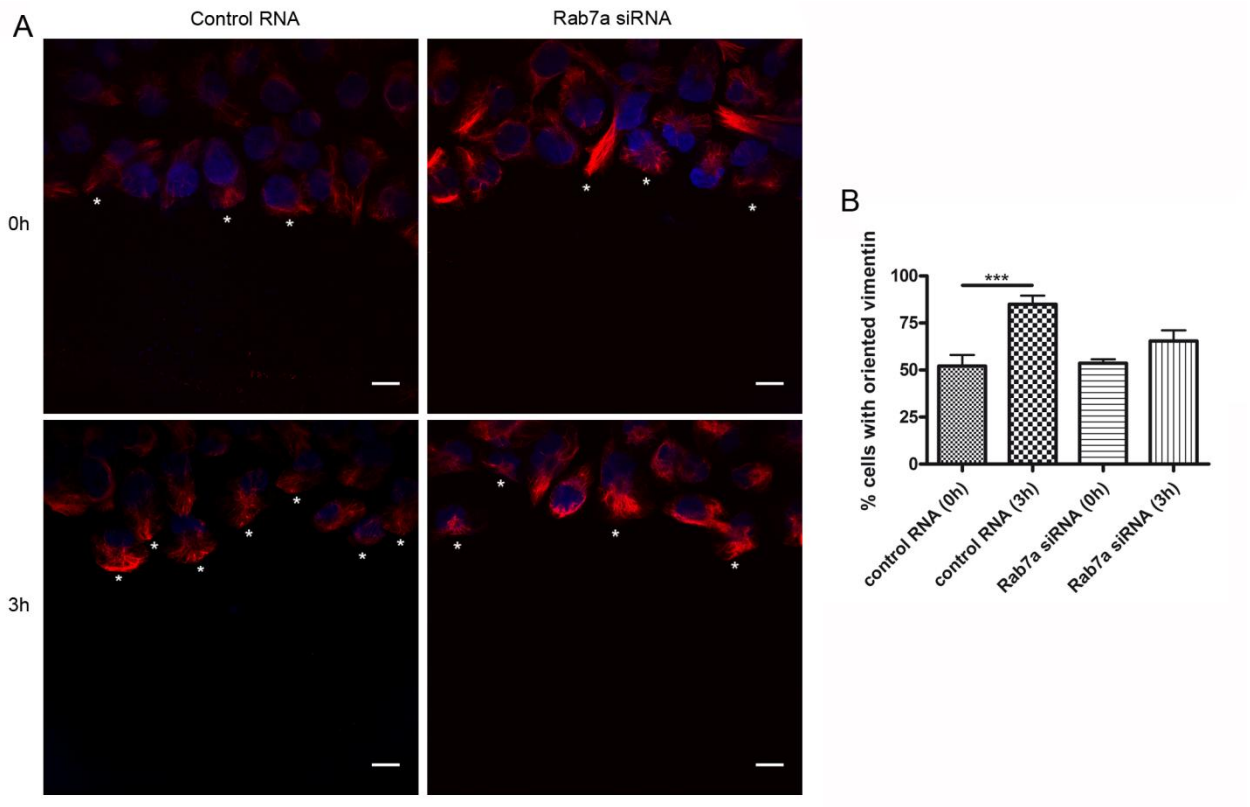

Figure 4.30 Rab7a impairs vimentin filaments reorganization and re-orientation during migration. (A) NCI H1299 cells transfected with control RNA or siRNA against Rab7a were stained after wound healing assay with vimentin (red) and Hoechst (blue). Images refer to wounds made at two different time points before the permeabilization and fixation steps: 0 hours indicates non-migrating cells and 3 hours indicate migrating cells. * indicates a polarized cell with vimentin filaments oriented into the direction of the wound. Scale bar = 10 µm. (B) Quantification of the percentage of cells with oriented vimentin in control and Rab7a-depleted cells at the initial (0 hours) and final (3 hours) time points (n=50).

4.1.12 Rab7a is localized in the area of the cell facing the wound during migration

Given that Rab7a could affect vimentin filaments re-orientation during migration we evaluated the localization of Rab7a in NCI H1299 migrating cells. Therefore, we transfected NCI H1299 cells with a construct coding for GFP-Rab7a and we performed a wound healing assay. Interestingly, we found that about 80% of Rab7a-positive vesicles in migrating cells expressing GFP-Rab7a were localized between the nucleus and the leading edge, facing the wound (Figure 4.31).

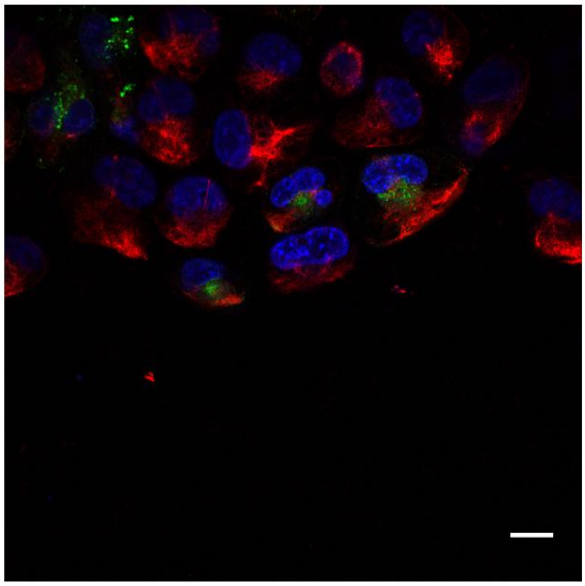

Figure 4.31 Rab7a localizes between the nucleus and the leading edge. (A) NCI H1299 cells transfected with GFP-Rab7a wt were subjected to wound healing assay and permeabilized, fixed and stained after three hours with anti-vimentin antibody (red) and Hoechst (blue). Scale bar = 10 µm.

4.2 STUDY ON THE ROLE OF RAB7A MUTANTS IN CELL MIGRATION

We demonstrated that Rab7a is an important player in cell migration. Mutations in Rab7a might alter Rab7a functions. For instance, specific mutations in Rab7a lead to the onset of the Charcot-Marie-Tooth 2B neuropathy. Moreover, studying the functions of mutated proteins increases the knowledge on the role of the wild type protein by comparison and defines the importance of a specific domain in interactions or functions. We therefore created some Rab7a mutants in order to understand more the role of Rab7a in cell migration. In addition, we evaluated the role of CMT2B-associated Rab7a mutants in some aspects of cell migration. In fact, it is still not known the molecular mechanism underlying the onset of CMT2B and it is not clear how specific mutations in an ubiquitous protein, such as Rab7a, lead to a disease that affects specifically peripheral neurons.

4.2.1 Construction of HA-Rab7a mutants

In order to investigate deeper the role of Rab7a in cell migration we created mutated Rab7a proteins. Rab7a protein is composed by several α helices and β sheets. Rab-conserved sequences have been defined and named Rab family (RabF) motifs. They were used as diagnostic Rab sequences in order to define a Rab protein on the basis of its primary structure. In particular, five RabF motifs have been found. Moreover, RabF regions cluster in and around switch I and switch II regions which are involved in the conformational change upon GDP or GTP binding (Pereira-Leal and Seabra, 2000). Based on this and on several data on the structure and the interaction of Rab GTPases with effectors, Pereira-Leal and Seabra proposed a model where effectors bind not only to RabF regions to discriminate between nucleotide-bound states but also to other regions that confer specificity to the interaction. Pereira-Leal and Seabra defined these regions as Rab subfamily (RabSF) regions (Pereira-Leal and Seabra, 2000) (Figure 4.32).

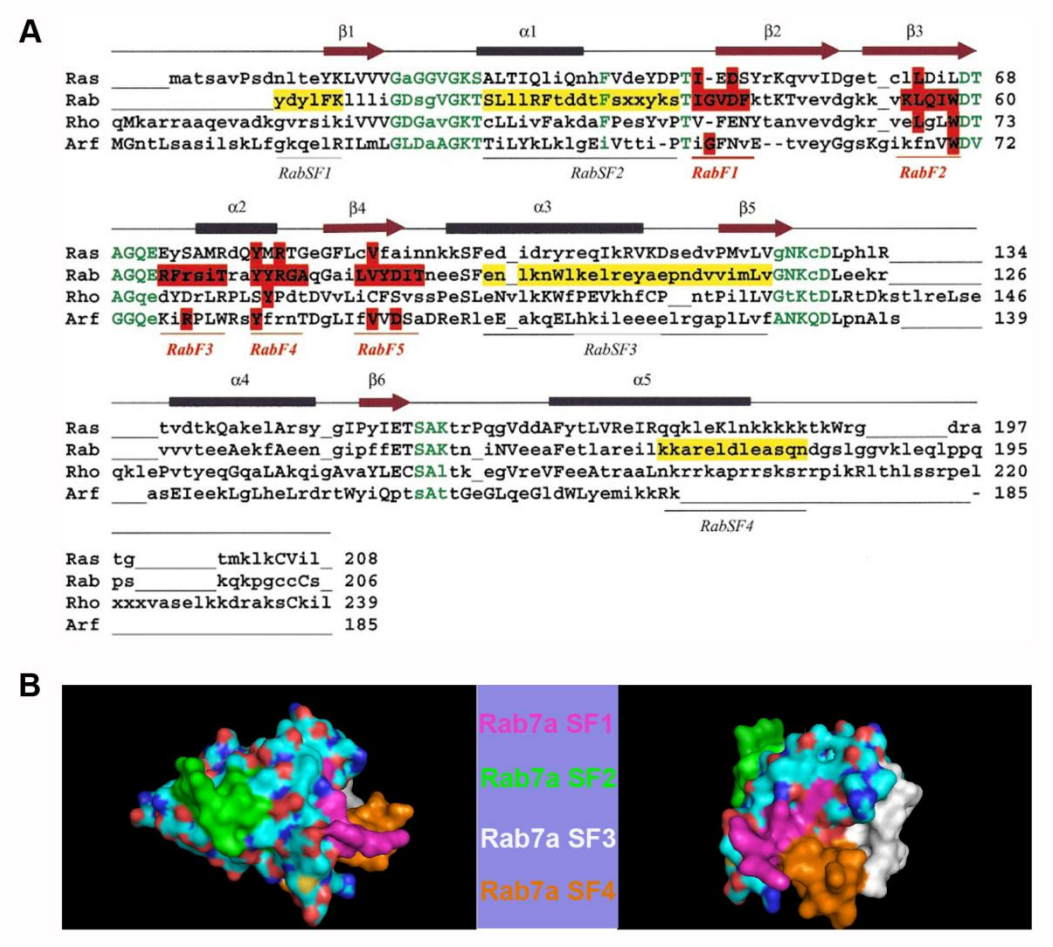

Figure 4.32 Rab family and Rab subfamily regions. (A) Alignment of Ras, Rab, Rho and Arf model sequences. α helices, β sheets, RabFs and RabSFs are indicated (Pereira-Leal and Seabra, 2000). (B) Representation of Rab7a protein structure by using PyMol software. RabSF1, RabSF2, RabSF3 and RabSF4 are indicated with different colours as illustrated (based on the crystallographic data on GDP-bound Rab7a protein).

Rab7a exerts its functions through the interaction with several effectors. In order to investigate deeper the functions of Rab7a mediated by interactions with effector proteins, we created Rab7a proteins mutated in RabSF regions. Moreover, as deletion of part of Rab7a involved in α helices and β sheets could lead to alterations in the protein conformation or function, we created two deleted mutants lacking the N-terminal domain or the C-terminal domain where the RabSF1 and RabSF4 regions have place, respectively. Instead, we created mutants with point mutations in the RabSF2 and RabSF3 regions focusing on amino acids that were predicted to be on the surface of the Rab7a protein according to studies conducted by using PyMol software and available crystallographic data. This was made in order to possibly create mutants that weren't able to interact with some Rab7a effectors and therefore could disrupt Rab7a functions. Therefore the point mutations generated affected the codons so that the coded new amino acids had different biochemical properties (Table 4.2).

RAB7A MUTANTS WITH POINT MUTATION	DELETED MUTANTS OF RAB7A	RabSF involved in the mutation
	Rab7a 11-207	RabSF1
Rab7a N30A (asparagine to alanine)		RabSF2
Rab7a S34I (serine to isoleucine)		RabSF2
Rab7a S111G (serine to glycine)		RabSF3
Rab7a N117A (asparagine to alanine)		RabSF3
Rab7a K175E (lysine to glutamate)		RabSF4
	Rab7a 1-176	RabSF4

Table 4.2 List of mutants of Rab7a created and brief information on the amino acids and RabSF involved.

In order to create the Rab7a mutants with point mutations we used site-directed mutagenesis. Complementary oligonucleotide primers, containing the point mutation, were used in the mutagenesis reaction, together with the plasmid containing the DNA coding the wild type protein (parental DNA template). This plasmid derived from the pcDNA3 vector (Figure 4.33 A). HA tag and the DNA coding Rab7a (*Canis familiaris*) were cloned in this vector, thus creating the plasmid that was used in site-directed mutagenesis (Figure 4.33 B). PCR reaction was carried out as indicated in "Matherial and Methods" section. PCR products were then treated with DpnI enzyme. DpnI endonuclease is specific for mehtylated and hemimethylated DNA and digested the parental DNA template, thus selecting for mutation-containing synthesized DNA. In fact, the plasmid containing the DNA coding for the wild type protein, which was used as parental DNA template, was previously isolated from dam^+ *E. coli* strain (DH5α), thus it was methylated and susceptible to DpnI digestion.

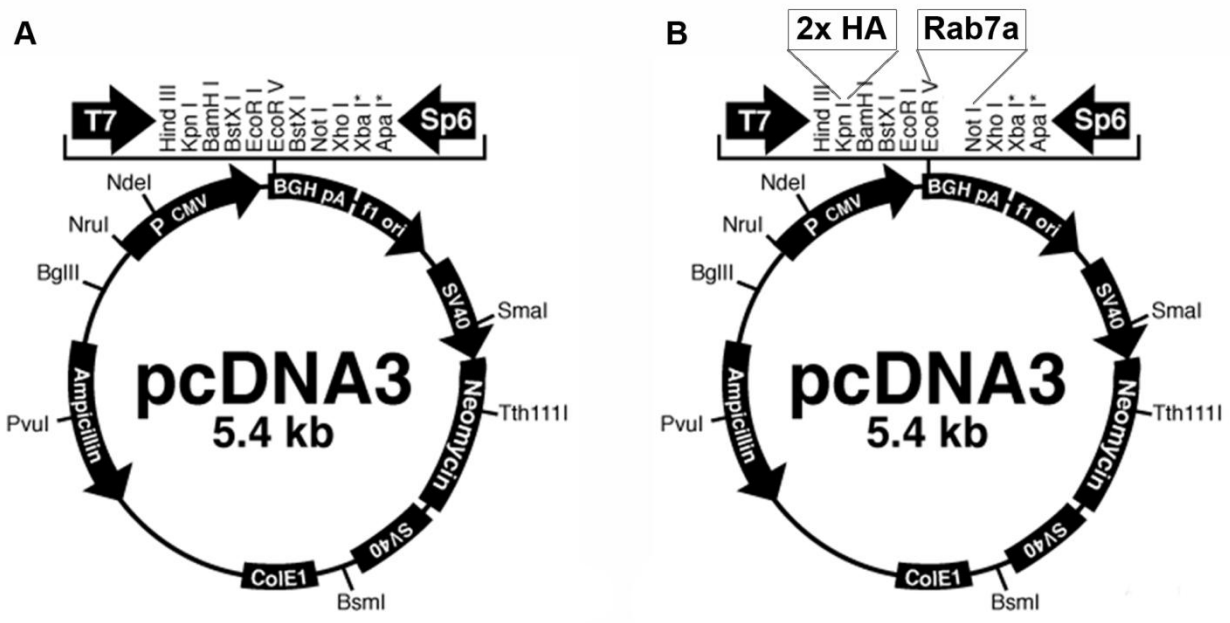

Figure 4.33 Map of the plasmid used in the site-directed mutagenesis experiments. (A) Map of the pcDNA3 vector. (B) Map of the pcDNA3 2xHA-tagged Rab7a wt plasmid which differs from A for the fragment encoding 2xHA tag between the cloning sites KpnI/KpnI and the fragment encoding Rab7a wt between the cloning sites EcoRV and NotI. Both plasmids are characterized by a CMV promoter which drives protein expression in mammalian cells and antibiotic selection cassettes that confer resistance to ampicillin in *E. coli* and neomycin analogs in mammalian cells.

Competent *E. coli* DH5α cells were transformed with the circular, nicked dsDNA obtained after the digestion step and were plated on LB-agar containing ampicillin. After transformation, the competent cells repaired the nicks in the mutated plasmids that were then isolated from the bacteria through mini-preparation of DNA as described in "Material and Methods" section.

DNA sequencing verified the presence of the mutated amino acid.

In order to create deleted mutants of Rab7a, we designed specific primers containing the EcoRV/NotI restriction sites there were able to amplify the region of interest of Rab7a wt. These mutants were cloned into pcDNA3 2xHA Rab7a wt (Figure 4.33 B) by removing the fragment coding for Rab7a wt and adding the fragments coding for the Rab7a deleted mutants.

The coding regions of Rab7a deleted mutants were amplified by PCR using synthetic oligonucleotides. PCR products were then purified as described in "Matherial and Methods". After digesting PCR products and the acceptor plasmid (Figure 4.33 B) with the restriction enzymes (EcoRV and NotI), a purification step was performed. Digested PCR products were inserted into the EcoRV/NotI linearized pcDNA3 2xHA plasmid with a ligation reaction. We transformed the ligation products into *E. coli* cells and obtained the final products after colony screening and DNA sequencing (Figure 4.34).

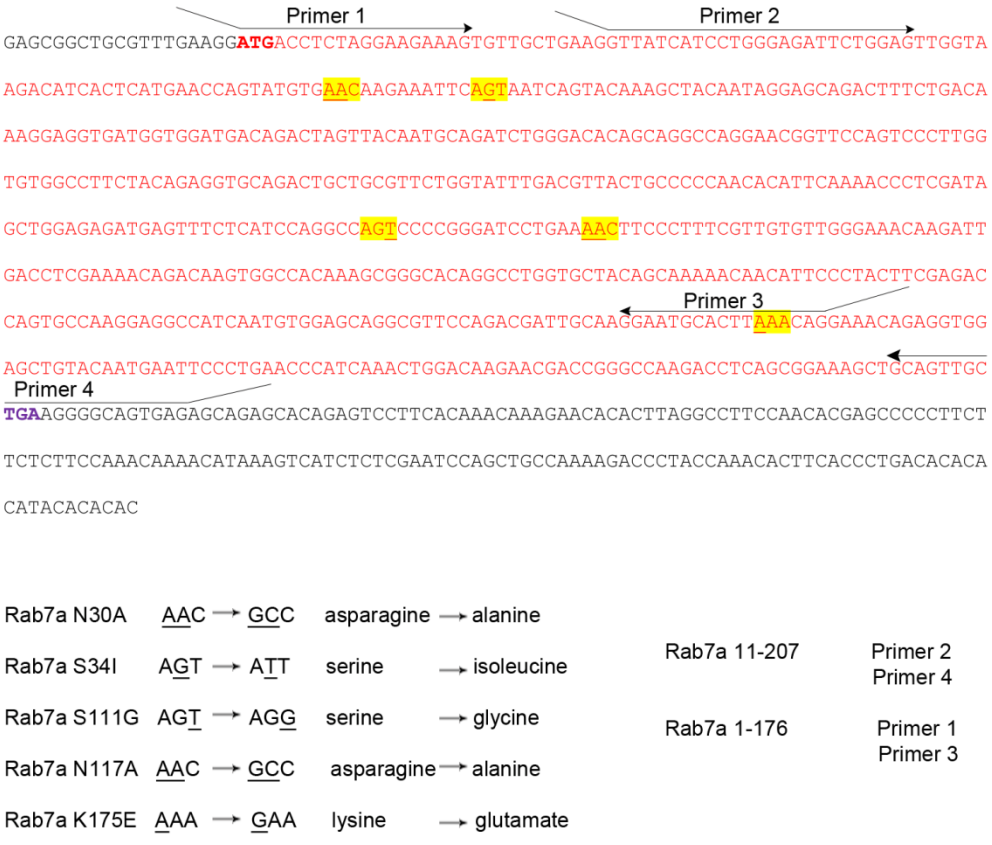

Figure 4.34 Scheme representing the Rab7a mutants created. mRNA sequence of Rab7a (NCBI Reference sequence: NM_001003316.1). CDS in red. Codons and bases that have been mutated in site-directed mutagenesis experiments are highlighted and underlined, respectively. Primers that have been used to make Rab7a deleted mutants are shown.

4.2.2 Expression of HA-Rab7a mutants

After having made the Rab7a mutants, we tested their expression in HeLa cells. The dominant negative Rab7a mutant (Rab7a T22N) and the active Rab7a mutant (Rab7a Q67L) were used as controls. Cells were lysed and lysates were analyzed by western blot using antibodies against HA and tubulin. The mutant HA-Rab7a 11-207 showed low expression (Figure 4.35).

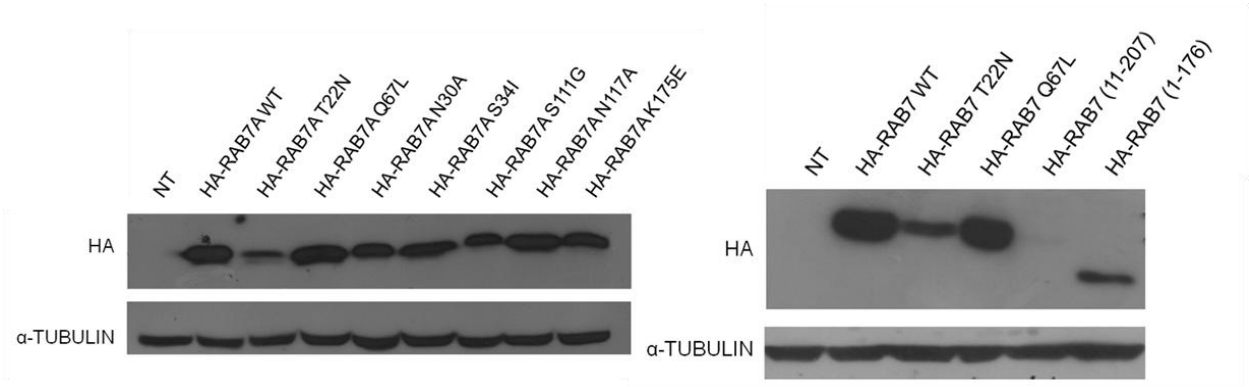

Figure 4.35 Rab7a 11-207 mutant shows low expression. Lysates of control HeLa cells or of cells expressing wt or mutated Rab7a were subjected to western blot analysis using anti-HA and anti-tubulin antibodies.

4.2.3 Rab7a mutants expression does not impair cell adhesion

As Rab7a has an important role in cell migration we investigated whether the expression of Rab7a mutants were able to re-induce cell spreading onto fibronectin after Rab7a knock down as we demonstrated for the wild type protein. Therefore, NCI H1299 Rab7a-depleted cells expressing wt or mutated Rab7a were subjected to adhesion assay. Cells were seeded on fibronectin-treated coverslips and after 30 min cells were fixed, permeabilized and stained by Rhodamine-conjugated phalloidin in order to look at the actin cytoskeleton and anti-HA antibody. The average cell area was calculated and we didn't notice any differences between the recovery of the function mediated by either wt or mutated Rab7a (Figure 4.36).

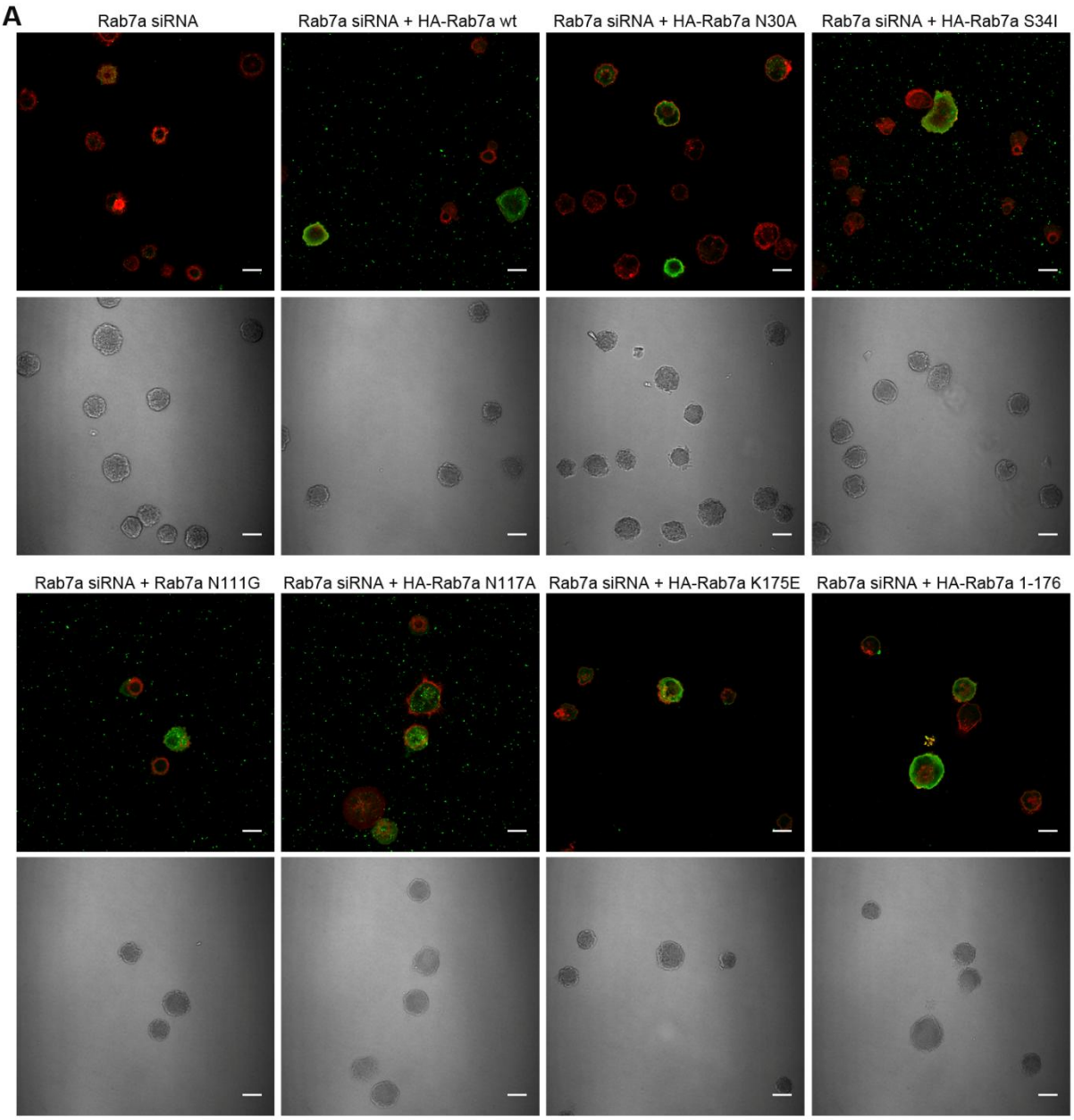
A
Rab7a siRNA
Rab7a siRNA + HA-Rab7a wt
Rab7a siRNA + HA-Rab7a N30A
Rab7a siRNA + HA-Rab7a S34I
Rab7a siRNA + Rab7a N111G
Rab7a siRNA + HA-Rab7a N117A
Rab7a siRNA + HA-Rab7a K175E
Rab7a siRNA + HA-Rab7a 1-176

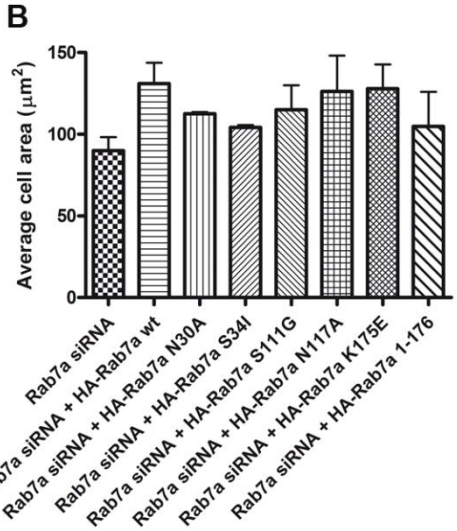
B
Average cell area (μm²)
150
100
50
0
Rab7a siRNA
Rab7a siRNA + HA-Rab7a wt
Rab7a siRNA + HA-Rab7a N30A
Rab7a siRNA + HA-Rab7a S34I
Rab7a siRNA + HA-Rab7a S111G
Rab7a siRNA + HA-Rab7a N117A
Rab7a siRNA + HA-Rab7a K175E
Rab7a siRNA + HA-Rab7a 1-176

Figure 4.36 Rab7a mutants act in a similar way to Rab7a wt. A) NCI H1299 cells transfected with siRNA against Rab7a or depleted for Rab7a and transfected afterward with HA-Rab7a wt, HA-Rab7a N30A, HA-Rab7a S34I, HA-Rab7a S111G, HA-Rab7a N117A, HA-Rab7a K175E or HA-Rab7a 1-176 were plated on fibronectin-coated coverslips and left to adhere for 30 minutes. Samples were subsequently fixed and stained with Rhodamine-conjugated phalloidin and anti-HA antibody. Confocal images of each sample were taken and subsequently analyzed. Relative transmission images are shown. B) Quantification of the average area (in μm^2) of NCI H1299 cells transfected as described in A after 30 minutes of adhesion on fibronectin. Data represent the mean ± s.e.m. of two different experiments.

4.2.4 Rab7a CMT2B mutants behave like the wild type protein in cell adhesion assays

Specific mutations in Rab7a are responsible for the onset of CMT2B disease (Meggouh *et al.*, 2006; Houlden *et al.*, 2004; Verhoeven *et al.*, 2003; Wang *et al.*, 2014). As Rab7a-dependent lysosomal degradation affected the final phase of migration of immature neurons during the development of cerebral cortex *in vivo* (Kawauchi *et al*., 2010; Kawauchi, 2011), we decided to investigate whether CMT2B-associated Rab7a proteins were able to re-induce cell spreading onto fibronectin after Rab7a knock down as the wild type protein. NCI H1299 Rab7a-depleted cells expressing the CMT2B-causing Rab7a mutants acted in a similar way of the Rab7a wild type protein (Figure 4.37).

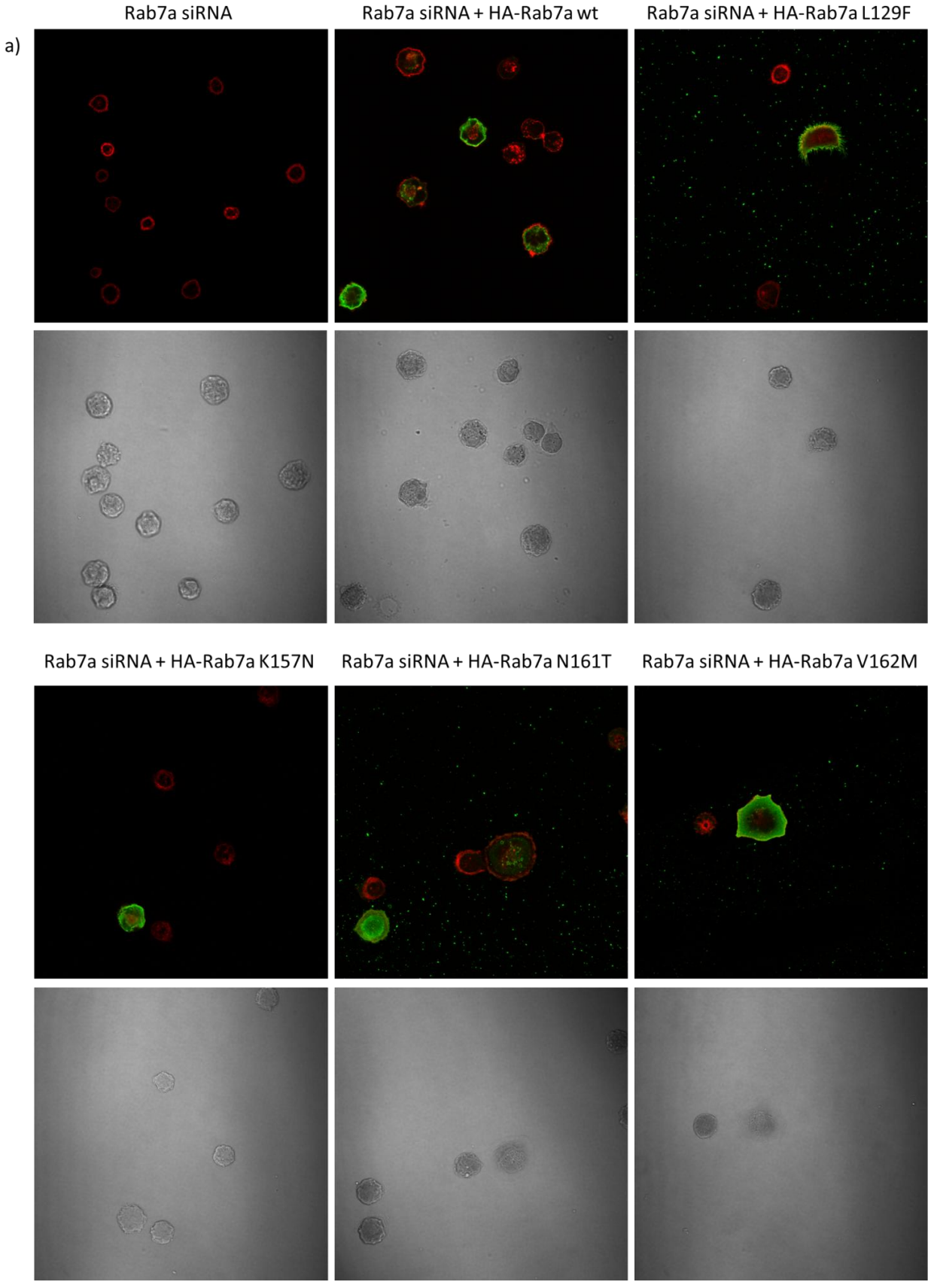
a)
Rab7a siRNA
Rab7a siRNA + HA-Rab7a wt
Rab7a siRNA + HA-Rab7a L129F
Rab7a siRNA + HA-Rab7a K157N
Rab7a siRNA + HA-Rab7a N161T
Rab7a siRNA + HA-Rab7a V162M

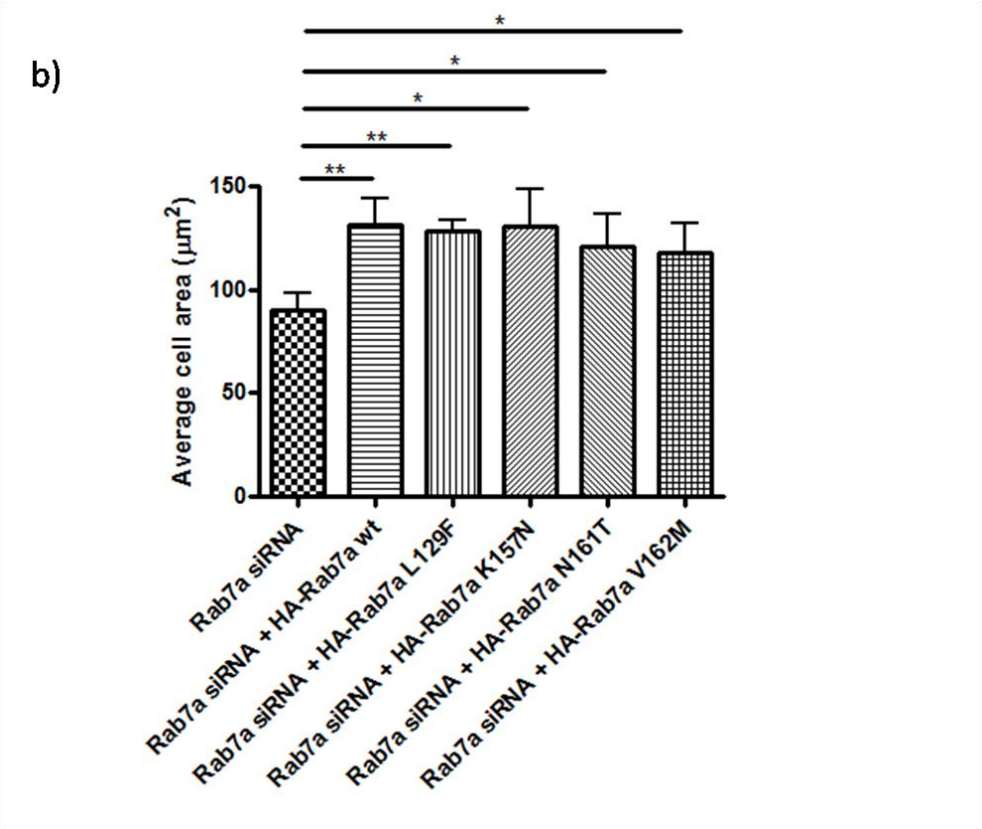

Figure 4.37 CMT2B-associated Rab7a mutants act in a similar way to Rab7a wt. a) NCI H1299 cells transfected with siRNA against Rab7a or depleted for Rab7a and transfected afterward with HA-Rab7a wt, HA-Rab7a L129F, HA-Rab7a K157N, HA-Rab7a N161T or HA-Rab7a V162M were plated on fibronectin-coated coverslips and left to adhere for 30 minutes. Samples were subsequently fixed and stained with Rhodamine-conjugated phalloidin and anti-HA. Confocal images of each sample were taken and subsequently analyzed. Relative transmission images are shown. b) Quantification of the average area (in μm^2) of NCI H1299 cells transfected as described in a) after 30 minutes of adhesion on fibronectin. Data represent the mean ± s.e.m. of at least three different experiments.

4.2.5 CMT2B-associated Rab7a mutants do not alter vimentin reorientation during migration

As Rab7a regulates vimentin re-orientation during migration we wondered whether the expression of these mutant proteins prevented vimentin filaments reorientation in wound healing assay. Therefore, we expressed wt or mutated GFP-Rab7a and we performed a wound healing assay. After three hours from the start of the assay, a new wound was made and cells were permeabilized, fixed and stained with anti-vimentin antibody and Hoechst (Figure 4.38). We quantified the percentage of cells with vimentin oriented in the direction of the wound after 3 hours of migration and at 0 hours of migration (non-migrating cells). We observed that Rab7a mutants didn't interfere with vimentin filaments reorganization (Figure 4.39).

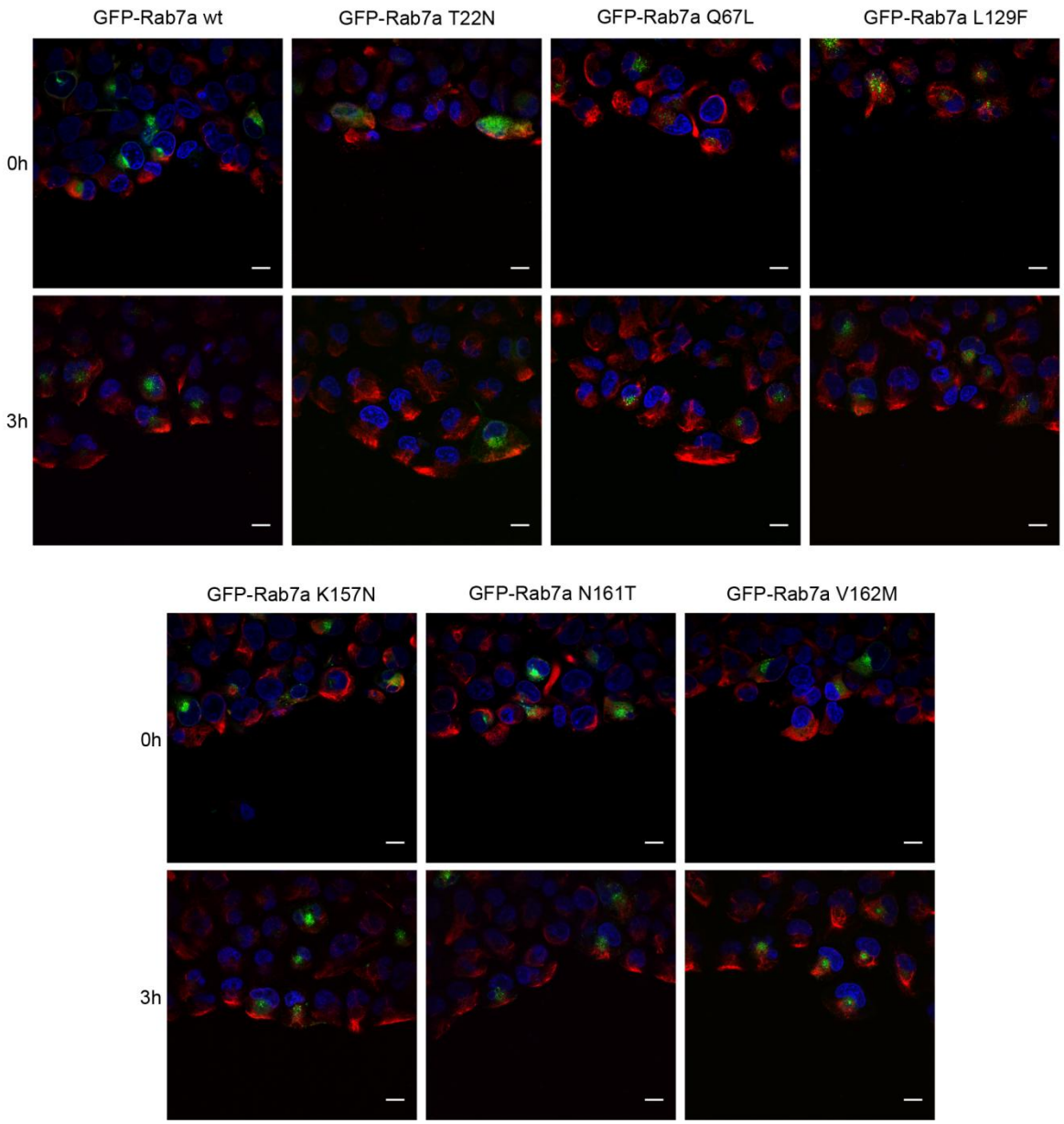

Figure 4.38 CMT2B-associated Rab7a mutants do not affect vimentin filaments re-orientation during migration. (A) NCI H1299 cells transfected with GFP-Rab7a wt, GFP-Rab7a T22N, GFP-Rab7a Q67L, GFP-Rab7a L129F, GFP-Rab7a K157N, GFP-Rab7a N161T or GFP-Rab7a V162M were subjected to wound healing assay and permeabilized, fixed and stained after three hours with anti-vimentin antibody (red) and Hoechst (blue). Scale bar = 10 µm.

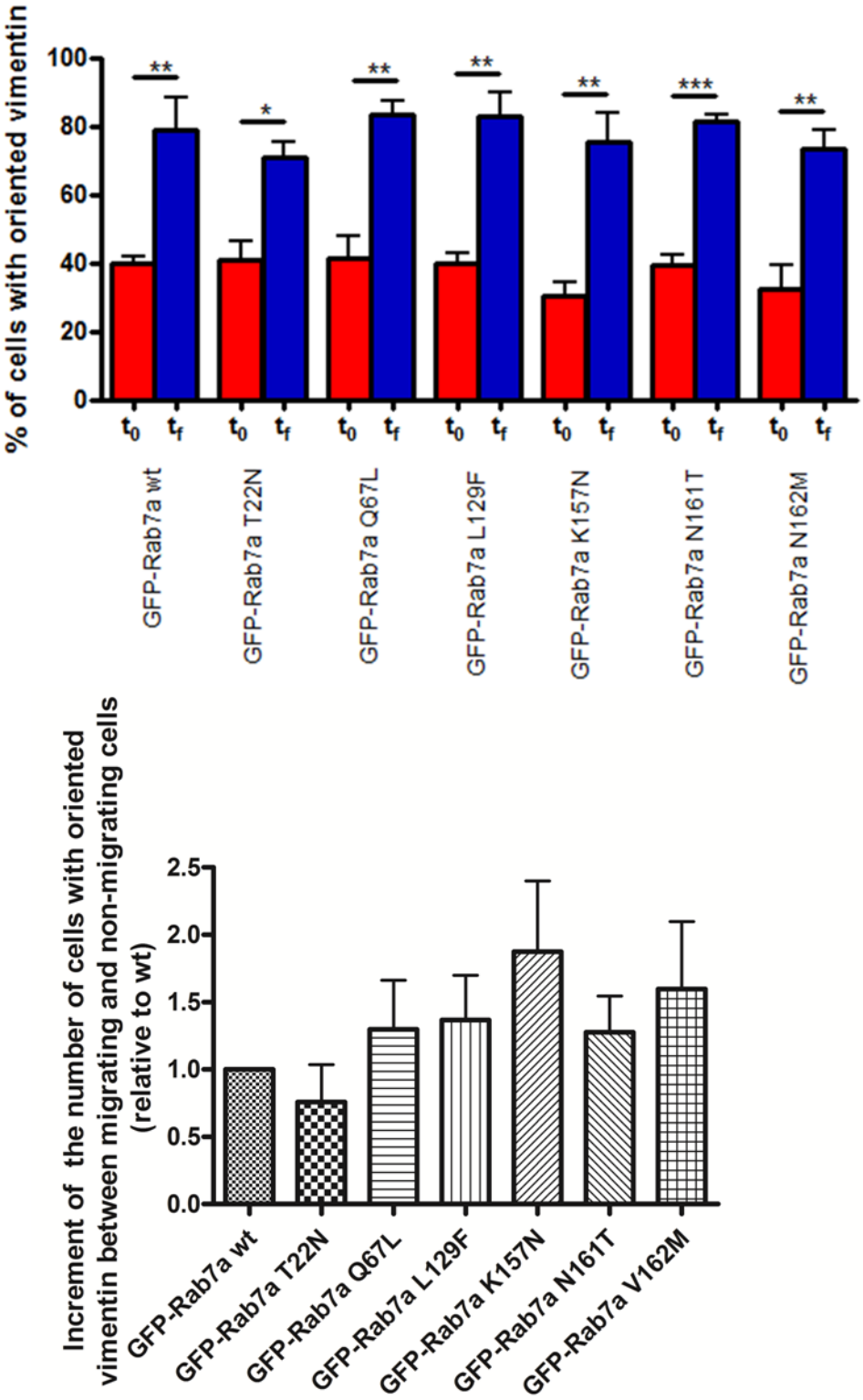

Figure 4.39 Rab7a mutants don't alter vimentin re-organization toward the leading edge during migration. Quantification of the percentage of cells transfected with GFP-Rab7a wt, GFP-Rab7a T22N, GFP-Rab7a Q67L, GFP-Rab7a L129F, GFP-Rab7a K157N, GFP-Rab7a N161T or GFP-Rab7a N162M with vimentin oriented at the front of the cell. T_0 indicates non-migrating cells (0h); T_f indicates migrating cells (3h) (top graph). Quantification of the increase of the number of migrating cells with oriented vimentin compared to the number of non-migrating cells with vimentin facing the wound in cells transfected as indicated (bottom graph). Data represent the mean ± s.e.m. of three different experiments.

4.2.6 CMT2B-causing Rab7a mutants are localized in the area of the cell facing the wound during migration

As Rab7a localized at the front of the cell during migration (Figure 4.31) we wondered whether Rab7a mutants-positive vesicles localized at the same site in migrating cells after wound healing assay.

Therefore, we quantified the percentage of cells with Rab7a oriented in the direction of the wound after 3 hours of migration (migrating cells) and in non-migrating cells (0h) after expressing wt or mutated GFP-Rab7a (Figure 4.38). Both active and CMT2B-causing Rab7a mutants were able to localize at the side of the cell facing the wound, as the wild type protein (Figure 4.39).

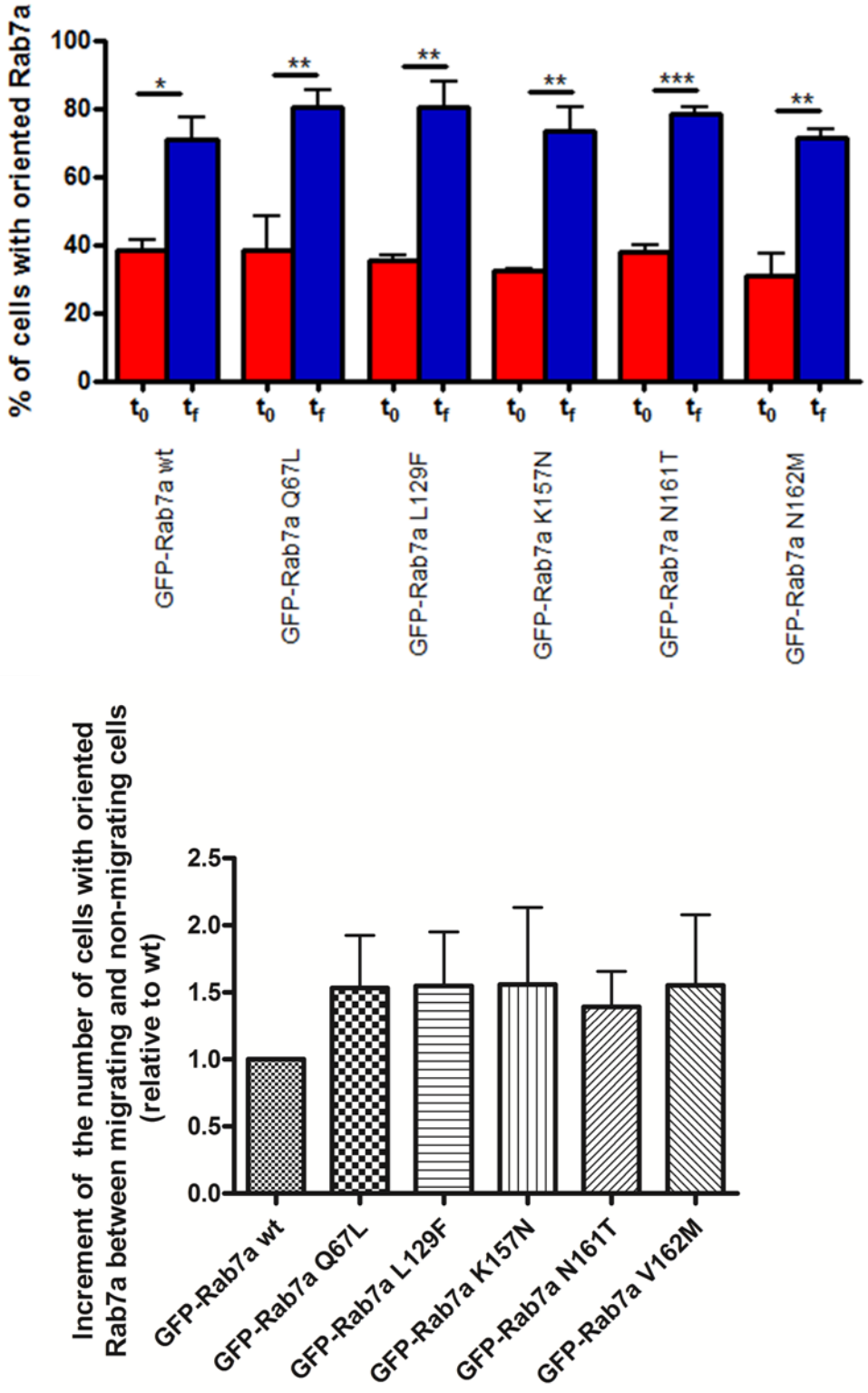

Figure 4.39 Rab7a mutants localize on vesicles at the front of the cell during migration. Quantification of the number of cells with either wt or mutated Rab7a-positive vesicles oriented at the front of the cell. T_0 indicates non-migrating cells; T_f indicates migrating cells (top graph). Quantification of the increase of the number of migrating cells with oriented Rab7a-positive vesicles compared to the number of non-migrating cells with Rab7a facing the wound in NCI H1299 cells transfected as indicated (bottom graph). Data represent the mean ± s.e.m. of three different experiments.

4.3 CHARACTERIZATION OF THE EFFECTS OF RILP ON CELL MIGRATION

Cell migration is a fundamental process in the development and maintenance of multicellular organisms. It includes the generation of temporal-spatial cues that result in cytoskeleton rearrangements, asymmetric polarization and cell adhesion (Vicente-Manzanares *et al.*, 2005). Given that we demonstrated that Rab7a has an important role in several aspects of cell migration and that RILP is a Rab7a effector we decided to evaluate the role of RILP in migration by characterizing its effects on cell motility, microtubules cytoskeleton, cell polarization and adhesion.

4.3.1 RILP affects cell velocity and accumulated distance of migrating cells

In order to investigate how RILP affect cell motility we performed a wound-healing assay on NCI H1299 cells transfected with either control RNA or siRNA against RILP. Confluent monolayers of cells were scratched with a pipette tip and migrating cells were imaged at time intervals of 30 min over a 8 hour time period. The effective silencing of RILP was checked by western blot of control and RILP-depleted cells lysates (Figure 4.40). As shown in Figure 4.40, RILP abundance was strongly reduced.

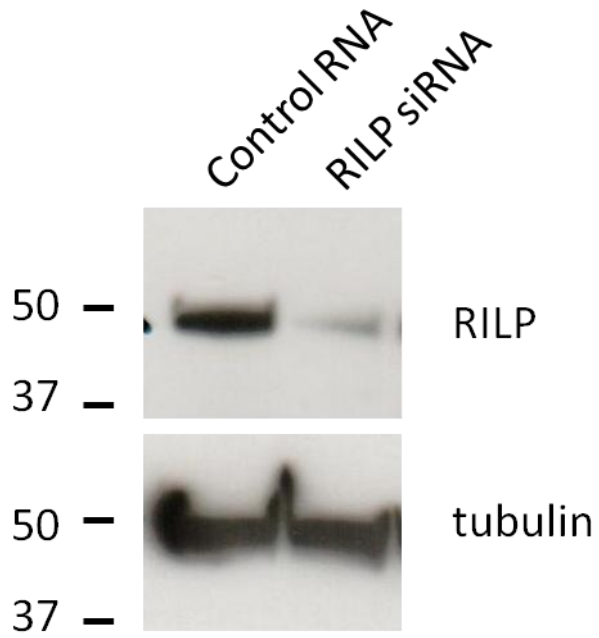

Figure 4.40 RILP abundance is reduced after silencing. NCI H1299 control and RILP-depleted cells were lysed and lysates were subjected to western blotting analysis using anti-RILP

and anti-tubulin antibodies. Tubulin serves as loading control. The migration of protein molecular weight size markers is indicated.

First of all, we demonstrated in NCI H1299 cells the role of RILP in cell motility. In fact, RILP-depleted NCI H1299 cells migrated faster than control cells (Figure 4.41 A; Movie 5),. Moreover, cells depleted for RILP seemed not to migrate collectively, as it was observed in control cells (Movie 5). Then, we evaluated several parameters in order to understand better the effect of RILP on cell motility. We analyzed in control and RILP-depleted migrating cells velocity, accumulated distance, euclidean distance and directness (Figure 4.41 B-E). Interestingly, in case of the lack of RILP, cells speeded up of about the 21% compared to control cells (Figure 4.41 B). In accordance with this data, we saw a similar increase in the accumulated distance (of about 24%), which is the total distance that cells travelled in a certain amount of time, whereas euclidean distance and directness were not impaired after RILP silencing (Figure 4.41 C-E).

These data demonstrate that RILP is required for proper cell motility and modulates cell velocity.

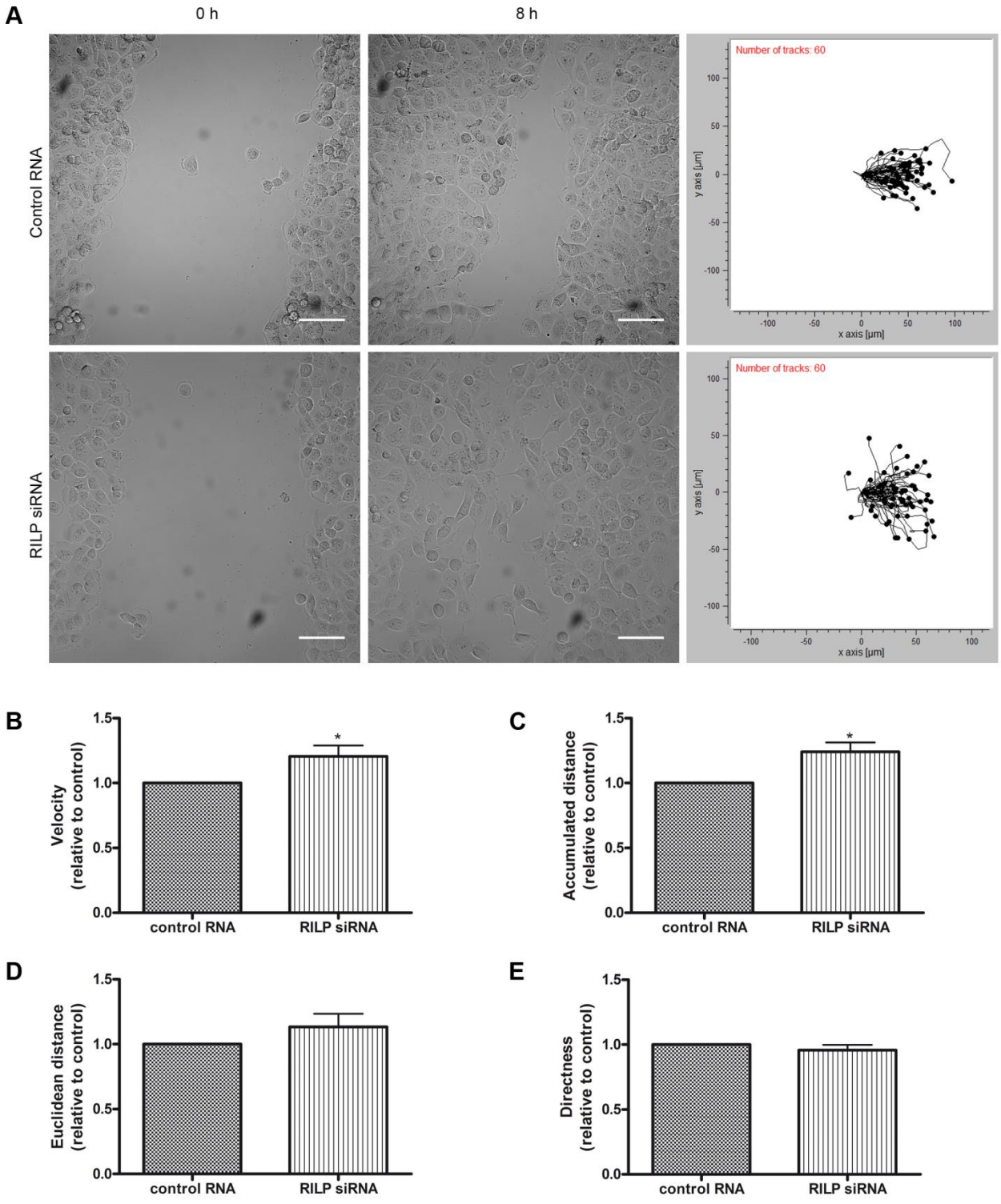

Figure 4.41 RILP silencing affects cell velocity and accumulated distance in migrating cells. NCI H1299 cells transfected with control RNA or with RILP siRNA were imaged every 30 min over a 8 hours period during a wound-healing assay. (A) Images refer to the initial time point (0 hours) or after the closure of the wound (8 hours). On the right panel the migratory tracks of some representative cells are shown for control and RILP-depleted cells. Migration velocity (B), accumulated distance (C), euclidean distance (D) and directness (E) have been quantified and relative graphs are shown. Data represents the mean ± s.e.m. of four independent experiments (n=60). Scale bar = 50 µm.

4.3.2 RILP depletion does not alter Golgi apparatus reorientation

Cell polarity is essential for directional migration and it is defined by cytoskeleton rearrangements, positioning of the nucleus and reorientation of the Golgi complex and the microtubule-organizing center (MTOC) into the direction of the wound (Vicente-Manzanares *et al*, 2005). Therefore, we evaluated a possible role of RILP on cell polarization by measuring the reorientation of the Golgi complex towards the leading edge. As suggested by the fact that directness was not affected by RILP silencing (Fig. 4.41 E), RILP depletion did not interfere with cell polarization and, in particular, with the Golgi apparatus reorientation (Fig. 4.42 A). In fact, ~80% of cells had the Golgi apparatus correctly oriented between the nucleus and the leading edge in both control and RILP-depleted cells (Fig. 4.42 B).

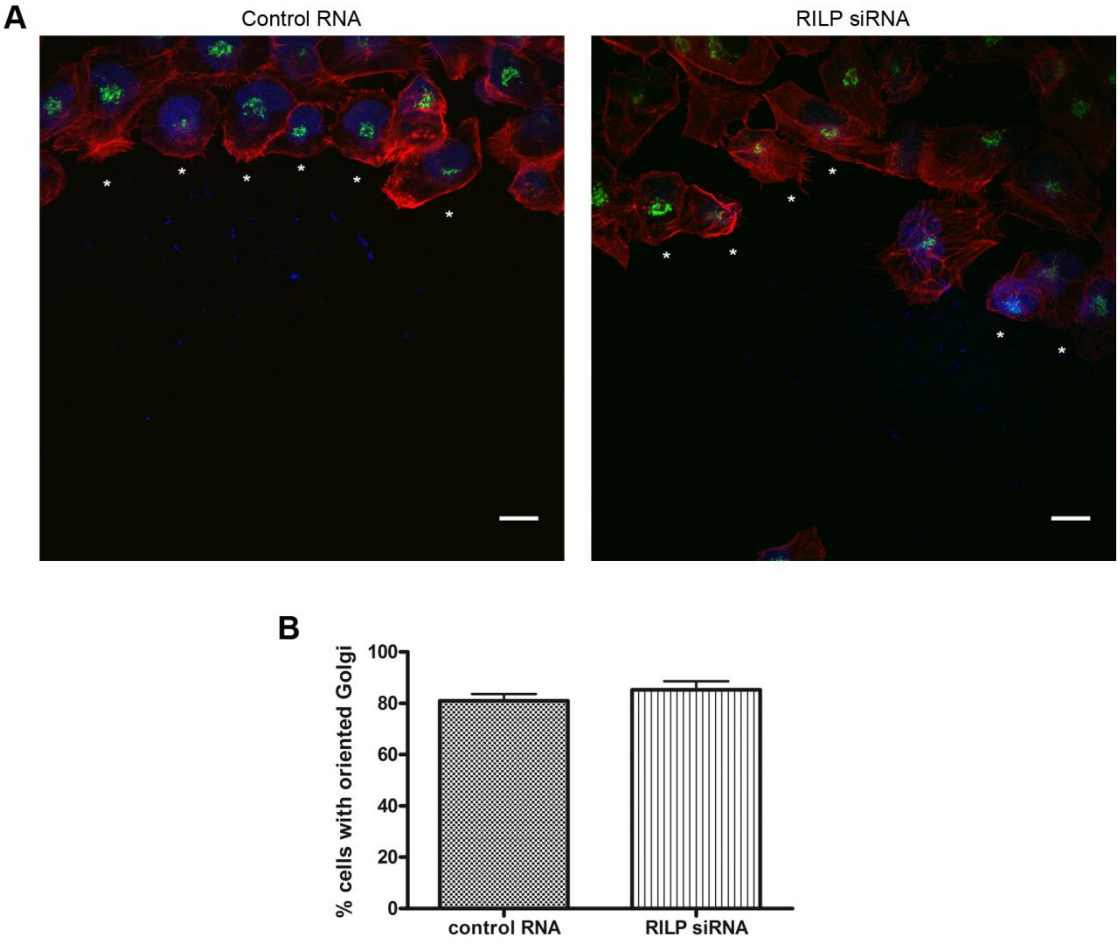

Figure 4.42 Golgi apparatus reorientation during migration is not impaired in RILP-depleted cells. (A) NCI H1299 cells transfected with either control RNA or siRNA against RILP were subjected to wound healing assay and stained after three hours with anti-giantin antibody (green), rhodamine-conjugated phalloidin (red) and Hoechst (blue). * indicates a polarized cell with Golgi complex oriented into the direction of the wound. (B) Quantification of NCI H1299 cells transfected as described in (A) and showing oriented Golgi into the direction of the wound. Data represent the mean ± s.e.m. of three independent experiments (n=50). Bars = 10 µm.

4.3.3 RILP does not influence microtubule cytoskeleton rearrangements

Given that microtubule cytoskeleton is reorganized during migration we investigated whether RILP could affect microtubules organization. As shown in Figure 4.43 control migrating cells showed oriented microtubules, however we didn't detect any visible alteration of microtubule cytoskeleton in migrating cells depleted for RILP (Figure 4.43 A). The percentage of migrating cells with oriented microtubules was about 85% for both control and RILP-depleted cells (Figure 4.43 B). In addition, TIRF analysis of tubulin filaments showed a similar pattern for both control cells and cells silenced for RILP (Figure 4.43C). Overexpression of RILP confirmed the lack of any visible effect of RILP on the reorganization of microtubule cytoskeleton after wound healing assay (Figure 4.43 D). Moreover, we observed RILP effects on tubulin filaments dynamics by live imaging of control and RILP-depleted cells that were subsequently transfected with GFP-tubulin. We demonstrated that RILP depletion does not affect tubulin filaments dynamics (Movie 6).

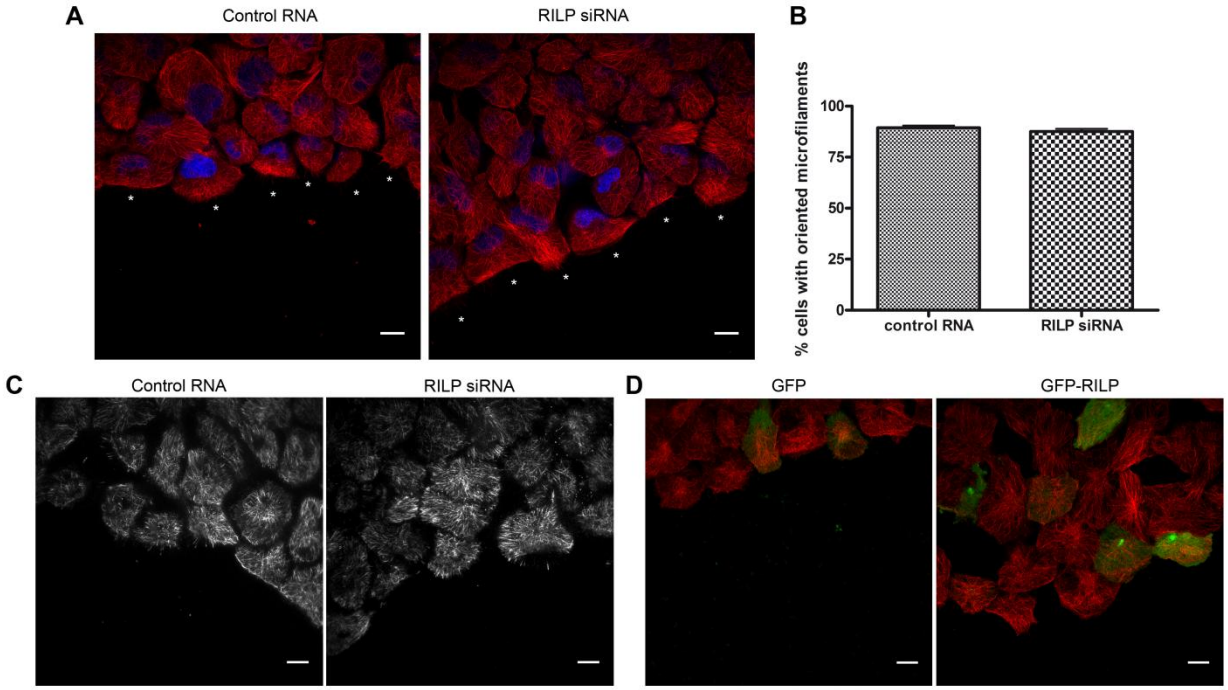

Figure 4.43 RILP depletion does not alter microtubule cytoskeleton. (A) NCI H1299 cells transfected with either control RNA or siRNA against RILP were stained after wound healing assay with anti-tubulin antibody (red) and Hoechst (blue) at 3 hours from the start of the experiment. * indicates a polarized cell with tubulin filaments oriented into the direction of the wound. (B) Quantification of the percentage of cells with oriented tubulin in control and RILP-depleted cells after 3 hours of migration. Data represent the mean ± s.e.m. of two different experiments. (C) Total internal reflection fluorescence microscopy (TIRF) images of migrating NCI H1299 cells transfected with control RNA or siRNA against RILP and stained by using

anti-tubulin antibody. Images were taken at 110 nm depth. (D) NCI H1299 cells expressing either GFP or GFP-RILP were stained after wound healing assay with anti-tubulin (red) at 3 hours from the start of the experiment.

4.3.4 RILP modulates cell adhesion

We further investigated the role of RILP in cell migration by analizing the effect of RILP on cell adhesion. We proved that Rab7a, a RILP interactor, is required for cell migration and cell adhesion on fibronectin substrate. In particular, we showed that Rab7a-depleted cells migrated slower and adhere and spread out less on fibronectin-coated coverslips. We therefore evaluated the effect of expression of either exogenous HA-RILP or the truncated form of RILP, HA-RILP-C33, on cell adhesion. HA-RILP-C33 retains the Rab7a-interacting domain but not N-terminal domain which is responsible for the interaction with the dynein-dynactin complex (Cantalupo *et al*, 2001; Jordens *et al*, 2001). We studied the role of control and RILP expressing cells to spread out on fibronectin-coated coverslips in 30 min by staining with rhodamine-phalloidin and, then, looking at the actin cytoskeleton. Interestingly, the overexpression of RILP determined a lower ability to spread compared to control cells (Figure 4.44 A). The average cell area of control cells was of 200 μm^2. In contrast, HA-RILP and HA-RILP-C33 expressing cells had a decrease in the average area of about 45% and 41%, respectively (Figure 4.44 B).

These data demonstrate that RILP is important for cell adhesion to fibronectin and this effect might involve Rab7a.

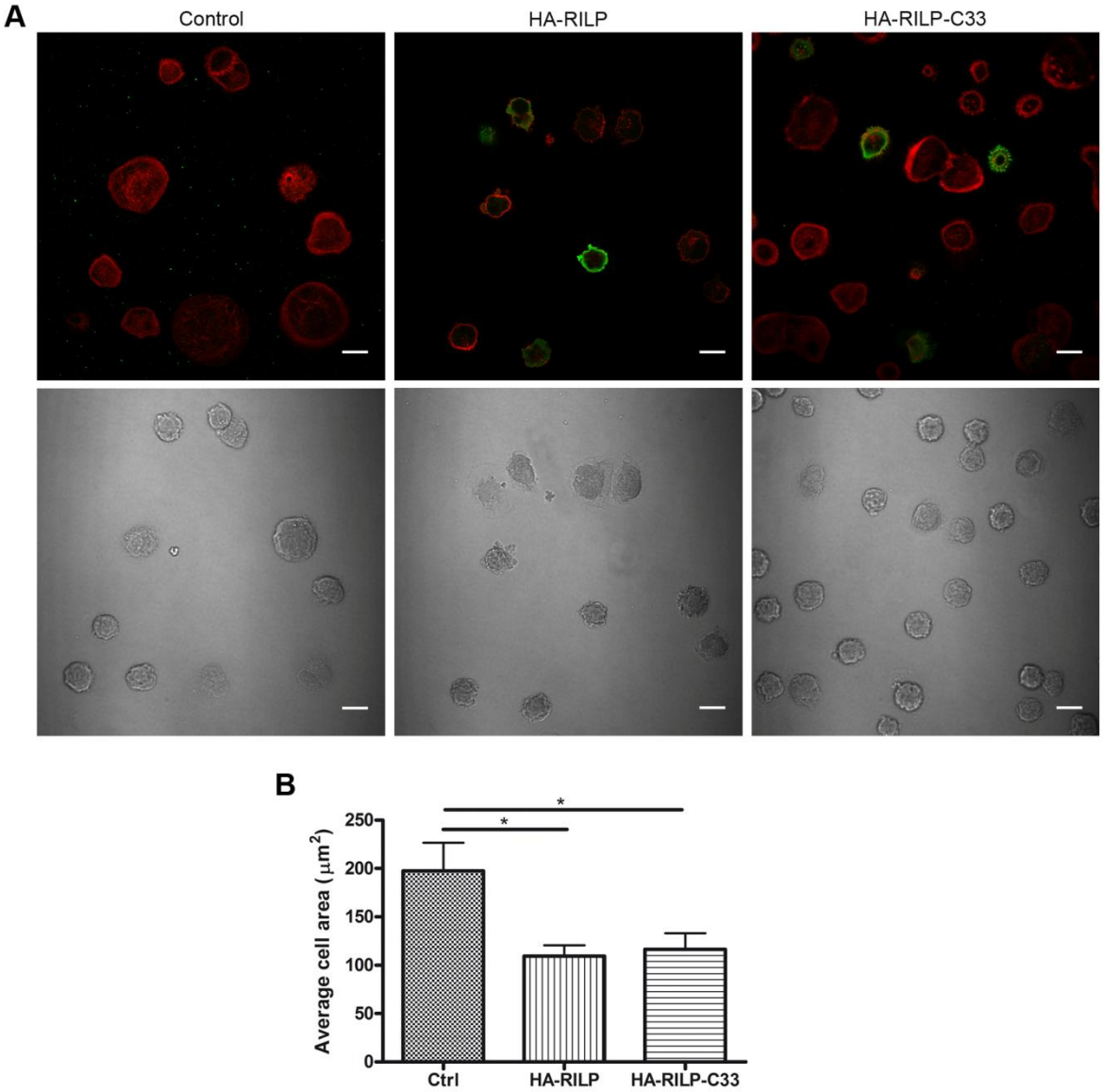

Figure 4.44 Overexpression of RILP alters cell adhesion on fibronectin. NCI H1299 control cells or transfected with either HA-RILP or HA-RILP-C33 were plated on fibronectin-coated coverslips and left to adhere for 30 minutes. (A) Coverslips were then fixed and stained with rhodamine-conjugated phalloidin and anti-HA antibody. Confocal and relative transmission images are shown. (B) Quantification of the average area (in μm^2) of NCI H1299 cells treated as described before. Data represent the mean ± s.e.m. of at least three different experiments (n=50). Scale bar = 10 μm.

DISCUSSION

Here, we set out to investigate the role of Rab7a in cell migration and we discovered that this small GTPase has a key role in regulating this process.

First of all, we analyzed cell motility of control and Rab7a-depleted cells by wound-healing assay (Movie 1; Figure 4.2). We demonstrated that Rab7a is fundamental for cell movement as the motility of Rab7a-depleted cells was slower than that of control cells (Movie 1; Figure 4.2). Analyzing several migration parameters in Rab7a-depleted cells we established that cell velocity, accumulated distance, euclidean distance and directness were decreased compared to control cells, proving that Rab7-depleted cells migrate slower and less persistently (Figure 4.4). Therefore, we demonstrated that Rab7a is essential for proper cell motility.

Furthermore, we investigated the role of Rab7a in other aspects of cell migration, such as Golgi apparatus orientation, which is a hallmark of cell polarization. However, the majority of Rab7a-depleted cells showed correctly oriented Golgi apparatus similarly to control cells (Figure 4.5) thus demonstrating that Rab7a depletion does not interfere with Golgi orientation.

In contrast, Rab7a depletion affected another important event occurring during migration which consists in the formation of protrusions (Vicente-Manzanares *et al.*, 2005). In fact, Rab7a-depleted cells showed 40% fewer filopodia at the leading edge compared to control cells (Figure 4.6). Filopodia sense the mechanical and chemical environment of a cell and represent the first contact with the extracellular matrix. Myosin X is a molecular motor responsible for filopodial formation and transporting cargoes toward the filopodial tip (Bornschlögl, 2013). Therefore, we investigated whether Rab7a could be involved in myosin X functions. We demonstrated that myosin X localized mainly at filopodia tips as expected and partially localized to Rab7a-positive endocytic vesicles and organelles (Figure 4.7, Movie 2), similarly to what has been seen by Plantard and colleagues (Plantard *et al.*, 2010). Rab7a-positive compartments transported this molecular motor to cell periphery where the Rab7a coat was lost (Figure 4.7, Movie 2). In contrast, in case of Rab7a depletion, myosin X mostly localized intracellularly (Figure 4.8 A), suggesting that Rab7a is important for myosin X trafficking. Myosin X is responsible for the regulation of the formation and elongation of filopodia. Plantard *et al* proved that myosin X binding to PtdIns(3,4,5)P_3 is necessary for myosin X promotion of filopodia and that, when myosin X is unable to bind to PtdIns(3,4,5)P_3, it is localized in Rab7a-positive endosomal vesicles (Plantard *et al.*, 2010), which is in line with our data. As Rab7a depletion alters myosin X trafficking and localization but not its abundance (Figures 4.8, 4.9 and 4.10), we suggest that, after Rab7a silencing, myosin X is mislocalized, does not reach the cell periphery and does not

bind to PtdIns(3,4,5)P_3 and, thus, does not promote filopodia formation, which is found to be impaired after Rab7a silencing (Figure 4.6). Interestingly, myosin X silencing decreases the number of endogenous filopodia (Courson and Cheney, 2015), situation which resembles the effect of Rab7a depletion, proving that both impaired trafficking or silencing of myosin X lead to alterations of filopodia formation. Therefore, Rab7a might be responsible for myosin X targeting to filopodial tips and, in turn, for filopodia formation and stabilization through myosin X interactions with the intracellular actin filaments and the β-integrin transmembrane receptors which constitute a link to the ECM. This could finally affect environment and cue sensing, decreasing the ability of Rab7a-depleted cells to migrate.

Myosin X seems also to drive cell invasion by transporting integrins to the tips of filopodia to tether the ECM (Jacquemet *et al*., 2015). Therefore, we tested the ability of Rab7a-depleted cells to spread on fibronectin substrate, an important component of the ECM. This ability is mediated by cell-matrix adhesions. We showed that Rab7a activity is important for spreading and adhesion on fibronectin (Figure 4.11). Therefore, integrins might be affected by Rab7a silencing. Myosin X binds β-integrin receptors through its tail domain in order to make connections with the ECM. Thus, cells expressing myosin X mutants lacking integrin binding showed decreased filopodial adhesion (Courson and Cheney, 2015). Moreover, β1-integrin is important for cell adhesion to fibronectin (Humphries *et al*., 2006) and it can exists in different conformational states. Inactive β1-integrin is mostly localized at the plasma membrane, whereas active β1-integrin seems to be more cytoplasmic (De Franceschi *et al.*, 2015). The localization of the active form of this integrin has been associated with late endosomes and lysosomes either for degradation or for ligand detachment, which allows the unbound free integrin to cycle back to the plasma membrane. Active β1-integrin has been seen to localize to Rab7a-positive compartments (Arjonen *et al*., 2012), thus we hypothesized that Rab7a could alter β1-integrin traffic. Here we confirmed the association between β1-integrin and Rab7a on the same vesicular structures as about 40% of β1-integrin colocalized with Rab7a in NCI H1299 cells overexpressing both proteins (Figure 4.12). In addition, we observed Rab7a vesicles positive for β1-integrin in live cells, suggesting that intracellular transport of β1-integrin is mediated by Rab7a (Figure 4.12; Movie 3). Moreover, we demonstrated that Rab7a-depletion alters the localization of the active form of the receptor during migration (Figure 4.14). In fact, we detected an increase of about 80% of the number of Rab7a-depleted cells with the active form of β1-integrin accumulated at the leading edge compared to control cells (Figure 4.15 B). In addition, we confirmed by TIRF analysis that Rab7a depletion inhibits filopodia formation as proved by the decrease of about 50% of the number of cells with β1-integrin-rich filopodia (Figure 4.15 A). Furthermore, we showed that the total amount of β1-integrin was similar in control and Rab7a-depleted cells,

while the amount of the active form of β1-integrin was decreased of about 25% after Rab7a silencing by western blot analysis (Figure 4.16). Similarly, the abundance of cytoplasmic active β1-integrin was lower after Rab7a depletion but, interestingly, the staining was more vesicular in cells silenced for Rab7a compared to control cells (Figure 4.17). In addition, the colocalization between the early endosomal marker EEA1 and active β1-integrin was four times higher in Rab7a-depleted cells compared to control cells (Figure 4.18). Nevertheless, the total amount of EEA1 was similar in control and Rab7a-depleted cells (Figure 4.19). These data let us hypothesize that Rab7a regulates β1-integrin trafficking. Active β1-integrin that accumulates at the leading edge after Rab7a silencing might be due to clustering of this form of integrin, probably after ligand binding. As active β1-integrin is internalized together with the ligand and more efficiently than the inactive form (Arjonen *et al*., 2012), we hypothesize that the ligand-bound β1-integrin conformer is internalized by EEA1-positive vesicles and the lack of Rab7a, which controls endosome maturation, block the transport of activated integrin to late endosomes and lysosomes which is important for ligand detachment and/or integrin degradation, causing accumulation of active β1-integrin at the level of early sorting endosomes. Active ligand-bound β1-integrin might cycle back to the plasma membrane at the leading edge through the short-loop pathway regulated by Rab4, the long-loop pathway mediated by Rab11 or through Rab25-regulated trafficking, explaining the higher amount of active integrins localized at the leading edge upon Rab7a silencing. Thus, integrin might be unable to bind other ligands as still associated with the previous ligand. Therefore, Rab7a-depleted cells might be less able to adhere to ECM, due to alterations in integrin trafficking and in the formation of protrusions. This hypothesis would be in line with the data on cell motility proving that after Rab7a silencing, cells migrate less. Moreover, all these events might affect, in turn, the activation of β1-integrin, due to the lower cell motility and the lack of new ligands to be used for traction and translocation of the cell. To support this explanation, it would be interesting to follow the internalization of fibronectin ligand and proving its recycling to the cell surrounding together with β1-integrin in case of Rab7a depletion. This would confirm that Rab7a controls ligand detachment from integrins. Moreover, a stronger binding of β1-integrin to SNX 17 or SNX 31 in Rab7a-depleted cells would support the fact that active β1-integrin is recycled back to the plasma membrane instead of being degraded. Finally, studying adhesion turnover when Rab7a is lacking would give more information about cell-matrix adhesions, whose integrin is a main component. For instance, vinculin is recruited to the cytoplasmic tails of β-integrins, through the interaction with talin and it is important in stabilizing focal adhesions. In fact, it has been demonstrated that the lack of vinculin decreases cell motility by impairing adhesions formation, both in size and number (Peng *et al.,* 2011). Here, we demonstrated that vinculin abundance is not altered after

Rab7a silencing (Figure 4.20). However, it would be necessary to evaluate also vinculin localization at adhesion sites by immunofluorescence in order to clarify the role of Rab7a on adhesions.

Recently, it has been demonstrated a novel trafficking pathway for β1-integrin (Shafaq-Zadah *et al.*, 2016). In fact, non-ligand-bound conformation of β1-integrin was found to localize at the trans-Golgi network (TGN), proving that β1-integrin is transported from the plasma membrane to the TGN in order to be resecreted in a polarized manner. Moreover, the activation of β1-integrin increased the retrograde transport efficiency of the non-ligand-bound pool of the protein. β1-integrin coimmunprecipitates and colocalizes with Vps35, a component of the retromer, a peripheral membrane protein complex which is responsible for recycling receptors from endosomes to TGN (Edgar and Polak, 2000). In particular, Vps35 overlapped only with non-ligand-bound form of β1-integrin. Retrograde trafficking inhibition abrogated cell adhesion in cells of developing mouse embryo and persistent cell migration in the developing posterior gonad arm of *Caenorhabditis elegans*. Depletion of some retrograde trafficking factors determined a decrease of total ad surface levels of β1-integrin and a higher colocalization between this integrin and LAMP-1 (Shafaq-Zadah *et al*., 2016). An exciting hypothesis involves a dual active β1-integrin trafficking pathway regulated by Rab7a. In fact, we speculate that active β1-integrin transport to Rab7a-positive vesicles is fundamental for ligand detachment and subsequent integrin degradation or, to a higher extent, integrin transport to TGN in order to be secreted to the leading edge of migrating cells. In fact, when retrograde trafficking is inhibited lysosomal integrin localization increases (Shafaq-Zadah *et al*., 2016). Rab7a regulates endosome maturation (Feng *et al*., 1995; Bucci *et al*., 2000) but also receptor recycling through recruitment of the retromer (Rojas *et al*., 2008). Indeed, the core retromer complex, composed of Vps26, Vps29 and Vps35, binds to active Rab7a and localizes to Rab7a positive endosomal compartments (Rojas *et al*., 2008). In particular, Rab7a interacts directly with Vps35 (Priya *et al*., 2014). When Rab7a is depleted, mannose 6-phosphate receptor retrograde transport is impaired and localizes in enlarged early endosomes (Rojas *et al*., 2008). Therefore, we suggest that Rab7a-depletion could block ligand detachment and impair integrin trafficking both to TGN and lysosomes, leading to accumulation of active-ligand-bound β1-integrin which is recycled back to the plasma membrane through EEA1- positive compartments. The impaired retrograde transport of β1-integrin to TGN would influence cell-matrix adhesion and persistent cell migration. When retrograde transport was inhibited, an impairment of the *de novo* formation of focal adhesions occurred, focal adhesion kinase (FAK) Tyr397 phosphorylation, which is dependent on integrin engagement to the ECM, was lower, and reduced integrin turnover led to enlarged focal adhesions which detached slower from the substrate (Shafaq-Zadah *et al*., 2016).

Rab7a depletion alters cell adhesion to fibronectin and directness during cell migration, whereas Golgi apparatus topology is not affected, similarly to retrograde transport alterations (Shafaq-Zadah *et al*., 2016). This prove that, both in cells silenced for Rab7a or components of the retromer, alterations of cell directionality are not due to defects in Golgi complex positioning. However, the FAK phosphorylation state has not been studied when Rab7a is lacking and detachment analysis should be conducted in order to evaluate whether Rab7a role in cell migration involves the regulation of β1-integrin trafficking to TGN.

β1-integrin is important for Rac1 activation (Nodari *et al*., 2007; Jacquemet *et al.*, 2013). Rac1 interacts directly with Rab7a and colocalizes with it in rat osteoclasts and fibroblast-like cells (Sun *et al.*, 2005). We confirmed the co-localization of Rac1 and Rab7a in a lung cancer cell line, showing that some vesicles positive for Rab7a are positive also for Rac1 and that these two proteins overlap during the movement of these vesicles (Figures 4.22 and 4.23, Movie 4). In Rab7a-depleted cells Rac1 abundance is not altered but its activity is impaired (Figures 4.21 and 4.24). Jacquemet *et al* demonstrated that active integrins, after initially activating Rac1, subsequently recruit a complex containing filamin A (FLNa) and IQ Motif Containing GTPase Activating Protein 1 (IQGAP1) and involving a GAP which is responsible for lowering Rac1 activity in order to limit protrusive activity during cell migration. FLNa is recruited specifically to the activated integrin (Jacquemet *et al.,* 2013). Therefore, we hypothesize that the accumulation of the active form of this β1-integrin at the leading edge, due to Rab7a silencing, is responsible for recruiting the complex containing FLNa and IQGAP1 and, in turn, RacGAP1, which is important for Rac1 inactivation. Therefore, the effect on the activation state of Rac1 after Rab7a depletion might be due to the impaired trafficking of β1-integrin. The subsequent recruitment of the FLNa-IQGAP1 complex to sites of integrin activation and therefore the recruitment of RacGAP1 may explain the impaired activation state of Rac1, which is involved in cell migration as it is important in the reorganization of the actin cytoskeleton (Jacquemet *et al.,* 2013; Bosco *et al.,* 2009). As a consequence, protrusive force mediated by localized polimerization of actin is reduced. Our data on Rac1 are in line with a recent work which has shown that Rab7a depletion caused a lower Rac1 activity (Mascia *et al*., 2015).

Both Rab7a and Rac1 have been linked to vimentin, which has been associated to cell migration in several works (Dave and Bayless, 2014). Rab7a interacts with vimentin and silencing of this small GTPase determines a lower phosphorylated state of the head domain of vimentin and a higher abundance of vimentin in the insoluble, filamentous fraction (Cogli *et al.*, 2013a). By creating vimentin deletion mutants, we demonstrated that Rab7a interacts with coil1A of vimentin (Figure 4.28). In addition, vimentin depletion modulates Rab7a abundance (Figure 4.29), proving that the two proteins are able to affect each other. Moreover, vimentin regulates

Rac1 activation whereas Rac1 activation determines vimentin phosphorylation and disassembly (Havel *et al*., 2015; Meriane *et al*., 2000; Lee *et al*., 2001; Helfand *et al*., 2011). As both Rab7a and Rac1 regulate vimentin assembly and since vimentin filaments are reoriented towards the direction of the wound during migration (Sakamoto *et al*., 2013), we investigated whether vimentin filament orientation was altered in Rab7a-depleted migrating cells. Here, we showed that Rab7a silencing alters vimentin filament reorganization during migration (Figure 4.30). In fact, the number of cells which reorganized vimentin filaments during migration was ~ 25% lower in cells silenced for Rab7a (Figure 4.30 B). Therefore, we suggest that Rab7a depletion might influence vimentin phosphorylation and assembly by modulating Rac1 activity and, in turn, impairing vimentin reorientation during cell migration. Moreover, we showed that Rab7a-positive compartments are localized at the front of the cell during migration (Figure 4.31). We hypothesize that proper Rab7a localization during migration regulates different cellular elements, including the reorganization of vimentin filaments.

In light of the above, our data prove that Rab7a has a role in cell migration and its depletion may cause several effects on different proteins that regulate cell migration such as Rac1, β1-integrin, myosin X and vimentin. All together the effects of Rab7a on these proteins might explain the lower cell velocity, directness and cell adhesion with the extracellular matrix shown by Rab7a-depleted cells (Figure 5.1).

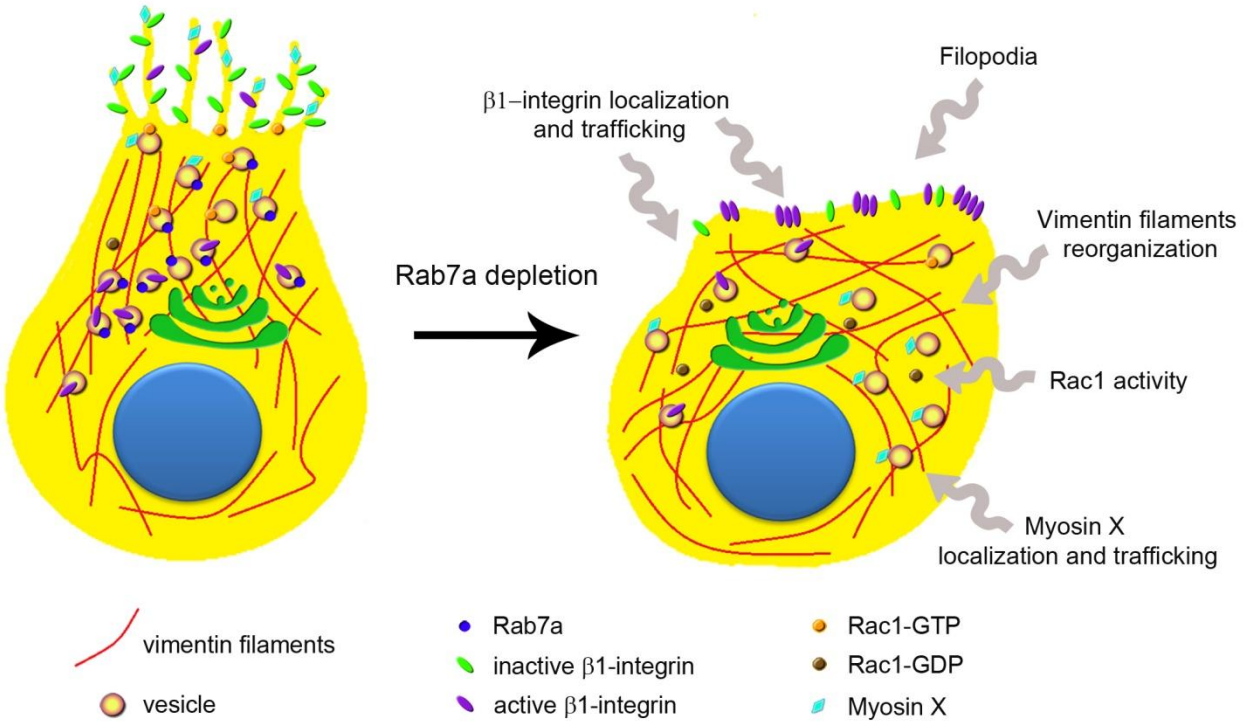

Figure 5.1 Proposed model for the role of Rab7a in cell migration. Processes affected by Rab7a silencing in migrating cells. Rab7a controls cell migration by regulating vimentin filament

assembly and organization, Rac1 activity, myosin X localization, filopodial formation and β1-integrin localization, activation and trafficking.

This discovery could open new scenarios on the role of Rab7a both in physiological and pathological situations. In fact, cell migration is fundamental for homeostatic processes, such as immune response and repairing of injured tissues. Indeed, leukocytes migrate from the circulation into lymph nodes and inflamed tissues to develop the immunoresponse. Moreover, skin continuous renovation is based on migration of precursors from the basal layer. Cell migration can be important in some pathologies, such as vascular disease, chronic inflammatory disease but also tumor formation and metastasis. During tumor formation, the invasion of blood vessels is due to proliferation and migration of endothelium components, whereas at later stages some cancer cells acquire the ability to migrate out of the initial tumor reaching other tissues and giving rise to metastasis (Horwitz and Webb, 2003). As during cell migration several activities are integrated, all the molecular events that characterize this process are still unclear. Understanding the role of Rab7a in cell migration could be useful to clarify some of these molecular events and find therapies for some of these pathologies where alterations of migration play a key role. Therefore, we created some Rab7a mutants in order to understand deeply the role of Rab7a in cell migration by altering its amino acidic composition. We generated Rab7a mutants with point or deletion mutations in the RabSF regions focusing on amino acids that were predicted to be on the surface of the Rab7a protein according to studies conducted by using PyMol software and available crystallographic data (Table 4.2; Figure 4.34). This was made in order to possibly create mutants that weren't able to interact with some Rab7a effectors and therefore could disrupt Rab7a functions. Rab7a N30A, Rab7a S34I, Rab7a S111G, Rab7a N117A, Rab7a K175E, Rab7a 11-207 and Rab7a 1-176 were generated. Only the Rab7a 11-207 mutant showed low proteic level expression, probably due to the lack of the first ten amino acids which, then, might be important for Rab7a stability (Figure 4.35). However, the expression of the generated Rab7a mutants after Rab7a silencing recovered, although partially, Rab7a function in cell adhesion (Figure 4.36), suggesting that the amino acids mutated or deleted were not of importance for exerting this role. Nevertheless, since Rab7a is involved in several aspects of cell migration, other studies involving these mutants should be conducted in order to better understand the role of these amino acids in Rab7a functions.

It has been demonstrated that specific mutations in Rab7a gene, which give rise to mutated proteins (Rab7a L129F, Rab7a K157N, Rab7a N161T, Rab7a N161I, Rab7a V162M), are responsible for the onset of CMT2B disease, a peripheral neuropathy (Meggouh *et al.*, 2006; Houlden *et al.*, 2004; Verhoeven *et al.*, 2003; Wang *et al.*, 2014). As Rab7a is ubiquitous but

CMT2B Rab7a mutant proteins affect only the peripheral nervous system, it is probable that some specific Rab7a functions are impaired when these mutants are expressed. Moreover, the peripheral nervous system has an intrinsic regenerative ability in response to traumatic injury, which involves coordination among specific cellular and molecular events in order to favor axonal regrowth and target reinnervation. For instance, inflammatory cells are needed to remove myelin and axon debris, while Schwann cells proliferate and migrate and support axon regrowth (Lang *et al*., 2014). Furthermore, a first link between Rab7a and neuronal migration has been demonstrated during the development of cerebral cortex *in vivo* (Kawauchi *et al*., 2010; Kawauchi, 2011). In fact, impairment of Rab7a activity led to defects in the final phase of migration of immature neurons. In particular, the distances from the nuclei to the pial edge of the cortical plate were increased when Rab7a was lacking or Rab7a T22N was expressed (Kawauchi *et al*., 2010; Kawauchi, 2011). Furthermore, the dendritic shafts in some immature neurons expressing Rab7a T22N were thicker and longer than control whereas the dendritic branches were more elongated (Kawauchi *et al*., 2010; Kawauchi, 2011). Therefore, we investigated whether Rab7a L129F, Rab7a K157N, Rab7a N161T, Rab7a V162M mutants could act in a different way compared to wild type protein in some aspects of cell migration. Nevertheless, CMT2B-causing Rab7a proteins were able to re-induce cell spreading onto fibronectin after Rab7a silencing as the wild type protein (Figure 4.37). In addition, expression of CMT2B-associated Rab7a mutants and the constitutively active (Rab7a Q67L) and the dominant negative (Rab7a T22N) mutants of Rab7a did not significantly interfere with vimentin re-orientation during cell migration (Figure 4.38), which was affected after Rab7a silencing. However, the increment of cells which showed reoriented vimentin filaments after migration was lower in cells expressing the dominant negative mutant of Rab7a compared to the wild type protein, whereas, when CMT2B-causing Rab7a mutants were expressed, it was higher compared to the wild type protein and similar to the constitutively active Rab7a mutant behavior. This is in line with previous work which showed that CMT2B-associated Rab7a mutants act as active proteins (Spinosa *et al*., 2008; De Luca *et al*., 2008). In addition, Rab7a Q67L, Rab7a L129F, Rab7a K157N, Rab7a N161T, Rab7a V162M localized at the front of the cell during migration as the wild type protein (Figure 4.39). Further studies should be conducted in order to understand whether CMT2B-causing Rab7a mutants could impair specific events occurring during cell migration. In particular, it would be interesting to investigate whether these mutants and, more specifically Rab7a K157N, alter β1-integrin trafficking as it has been demonstrated that Rab7a K157N reduced endosomal localization of the retromer, which might be involved in receptor recycling and function (Seaman *et al*., 2009; Shafaq-Zadah *et al*., 2016). In fact, it is still not known how specific Rab7a mutations lead to this disease that affects specifically peripheral

neurons, therefore understanding which Rab7a functions are altered when CMT2B-causing Rab7a mutants are expressed will help to elucidate the molecular mechanisms underlying the onset of this neuropathy.

Here, we proved that Rab7a has a key role in cell migration. Active Rab7a recruits RILP to endosomal membranes and, together, they control late endocytic traffic, phagosome and autophagosome maturation and are responsible for signalling receptor degradation (Cantalupo *et al*., 2001; Jordens *et al*., 2001; Harrison *et al*., 2003; Progida *et al*., 2007). Overexpression of RILP arrests Rab7a in the active form and late endosomes and lysosomes are accumulated around the MTOC, whereas overexpression of RILP-C33 induces dispersed lysosomes (Cantalupo *et al*., 2001; Jordens *et al.*, 2001). Therefore, we set out to investigate whether also RILP could have a role in cell migration. Here we characterized the effects of RILP on this process by evaluating its role on cell motility, microtubule cytoskeleton, cell polarization and adhesion. First of all, we established that RILP is an important player in cell motility by fostering wound closure in NCI H1299 cells when depleted (Figure 4.41; Movie 5), on the contrary of what occurred when Rab7a was depleted. These data are in line with a recent work proving that in wound-healing assay, after RILP depletion, MDA-MB-231 cells close the wound faster (Wang *et al*, 2015). This demonstrates that the role of RILP in migration is not cell-specific as it affects cell migration both in breast and lung cancer cells. In particular, we showed that cell velocity and distance travelled by cells were increased after RILP silencing (Figure 4.41). Moreover, RILP-depleted migrating cells seemed to not migrate together as a sheet, rather they appeared to loose cell-cell contacts (Movie 5). This aspect should be investigated deeply as cell-cell adhesions are usually disrupted in metastatic cells, which migrate individually (Conacci-Sorrell *et al*., 2002). Similarly to Rab7a depletion, the loss of RILP does not influence Golgi apparatus reorientation (Figure 4.42). RILP interacts with its N-terminal domain with dynactin, thus recruiting the dynactin-dynein complex to vesicles that are transported toward the minus end of microtubules (Jordens *et al*., 2001). Moreover, during migration microtubules are reorganized along the direction of migration and dynein and dynactin are enriched at the leading edge (Etienne-Manneville, 2013; Dujardin *et al*., 2003). Inhibition of dynein and dynactin interfere with microtubule network reorientation and persistent directed cell migration (Dujardin *et al*., 2003). Therefore, we evaluated whether RILP proteic modulation could alter microtubule cytoskeleton reorganization mediated by the dynein-dynactin complex in migrating cells. However, our data did not indicate a detectable effect of RILP on tubulin cytoskeleton. In fact, both silencing and overexpression of RILP did not alter microtubule orientation during migration (Figure 4.43). In addition, TIRF analysis of microtubules showed a similar pattern for both

control and RILP-depleted cells (Figure 4.43). These data were confirmed by live imaging where we detected no effect on tubulin filaments dynamics after RILP silencing (Movie 6).

We previously demonstrated that Rab7a-depleted cells migrated slower and adhere and spread out less on fibronectin-coated coverslips. Therefore, we evaluated the effect of expression of either exogenous HA-RILP or HA-RILP-C33 on cell adhesion. HA-RILP-C33 retains the Rab7a-interacting domain but not N-terminal domain, which is responsible for the interaction with the dynein-dynactin complex (Cantalupo *et al*, 2001; Jordens *et al*, 2001). Interestingly, both the expression of HA-RILP and HA-RILP-C33 decreased cell adhesion on fibronectin substrate (Figure 4.44). These data demonstrate that RILP is important for cell adhesion and this effect might involve Rab7a. It has been demonstrated a role of RILP in controlling actin cytoskeleton through the interaction with RalGDS, which in turn regulates RalA, a modulator of actin cytoskeleton organization (Wang *et al.*, 2015), thus both RILP and Rab7a modulations influence actin filaments rearrangements even if in an opposite manner. In fact, overexpression of RILP led to inhibition of RalA and, in turn, to the decrease of stress actin fibers and cortical actin (Wang *et al.*, 2015), whereas Rab7a depletion affects negatively actin cytoskeleton by inactivating Rac1 and impairing filopodial formation. As HA-RILP-C33 does not retain the N-terminal domain, which is responsible for the interaction with RalGDS (Wang *et al.*, 2015), we suggest that the role of RILP in cell adhesion involves Rab7a but not RalA or the dynactin/dynein complex. Therefore, RILP controls cell velocity, cell adhesion and actin filaments rearrangements, but not Golgi apparatus reorientation and microtubules reorganization (Figure 5.2).

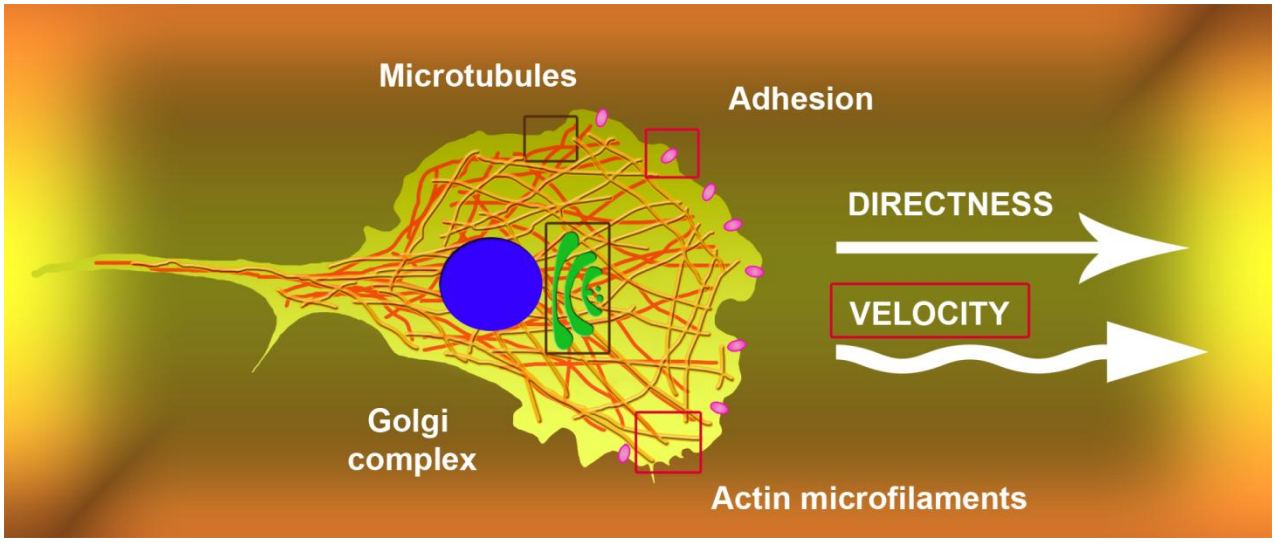

Figure 5.2 Model which shows the aspects of cellular migration regulated by RILP. RILP controls cell velocity, adhesion and actin reorganization but not Golgi apparatus and microtubules reorientation.

Taking all these data into account, we showed that both Rab7a and RILP have a key role in cell migration by regulating several processes. However, it seems that Rab7a and RILP conversely regulate several aspects of migration, therefore it might be hypothesized that they act in the same pathway and proper levels of these two proteins are necessary for correct cell migration. Therefore, in order to confirm this, it would be interesting to evaluate the role of RILP on Rac1 activity, myosin X localization, filopodia formation, β1-integrin trafficking and vimentin filaments reorganization that we have proved to be regulated by Rab7a. Moreover, specific experiments should be set to prove which of the two proteins is downstream in this pathway. For instance, it would be interesting to see the effects on cell spreading on fibronectin of overexpression of both Rab7a and RILP, or whether depletion of both RILP and Rab7a determines a higher or lower cell velocity during migration assay compared to control cells. However, the reason why Rab7a and RILP regulate in an opposite manner this process is not clear and further studies will be necessary to understand how these key proteins of vesicular trafficking control cell migration and might be modulated in the future in relation to pathologies.

APPENDIX

Movie 1. Silencing of Rab7a affects wound closure. Monolayers of NCI H1299 cells transfected with control RNA (top) or Rab7a siRNA (bottom) were subjected to wound healing assay. Cell migration was imaged with a Olympus confocal microscope every 30 minutes.

Movie 2. Myosin X is transported to the cell periphery in Rab7a-positive compartments. NCI H1299 cells co-expressing GFP-myosin X (green) and mCherry-Rab7a wt (red) were imaged with a Spinning Disk confocal microscope at 5 second intervals.

Movie 3. Rab7a and β1-integrin overlap and move together. NCI H1299 cells co-expressing GFP-β1-integrin (green) and mCherry-Rab7a wt (red) were imaged with a Spinning Disk confocal microscope at 2 second intervals.

Movie 4. Rab7a and Rac1 overlap and move together. NCI H1299 cells co-expressing GFP-Rac1 (green) and mCherry-Rab7a wt (red) were imaged with a Spinning Disk confocal microscope at 2 second intervals.

Movie 5. RILP depletion fosters cell motility and the closure of the wound. Monolayers of NCI H1299 cells transfected either with control RNA (top) or RILP siRNA (bottom) were scratched by a pipette tip. Cell migration was imaged with a Olympus confocal microscope every 30 minutes.

Movie 6. RILP silencing does not influence microtubules dynamics. Control and RILP-depleted NCI H1299 cells expressing GFP-tubulin (green) and treated with LysoTracker Red (red). Cells were imaged with a Spinning Disk confocal microscope at 2 second intervals.

REFERENCES

Arjonen A, Alanko J, VelteI S, Ivaska J. (2012). Distinct recycling of active and inactive β1 integrins. *Traffic* 13:610-25.

BasuRay S, Mukherjee S, Romero E, Wilson MC, Wandinger-Ness A. (2010). Rab7 Mutants Associated with Charcot-Marie-Tooth Disease Exhibit Enhanced NGF-Stimulated Signaling. *PLoS ONE* 5:e15351.

Bershadsky AD, Tint IS, Svitkina TM. (1987). Association of intermediate filaments with vinculin-containing adhesion plaques of fibroblasts. *Cell Motil Cytoskeleton* 8:274-83.

Bhuin T and Roy JK. (2014). Rab proteins: the key regulators of intracellular vesicle transport. *Exp Cell Res* 328:1-19.

Blanchoin L, Boujemaa-Paterckі R, Plastino J. (2014). Actin dynamics, architecture, and mechanics in cell motility. *Physiol Rev* 94:235-63.

Bohil AB, Robertson BW, Cheney RE. (2006). Myosin-X is a molecular motor that functions in filopodia formation. *Proc Natl Acad Sci U S A* 103:12411-16.

Borg M, Bakke O, Progida CA. (2014). A novel interaction between Rab7b and actomyosin reveals a dual role in intracellular transport and cell migration. *J Cell Sci* 127:4927-39.

Bornschlögl T. (2013). How filopodia pull: what we know about the mechanics and dynamics of filopodia. *Cytoskeleton* 70:590-603.

Bosco EE, Mullov JC, Zheng Y. (2009) Rac1 GTPase: a "Rac" of all trades. *Cell Mol Life Sci* 66:370-4.

Bucci C, De Luca M. (2012). Molecular basis of Charcot-Marie-Tooth type 2B disease. *Biochem Soc Trans* 40:1368-72.

Bucci C, Thomsen P, Nicoziani P, McCarthy J, van Deurs B. (2000). Rab7: a key to lysosome biogenesis. *Mol Biol Cell* 11:467-480.

Byron A, Humphries JD, Askari JA, Craig SE, Mould AP, Humphries MJ. (2009). Anti-integrin monoclonal antibodies. *J Cell Sci* 122:4009-11.

Cantalupo G, Alifano P, Roberti V, Bruni CB, Bucci C. (2001). Rab-interacting lysosomal protein (RILP): the Rab7 effector required for transport to lysosomes. *EMBO J* 20:683-93.

Carroll B, Mohd-Naim N, Maximiano F, Frasa MA, McCormack J, Finelli M, Thoresen SB, Perdios L, Daigaku R, Francis RE, Futter C, Dikic I, Braga VM. (2013). The

TBC/RabGAP Armus coordinates Rac1 and Rab7 functions during autophagy. *Dev Cell* 25:15-28.

Caswell PT, Spence HJ, Parsons M, White DP, Clark K, Cheng KW, Mills GB, Humphries MJ, Messent AJ, Anderson KI, McCaffrey MW, Ozanne BW, Norman JC. (2007). Rab25 associates with alpha5beta1 integrin to promote invasive migration in 3D microenvironments. *Dev Cell* 13:496-510.

Ceresa BP, Bahr SJ. (2006). rab7 activity affects epidermal growth factor: epidermal growth factor receptor degradation by regulating endocytic trafficking from the late endosome. *J Biol Chem* 281:1099-106.

Cogli L, Progida C, Bramato R, Bucci C. (2013a). Vimentin phosphorylation and assembly are regulated by the small GTPase Rab7a. *Biochim Biophys Acta* 1833:1283-93.

Cogli L, Progida C, Lecci R, Bramato R, Kruttgen A, Bucci C. (2010). CMT2B-associated Rab7 mutants inhibit neurite outgrowth. *Acta Neuropathol* 120:491-501.

Cogli L, Progida C, Thomas CL, Spencer-Dene B, Donno C, Schiavo G, Bucci C. (2013b). Charcot-Marie-Tooth type 2B disease-causing RAB7A mutant proteins show altered interaction with the neuronal intermediate filament peripherin. *Acta Neuropathol* 125:257-72.

Conacci-Sorrell M, Zhurinsky J, Ben-Ze'ev A. (2002). The cadherin-catenin adhesion system in signaling and cancer. *J Clin Invest* 109:987-91.

Courson DS, Cheney RE. (2015). Myosin-X and disease. *Exp Cell Res* 334:10-5.

Damianovich L, Albelda SM, Mette SA, Buck CA. (1992). Distribution of integrin cell adhesion receptors in normal and malignant lung tissue. *Am J Respir Cell Mol Biol* 6:197-206.

Dave JM, Bayless KJ. (2014). Vimentin as an integral regulator of cell adhesion and endothelial sprouting. *Microcirculation* 21:333-44.

De Franceschi N, Hamidi H, Alanko J, Sahgal P, Ivaska J. (2015). Integrin traffic - the update. *J Cell Sci* 128:839-52.

De Luca A, Progida C, Spinosa MR, Alifano P, Bucci C. (2008). Characterization of the Rab7K157N mutant protein associated with Charcot-Marie-Tooth type 2B. *Biochem Biophys Res Commun* 372:283-7.

Deinhardt K, Salinas S, Verastegui C, Watson R, Worth D, Hanrahan S, Bucci C, Schiavo G. (2006). Rab5 and Rab7 control endocytic sorting along the axonal retrograde transport pathway. *Neuron* 52:293-305.

Dujardin DL, Barnhart LE, Stehman SA, Gomes ER, Gundersen GG, Vallee RG. (2003). A role for cytoplasmic dynein and LIS1 in directed cell movement. *J Cell Biol* 163:1205-11.

Dujardin DL, Barnhart LE, Stehman SA, Gomes ER, Gundersen GG, Vallee RB. (2003). A role for cytoplasmic dynein and LIS1 in directed cell movement. *J Cell Biol*. 163:1205-11.

Edgar AJ, Polak JM. (2000). Human homologues of yeast vacuolar protein sorting 29 and 35. *Biochem Biophys Res Commun* 277:622-30.

Edinger AL, Cinalli RM, Thompson CB. (2003). Rab7 prevents growth factor-independent survival by inhibiting cell-autonomous nutrient transporter expression. *Dev Cell* 5:571-82.

Etienne-Manneville S. (2013). Microtubules in cell migration. *Annu Rev Cell Dev Biol* 29:471-99.

Feng Y, Press B, Wandinger-Ness A. (1995). Rab7: an important regulator of late endocytic membrane traffic. *J Cell Biol* 131:1435-52.

Frasa MA, Maximiamo FC, Smolarczyk, Francis RE, Betson ME, Lozano E, Goldenring J, Seabra MC, Rak A, Ahmadian MR, Braga VM. (2010). Armus is a Rac1 effector that inactivates Rab7 and regulates E-cadherin degradation. *Curr Biol* 20:198-208.

Gilles C, Polette M, Zahm JM, Turnier JM, Volders L, Foidart JM, Birembaut P. (1999). Vimentin contributes to human mammary epithelial cell migration. *J Cell Sci* 112:4615-25.

Gonzales M, Weksler B, Tsuruta D, Goldman RD, Yoon KJ, Hopkinson SB, Flitney FW, Jones JC. (2001). Structure and function of a vimentin-associated matrix adhesion in endothelial cells. *Mol Biol Cell* 12:85-100.

Harrison R, Bucci C, Vieira O, Schroer T, Grinstein S. (2003). Phagosomes fuse with late endosomes and/or lysosomes by extension of membrane protrusions along microtubules: role of Rab7 and RILP. *Mol Cell Biol* 23:6494-506.

Havel LS, Kline ER, Salgueiro AM, Marcus AI. (2015). Vimentin regulates lung cancer cell adhesion through a VAV2-Rac1 pathway to control focal adhesion kinase activity. *Oncogene* 34:1979-90.

Helfand BT, Mendez MG, Murthy SN, Shumaker DK, Grin B, Mahammad S, Aebi U, Wedig T, Wu YI, Hahn KM, Inagaki M, Herrmann H, Goldman RD. (2011). Vimentin organization modulates the formation of lamellipodia. *Mol Biol Cell* 22:1274-89.

Homan SM, Mercurio AM, LaFlamme SE. (1998). Endothelial cells assemble two distinct alpha6beta4-containing vimentin-associated structures: roles for ligand binding and the beta4 cytoplasmic tail. *J Cell Sci* 111:2717-28.

Horwitz R, Webb D. (2003). Cell migration. *Curr Biol* 13:R756-9.

Houlden H, King RH, Muddle JR, Warner TT, Reilly MM, Orrell RW, Ginsberg L. (2004). A novel RAB7 mutation associated with ulcero-mutilating neuropathy. *Ann Neurol*. 56:586–590.

Humphries JD, Byron A, Humphries MJ. (2006). Integrin ligands at a glance. *J Cell Sci* 119:3901-3.

Hyttinen JM, Niittykoski M, Salminen A, Kaarniranta K. (2013). Maturation of autophagosomes and endosomes: a key role for Rab7. *Biochim Biophys Acta* 1833:503-10.

Inoue H, Nojima H, Okayama H. (1990). High efficiency transformation of *Escherichia coli* with plasmids. *Gene* 96:23-28.

Jacquemet G, Hamidi H, Ivaska J. (2015). Filopodia in cell adhesion, 3D migration and cancer cell invasion. *Curr Opin Cell Biol* 36:23-31.

Jacquemet G, Morgan MR, Byron A, Humphries JD, Choi CK, Chen CS, Caswell PT, Humphries MJ. (2013). Rac1 is deactivated at integrin activation sites through an IQGAP1–filamin-A–RacGAP1 pathway. *J Cell Sci* 126:4121-35.

Jordens I, Fernandez-Boria M, Marsman M, Dusseliee S, Janssen L, Calafat J, Janssen H, Wubbolts R, Neefies J. (2001). The Rab7 effector protein RILP controls lysosomal transport by inducing the recruitment of dynein-dynactin motors. *Curr Biol* 11:1680-5.

Kawauchi T, Sekine K, Shikanai M, Chihama K, Tomita K, Kubo K, Nakajima K, Nabeshima Y, Hoshino M. (2010). Rab GTPases-dependent endocytic pathways regulate neuronal migration and maturation through N-cadherin trafficking. *Neuron* 67:588-602.

Kawauchi T. (2011). Regulation of cell adhesion and migration in cortical neurons: Not only Rho but also Rab family small GTPases. *Small GTPases* 2:36-40.

Kessler D, Gruen GC, Heider D, Morgner J, Reis H, Schmid KW, Jendrossek V. (2012). The action of small GTPases Rab11 and Rab25 in vesicle trafficking during cell migration. *Cell Physiol Biochem* 29:647-56.

Kim TK and Eberwine JH. (2010). Mammalian cell transfection: the present and the future. *Anal Bioanal Chem* 397:3173-8.

Lang BT, Wang J, Filous AR, Au NP, Ma CH, Shen Y. (2014). Pleiotropic molecules in axon regeneration and neuroinflammation. *Exp Neurol* 258:17-23.

Lauffenburger DA, Horwitz AF. (1996). Cell migration: a physically integrated molecular process. *Cell* 84:359-69.

Leduc C and Etienne-Manneville S. (2015). Intemediate filaments in cell migration and invasion: the unusual suspects. *Curr Opin Cell Biol* 32:102-112.

Lee SY, Song EJ, Kim HJ, Kang HJ, Kim JH, Lee KJ. (2001). Rac1 regulates heat shock responses by reorganization of vimentin filaments: identification using MALDI-TOF MS. *Cell Death Differ* 8:1093-102.

Maninová M, Klimová Z, Parsons JT, Weber MJ, Iwanicki MP, Vomastek T. (2013). The reorientation of cell nucleus promotes the establishment of front-rear polarity in migrating fibroblasts. *J Mol Biol* 425:2039-55.

Mascia A, Gentile F, Izzo A, Mollo N, De Luca M, Bucci C, Nitsch L, Calì G. (2015). Rab7 Regulates CDH1 Endocytosis, Circular Dorsal Ruffles Genesis and Thyroglobulin Internalization in a Thyroid Cell Line. *J Cell Physiol*: in press doi: 10.1002/jcp.25267.

Meggouh F, Bienfait HM, Weterman MA, De Visser M, Baas F. (2006). Charcot– Marie-Tooth disease due to a de novo mutation of the RAB7 gene. *Neurology* 67:1476–1478.

Mendoza P, Ortiz R, Diaz J, Quest AF, Leyton L, Stupack D, Torres VA. (2013). Rab5 activation promotes focal adhesion disassembly, migration and invasiveness in tumor cells. *J Cell Sci* 126:3835-47.

Meriane M, Mary S, Comunale F, Vignal E, Fort P, Gauthier-Rouviére C. (2000). Cdc42Hs and Rac1 GTPases induce the collapse of the vimentin intermediate filament network. *J Biol Chem* 275:33046-52.

Muthuswamy SK, Xue B. (2012). Cell polarity as a regulator of cancer cell behavior plasticity. *Annu Rev Cell Dev Biol* 28:599-625.

Nodari A, Zambroni D, Quattrini A, Court FA, D'Urso A, Recchia A, Tybulewicz VL, Wrabetz L, Feltri ML. (2007). Beta1 integrin activates Rac1 in Schwann cells to generate radial lamellae during axonal sorting and myelination. *J Cell Biol* 177:1063-75.

Pankiv S, Alemu EA, Brech A, Bruun JA, Lamark T, Overvatn A, Bjørkøy G, Johansen T. (2010). FYCO1 is a Rab7 effector that binds to LC3 and PI3P to mediate microtubule plus end-directed vesicle transport. *J Cell Biol* 188:253-269

Parsons JT, Horwitz AR, Schwartz MA. (2010). Cell adhesion: integrating cytoskeletal dynamics and cellular tension. *Nat Rev Mol Cell Biol* 11:633-43.

Paul NR, Jacquemet G, Caswell PT. (2015). Endocytic trafficking of integrins in cell migration. *Curr Biol* 25:R1092-105.

Peng X, Nelson ES, Maiers JL, DeMali KA. (2011). New insights into vinculin function and regulation. *Int Rev Cell Mol Biol* 287:191-231.

Pereira-Leal JB, Seabra MC. (2000). The mammalian Rab family of small GTPases: definition of family and subfamily sequence motifs suggests a mechanism for functional specificity in the Ras superfamily. *J Mol Biol* 301:1077-87.

Plantard L, Arjonen A, Lock JG, Nurani G, Ivaska J, Stromblad S. (2010). PtdIns(3,4,5)P3 is a regulator of myosin-X localization and filopodia formation. *J Cell Sci* 123:3525-34.

Priya A, Kalaidzidis IV, Kalaidzidis Y, Lambright D, Datta S. (2015). Molecular insights into Rab7-mediated endosomal recruitment of core retromer: deciphering the role of Vps26 and Vps35. *Traffic* 16:68-84.

Progida C, Malerød L, Stuffers S, Brech A, Bucci C, Stenmark H. (2007). RILP is required for the proper morphology and function of late endosomes. *J Cell Sci* 120:3729-37.

Raftopoulou M, Hall A. (2004). Cell migration: Rho GTPases lead the way. *Dev Biol* 265:23-32.

Raiborg C, Wenzel EM, Pedersen NM, Olsvik H, Schink KO, Schultz SW, Vietri M, Nisi V, Bucci C, Brech A, Johansen T, Stenmark H. (2015). Repeated ER-endosome contacts promote endosome translocation and neurite outgrowth. *Nature* 7546:234-238.

Ridley AJ, Schwartz MA, Burridge K, Firtel RA, Ginsberg MH, Borisy G, Parsons JT, Horwitz AR. (2003). Cell migration: integrating signals from front to back. *Science* 302:1704-9.

Rojas R, van Vlijmen T, Mardones GA, Prabhu Y, Rojas AL, Mohammed S, Heck AJ, Raposo G, van der Sluijs P, Bonifacino JS. (2008). Regulation of retromer recruitment to endosomes by sequential action of Rab5 and Rab7. *J Cell Biol* 183:513-26.

Romero Rosales K, Peralta ER, Guenther GG, Wong SY, Edinger AL. (2009). Rab7 activation by growth factor withdrawal contributes to the induction of apoptosis. *Mol Biol Cell* 20:2831-40.

Sakamoto Y, Boëda B, Etienne-Manneville S. (2013). APC binds intermediate filaments and is required for their reorganization during cell migration. *J Cell Biol* 200:249-58.

Saxena S, Bucci C, Weis J, Kruttgen A. (2005). The small GTPase Rab7 controls the endosomal trafficking and neuritogenic signaling of the nerve growth factor receptor TrkA. *J Neurosci* 25:10930-40.

Schwartz SL, Cao C, Pylypenko O, Rak A, Wandinger-Ness A. (2007). Rab GTPases at a glance. *J Cell Sci.* 120:3905-3910.

Seaman MN, Harbour ME, Tattersall D, Read E, Bright N. (2009). Membrane recruitment of the cargo-selective retromer subcomplex is catalysed by the small GTPase Rab7 and inhibited by the Rab-GAP TBC1D5. *J Cell Sci* 122:2371-82.

Seebohm G, Strutz-Seebohm N, Ureche ON, Henrion U, Baltaev R, Mack AF, Korniychuk G, Steinke K, Tapken D, Pfeufer A, Kääb S, Bucci C, Attali B, Merot J, Tavare JM, Hoppe UC, Sanguinetti MC, Lang F. (2008). Long QT syndrome-associated mutations in KCNQ1 and KCNE1 subunits disrupt normal endosomal recycling of IKs channels. *Circ Res* 103:1451-57.

Shafaq-Zadah M, Gomes-Santos CS, Bardin S, Maiuri P, Maurin M, Iranzo J, Gautreau A, Lamaze C, Caswell P, Goud B, Johannes L. (2016). Persistent cell migration and adhesion rely on retrograde transport of β1 integrin. *Nat Cell Biol* 18:54-64.

Shattil SJ, Kim C, Ginsberg MH. (2010). The final steps of integrin activation: the end game. *Nat Rev Mol Cell Biol* 11:288-300.

Shirane M, Nakayama KI. (2006). Protrudin induces neurite formation by directional membrane trafficking. *Science* 314:818-21.

Spinosa MR, Progida C, De Luca A, Colucci AM, Alifano P, Bucci C. (2008). Functional characterization of Rab7 mutant proteins associated with Charcot-Marie-Tooth type 2B disease. *J Neurosci* 28:1640-8.

Stenmark H. (2009). Rab GTPases as coordinators of vesicle traffic. *Nat Rev Mol Cell Biol* 10:513-25.

Sun Y, Buki KG, Ettala O, Vaaraniemi JP, Vaananen HK. (2005). Possible role of direct Rac1-Rab7 interaction in ruffled border formation of osteoclasts. *J Biol Chem* 280:32356-61.

Sutoh Yoneyama M, Hatakeyama S, Habuchi T, Inoue T, Nakamura T, Funyu T, Wiche G, Ohyama C, Tsuboi S. (2014). Vimentin intermediate filament and plectin provide a scaffold for invadopodia, facilitating cancer cell invasion and extravasation for metastasis. *Eur J Cell Biol* 93:157-169.

Tang DD. (2008). Intermediate filaments in smooth muscle. *Am J Physiol Cell Physiol* 294-C869-78.

Tiwari S, Askari JA, Humphries MJ, Bulleid NJ. (2011). Divalent cations regulate the folding and activation status of integrins during their intracellular trafficking. *J Cell Sci* 124:1672-80.

Tuloup-Minguez V, Hamai A, Greffard A, Nicolas V, Codogno P, Botti J. (2013). Autophagy modulates cell migration and β1 integrin membrane recycling. *Cell Cycle* 12:3317-28.

Vanlandingham PA, Ceresa BP. (2009). Rab7 regulates late endocytic trafficking downstream of multivesicular body biogenesis and cargo sequestration. *J Biol Chem* 284:12110-24.

Verhoeven K, De Jonghe P, Coen K, Verpoorten N, Auer-Grumbach M, Kwon JM, FitzPatrick D, Schmedding E, De Vriendt E, Jacobs A, Van Gerwen V, Wagner K, Hartung HP, Timmerman V. (2003). Mutations in the small GTP-ase late endosomal protein RAB7 cause Charcot–Marie-Tooth type 2B neuropathy. *Am J Hum Genet*. 72:722–727.

Vicente-Manzanares M, Webb DJ, Horwitz AR. (2005). Cell migration at a glance. *J Cell Sci* 118:4917-9.

Wang T, Ming Z, Xiaochun W, Hong W. (2011). Rab7: role of its protein interaction cascades in endo-lysosomal traffic. *Cell Signal* 23:516-21.

Wang X, Han C, Liu W, Wang P, Zhang X. (2014). A novel RAB7 mutation in a Chinese family with Charcot-Marie-Tooth type 2B disease. *Gene* 534:431-4.

Wang Z, Zhou Y, Hu X, Chen W, Lin X, Sun L, Xu X, Hong W, Wang T. (2015). RILP suppresses invasion of breast cancer cells by modulating the activity of RalA through interaction with RalGDS. *Cell Death Dis* 6:e1923.

Zhang H, Berg JS, Li Z, Wang Y, Lång P, Sousa AD, Bhaskar A, Cheney RE, Strömblad S. (2004). Myosin-X provides a motor-based link between integrins and the cytoskeleton. *Nat Cell Biol* 6:523-31.

ACKNOWLEDGEMENTS

At the end of my thesis I would like to thank all those people who made this thesis possible and an unforgettable experience for me.

First of all, I gratefully acknowledge my supervisor Prof. Cecilia Bucci for the chance to undertake a PhD project within her group, for the great effort she put into training me in the scientific field allowing me to grow as a research scientist, for insightful scientific discussion, and for the opportunities she gave me.

I would like to express my very sincere gratitude to Prof. Oddmund Bakke from University of Oslo for allowing me to work in his laboratory, to get access to the Imaging Platform and its advanced microscopes. I also thank him for allowing me to gain more knowledge in this field and for his support.

I would like to acknowledge my immense gratitude to Dr. Cinzia Progida for sharing her knowledge, for teaching me with patience, for being a mentor during my experience in Oslo.

Special thanks go to the people that I met during these years and that I had the pleasure to work with sharing everyday life in the lab. It has not always been easy, but we managed to find our own balance.

I wish to thank Mariangela who selflessly supported and encouraged me during these years, for sharing the same "adventure", for scientific and life discussions, for always being there when I needed, for our "nonsense conversation", for understanding me without the need to talk.

Thanks to Flora. The amount of time we shared in the lab doesn't correspond to the amount of precious advices and support you gave me. I really appreciated what you did for me.

I would also like to thank Maria who encouraged me to strive towards my goal and for her optimism.

Thanks to Veronica, always willing to help, and for life discussions. We shared both the beginning and the end of this experience.

Thanks to Aurora for the fun times we shared and for being herself.

Thanks for your friendship.

I would also like to thank Pier Paolo for fun and life discussions, for his selfless advices.

The members of the Bakke group have contributed immensely to my personal and professional experience at Oslo. Thanks for the technical assistance with microscopes and for the friendly support during my work. It has been an important experience in my life that I will never forget.

I am thankful to Carla for her precious friendship and for life discussions.

I give my sincere thank to Valentina for her true friendship throughout these long years. We shared this experience even if in different places.

I wish to thank my family for their continuous support during these years.